The Dissertation Committee for Sriramya Duddukuri Nair Certifies that this is the approved version of the following dissertation:

Adaptive Performance of Cement-based Materials Using a Magnetorheological Approach

Committee:

Raissa P. Ferron, Supervisor

Maria C.G. Juenger

David W. Fowler

Chadi S. El Mohtar

Eric van Oort

Adaptive Performance of Cement-based Materials Using a Magnetorheological Approach

by

Sriramya Duddukuri Nair, B. Tech.; M. S.

Dissertation

Presented to the Faculty of the Graduate School of

The University of Texas at Austin

in Partial Fulfillment

of the Requirements

for the Degree of

Doctor of Philosophy

The University of Texas at Austin

August 2013

Dedication

To my parents and my husband, for their support and encouragement.

Acknowledgements

First of all I would like to thank my advisor, Prof. Raissa Ferron for giving me this opportunity to work on this project and for introducing me to the world of rheology. Thank you for your guidance, support and encouragement over the years. Without you, this dissertation would not have been possible and I am greatly indebted to you.

I thank Prof. Maria Juenger for all her support and guidance. Thank you for spending time with me and guiding me through all my years at UT. I thank you as well for serving on my committee and for all your valuable inputs.

I would like to thank Prof. Eric van Oort and Kenneth "Mike" Cowan for their support both technically and financially towards the last year of this work. Thank you for sharing our excitement about this project and for all your input to the project. I'm really excited about joining your lab and I'm looking forward to it. I thank Prof. David Fowler and Prof. Chadi El Mohtar for taking time off their busy schedules to serve on my committee and for their guidance.

I thank Dr. Mohsen Ahmadian for helping me run the vibrating sample magnetometer and Zeynep Basaran for the scanning electron microscope images. The results were helpful for characterizing the materials. I also want to thank

Zeynep Basaran and Dongyeop Han for all the useful discussions we have had over the past few years. Working in the lab wouldn't have been fun without the two of you.

I express my gratitude to Sherian Williams and Tesse Smitherman for taking care of all the administrative nuances and for making it seem to seamless.

I thank Mike Rung and Michelle Shuck for their technical support with everything at both the labs. Thank you for listening to all the problems and providing feasible solutions. A special shout out to Chris Clement for all his ideas and help with fixing things at the lab. I would like to take a moment to thank everyone at 18B who have helped me in different ways ranging from experiments to ideas to emotional support when needed and for making this an unforgettable experience.

I express my sincere gratitude to all the undergraduate assistants who helped me with this project as well as other research projects that I have worked on at UT. A special recognition for Alex Martinez, Thomas Weng, Daniel Pelayo, Jessica Nguyen, Naomi Bhappu, Rukundo Gahigiro, Morgan Allford, Tania Vazquez and Kevin Nicoletta.

I thank the Civil Engineering Dept. and all the professors involved with CE 314K for supporting me financially through a teaching assistantship for a major chunk

of my stay at UT. Thanks to Wayne, Tyler, Phil, Amir, Craig, Jinwoo, Sarwar, Trevor, Wenyu, Zeynep and all the students for making it fun.

This PhD wouldn't have been possible without the support of my brother, my in-laws, my grandma's, uncles, aunts, cousins and especially all my friends in and out of Austin.

Growing up my father and his colleagues were my biggest inspiration and just like them I always wanted to be an engineer. My mother gets most of the credit for making my dreams come true. She had faith in my abilities and provided me with all the resources that I needed. I express my deepest gratitude to both my parents for their sacrifices and for being my strongest supporters throughout this long educational journey, which has lasted more than a couple of decades. I believe that I have made them proud today by finishing my doctoral degree.

These acknowledgements wouldn't be complete without the mention of my dearest husband, Hari. Being a fellow doctoral candidate he absolutely understood all the ups and downs of graduate school life and always knew the right thing to say to cheer me up during all the frustrating times when equipments or experiments wouldn't work. Even though I'm done with my PhD now, I cannot promise Hari that I won't show up at home all covered in cement because both Hari and cement (/concrete) are the two loves of my life.

Adaptive Performance of Cement-based Materials Using a Magnetorheological Approach

Sriramya Duddukuri Nair, Ph.D.

The University of Texas at Austin, 2013

Supervisor: Raissa P. Ferron

Today's concrete is no longer a simple combination of cement, aggregates and water. With increased use of various types of waste materials as supplementary cementitious materials and chemical admixtures, material incompatibility problems have been observed in concrete construction. As a result, some of the greatest problems in concrete manufacturing occur when concrete does not stiffen or harden on time. To this end, a new innovative type of cementing technique (based on the principles of magnetorheology) is presented that allows for the real-time control over the stiffening or setting behavior of concrete. In traditional magnetorheological (MR) fluids, magnetic particles are mostly submerged in Newtonian carrier fluids using high volumetric contents (40-50%) of magnetic particles. A key interest in this work was to investigate if using a non-Newtonian

carrier fluid like cement paste with low dosages of magnetic particles would yield an MR effect.

Rheological tests were conducted on paste mixtures containing small dosages of magnetic particles (less than 2% volume fraction) and when a magnetic field was applied, it was determined that the shear resistance of the paste could be altered significantly. The response of the paste was found to be dependent on the magnitude of the applied field, concentration of the magnetic particles and surface chemistry of magnetic particles. Furthermore the magnetic particles used in this research to create the MR cement paste did not have any effect on cement hydration products or on compressive strength results.

It was shown that the rheological behavior of cement paste could even be adapted to simulate "setting" behavior when an MR-based approach is used. Thus, the potential to create a cement-based material whose fresh state behavior can be adapted on-demand by the user to achieve a desired behavior may soon be a reality. Such a material can be useful in applications in which controlling the fresh-state behavior is critical, and could transform the way cement-based materials are cast. In addition, possibilities to create a smart cement-based composite from the fresh to the hardened state may be possible if the magnetic particles could later be used for structural health monitoring.

Table of Contents

List of Key Symbols

δ	Phase Lag (SAOS testing)
$\partial G'/\partial t$	Rate of change of G'
γ	Shear strain
$\dot{\gamma}$	Shear rate
γ_o	Constant shear strain
η	Newtonian viscosity
μ	Magnetic permeability
μ_B	Bingham viscosity
μ_c	Casson viscosity
τ	Shear stress
τ_o	Yield stress
χ	Volume susceptibility
ω	Angular frequency
B	Magnetic flux density (or magnetic field strength)
c	Hershel-Bulkley consistency index
d_x	Diameter where x represents the % of powder by volume containing particles with effective diameter less than that diameter
G'	Storage modulus
G''	Loss modulus
G*	Shear modulus
H	Applied magnetic field
H_c	Coercivity
k	Power law consistency index

M	Magnetization
M_r	Remnant magnetization
M_s	Saturation magnetization
n	Power exponent
t	time

List of Abbreviations

AEE	Atlantic Equipment Engineers
API	American Petroleum Institute
ASTM	American Society for Testing and Materials
C_2S	Dicalcium silicate
C_3S	Tricalcium silicate
C_3A	Tricalcium aluminate
CIP	Carbonyl Iron Powder
HRWR	High range water reducer
IPA	Isopropyl Alcohol
LVER	Linear viscoelastic region
MR	Magnetorheological
SAOS	Small amplitude oscillatory shear
VSM	Vibrating Sample Magnetometer

List of Tables

List of Figures

CHAPTER 1: INTRODUCTION

Today's concrete is no longer a simple combination of cement, aggregates and water. With the increased use of various types of supplementary cementitous materials and chemical admixtures, material incompatibility problems have been observed in concrete construction (Mehta and Monteiro 2006; Taylor et al. 2006; Taylor et al. 2006a; Roberts and Taylor 2007). As a result, some of the greatest problems in concrete manufacturing occur when concrete does not stiffen, set or harden on time (Taylor et al. 2006a). However, what if it was possible to create a concrete in which the user is able to control in real-time its stiffening/setting behavior? Cement-based magnetorheological (MR) fluids can potentially be used in civil engineering applications to act as a "set-on-demand" material, allowing the user greater control over the processing (e.g., pumping, placing, etc.) of concrete. MR fluids undergo large, rapid changes in their rheological properties when subjected to an external magnetic field. In the case of ideal MR fluids, these changes in rheological properties are completely reversible.

Such a material can be useful in applications where control of the fresh-state properties of concrete is critical. For example, in underwater concreting of drilled shafts, concrete is transported over large distances, and during this transportation, the concrete must not segregate. An MR approach could be used to maintain the desirable properties of concrete so that separation of the constituent ingredients is avoided. Furthermore, by

applying a magnetic field larger than the value used to control the flow behavior, washout of the concrete can be prevented. “Set-on-demand” properties of a material can be useful for other civil engineering applications such as:

- formwork pressure reduction of self-consolidating concrete;
- casting of narrow channels or long casting distances;
- improving segregation resistance of aggregates in concrete;
- to avoid sloughing or slumping of shotcrete from its receiving surface.

This new cementing technique could also play a major role in oil well cementing. Cementing problems were associated with 18 of 39 blowouts between 1992 and 2006 (Izon, Danenberger, and Mayes 2004), and based on a survey conducted in 1997, it was found that on average 5% of total well costs were spent on cementing and that 15% of the cementing jobs ended up in failure costing the industry $470 million/year in repairs (Sabins 2002). Failure of a cementing job could lead to oil spills (e.g. BP oil spill, 2010) that result in both immediate and long-term environmental damage and destruction of ecosystems. Furthermore, oil spills not only cause substantial monetary burdens to society, but they also have significant consequences to human health due to indirect and direct inhalation and ingestion of contaminated products (West 2011). The main goal of a cement job is to provide complete and durable zonal isolation from when the cement is placed, up until the well is abandoned. Zonal isolation is extremely important in the oil and gas industry since it prevents fluids (such as water or gas) in one zone from mixing with oil in another zone. The ability of the cement sheath to provide zonal isolation

depends on the cement/casing interface, the bulk cement and the cement/formation interface (Nelson and Guillot 2006). The bulk cement layer could be affected, for example, if there is gas or liquid migration into the cement during placing or if there are regions without any cement. Having better control over the rheological properties of cement slurry during placing could help avoid zonal isolation problems that arise from poor cementing.

In addition to controlling the fresh state properties, the development of an MR cement-based composite may also be helpful in the maintenance, repair and rehabilitation of concrete. Since the magnetic particles are embedded throughout the matrix of the concrete, the magnetic particles could potentially be used for structural health monitoring (Jiles 1988; Jiles 1990). Such monitoring could be critical to assess the performance of important structures (Brownjohn 2007), to reduce the risk of failures, to maintain the structures and to prolong their useful life.

The research presented here presents an innovative approach to control the fresh state performance of cement during cementing operations. Through better control of the fresh state properties, the quality and durability of the cementing operations can be improved (Kim, Ferron, and Shah 2012). This improvement in durability can extend the service life of the material and the improvement in quality control reduces the need for costly repairs and in addition reduces the need to use more materials to conduct the repairs. The aim of the current research was to:

- develop an cement-based MR fluid
- investigate the viscoelastic behavior of cement-based MR fluids over time
- examine the influence of magnetic particle type and magnetic particle size on the performance of cement-based MR fluids
- evaluate the influence of magnetic particles and magnetic field on cement hydration.

Chapter 2 gives brief introduction to rheology and magnetorheology. Chapter 3 gives detailed information about the characteristics of the materials used in this study and also the methods used to prepare the samples. Chapter 4 presents the results and discussion on an investigation conducted in which the viscoelastic properties of the cement-based MR fluids are investigated for a duration of two hours. This chapter also gives details about the influence of magnetic particle dosage, magnetic particle size, suspending medium rheological properties and the effects of cycling the applied magnetic field. Chapter 5 is about the effect of magnetic particles and magnetic field on hydration of cement-based MR fluids. Chapter 6 compares different types of magnetic particles and their effect on the rheological properties for a duration of two hours. Chapter 7 focuses on practical applications and investigated whether the changes in the rheological properties would actually translate into changes in the fresh state performance. Finally, chapter 8 gives a summary about the finding of the research and ideas for future work.

CHAPTER 2: BACKGROUND

To analyze the behavior of cement-based magnetorheological fluids, it is important to first understand the fresh state behavior of cementitious materials. Rheology has been widely used to characterize the behavior of fresh cement paste, fresh mortar or fresh concrete. Thus, the first part of this chapter gives a brief overview about rheology, the importance of rheology to the concrete industry and techniques used to measure the rheological properties. The phenomena of flocculation and thixotropy are also discussed as they influence the behavior of fresh cement paste or fresh concrete over the first few hours after mixing. Next, to get a background on magnetorheological (MR) fluids, basic concepts on magnetism, followed by a description of the current state of knowledge on MR fluids, is presented.

2.1 INTRODUCTION TO RHEOLOGY

Rheology is the study of flow and deformation of materials (Tattersall and Banfill 1983). It was coined by Eugene C. Bingham in 1920's and was derived from the Greek verb, *ρειυ* (to flow) (Macosko 1994); since the official birth of rheology in the 1920s it has grown into its own scientific field, with several research conferences and journals dedicated to this field. Rheology is extensively used in numerous scientific fields (such as physiology, geophysics, material science engineering, pharmaceutics and food industry) for manufacturing materials like plastics, paints, lubricants, detergents, asphalt, ketchup, yogurt, etcetera (Barnes, Hutton, and Walters 1989). The earliest published work on

rheology of fresh concrete is dated back to 1949 (L'Hermite 1949) and since then has received a lot of interest in the concrete community.

2.2 RHEOLOGICAL TESTS

2.2.1 Flow Curves

Rheological properties of cement pastes are typically characterized using flow curves (Ferraris, Obla, and Hill 2001; Tattersall and Banfill 1983; Williams, Saak, and Jennings 1999). A flow curve is a graphical representation of the shear stress versus the shear strain rate of a flowing material (see Figure 2.1) when the material is subjected to a varied shear strain rate (or conversely a varied shear stress). The shape of the flow curves provides insight about the flow behavior of a material, such as whether the viscosity of the material is shear-rate dependent or independent. Viscosity is a characteristic behavior

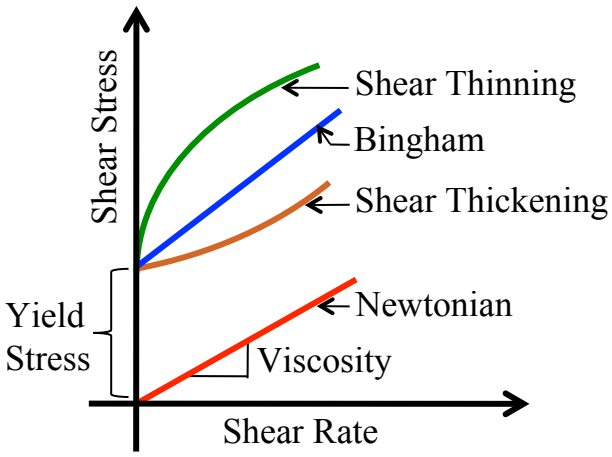

Figure 2.1 Illustration of common rheological behavior

of a fluid and is a measure of the fluids ability to resist shear-induced flow and is dependent on the internal friction between the neighboring particles in the fluid. From a flow curve, viscosity is determined from the slope of a shear stress vs. shear strain curve. If the flow curve has a linear response, then the viscosity is a constant, but if the response is non-linear then the value of viscosity is based on the shear rate at which it is measured. Apparent viscosity is defined as the ratio of shear stress to shear rate at any given shear rate.

Examination of the flow curve also provides insight about the existence of a yield stress in the material. Yield stress is the shear strength of a material, and ideally, it is the stress that has to be exceeded to initiate flow. When the level of stress is smaller than the yield stress, there is little or no deformation and above the yield stress the material flows with a resistance determined by the viscosity. The yield stress is determined by extrapolating the data of a flow curve and finding the intercept with the shear stress axis. Yield stress gives significant information regarding workability of concrete (higher yield stresses lead to less workable concrete). A balance between the yield stress and viscosity is required to achieve desired rheological properties in concrete. For self-consolidating concrete, low yield stresses allow for the concrete to flow under its own mass and the viscosity has to be sufficiently high in order to prevent segregation but low enough to ensure that the concrete flows at a reasonable speed.

The simplest type of rheological fluid is a Newtonian fluid. The viscosity of a Newtonian fluid is constant over the entire shear rate range; thus it is a shear rate independent material. In addition it does not have a yield stress. In the flow curve depicted in Figure 2.1, the Newtonian fluid is the line that demonstrates a linear response in a flow curve, which represents a constant viscosity and the line passes through the origin. The constitutive equation of a Newtonian fluid can be represented by:

$$\bar{\bar{\tau}} = \eta \, \bar{\bar{\dot{\gamma}}} \qquad \text{Equation 2.1}$$

where, $\bar{\bar{\tau}}$ is the shear stress response of the material, η is the Newtonian viscosity and $\bar{\bar{\dot{\gamma}}}$ is the rate of straining ($d\gamma/dt$) also known as shear strain rate or shear rate. Water and oils are some examples of Newtonian fluids, wherein the materials flow right after the application of a load and the material's resistance to flow is determined by the viscosity. If there is any deviation from the above behavior (either linearity and/or presence of yield stress), then the material is called as a non-Newtonian fluid. A few of the possible non-Newtonian behaviors are shown in Figure 2.1. If the material exhibits yielding behavior, then the yield stress could be calculated using various models (e.g. Bingham model) or estimated from visual inspection of the flow curve. A Bingham model can be represented by:

$$\tau = \tau_0 + \mu \, \dot{\gamma} \qquad \text{Equation 2.2}$$

where μ_b is the plastic or Bingham viscosity and τ_0 gives an indication for the yield stress of the material. The yield stress is determined by extrapolating the data and finding the intercept with the shear stress axis.

A material can also exhibit a shear thinning behavior, where in the apparent viscosity decreases with increasing shear rate or a shear thickening behavior where in the apparent viscosity increases with increasing shear rate (see Figure 2.1). A power law, Casson or Herschel-Bulkley model (see Equations 2.3, 2.4 and 2.5 respectively) can be used to calculate the rheological properties of these materials (Macosko 1994).

$$\tau = k\ \dot{\gamma}^{n} \qquad \text{Equation 2.3}$$

$$\tau^{1/2} = \tau_0^{\,1/2} + \left(\mu_c\ \dot{\gamma}\right)^{1/2} \qquad \text{Equation 2.4}$$

$$\tau = \tau_0 + c\ \dot{\gamma}^{n} \qquad \text{Equation 2.5}$$

where k and c represent a consistency index and n is the power exponent. For Newtonian fluids, $n = 1$, for shear thinning fluids, $n < 1$ and finally for shear thickening fluids, $n > 1$.

2.2.2 Stress Growth

As mentioned in the previous section, yield stress can be determined from a flow curve. Barnes and Walters (1985) tested a shear thinning material at different shear rates and determined the yield stress from a flow curve. Yield stress was obtained by extrapolating the results and finding the intercept with the shear stress axis. As they investigated the material at the lower shear rate regions, they found that the yield stress value dropped and, at very low shear rates, the material showed Newtonian behavior without any yield stress (Barnes and Walters 1985). Thus, the yield stress of a material is sensitive to the shear rate range that it is tested in; this is particularly important for high-shear thinning materials.

The stress growth technique is another technique that can be employed to measure the

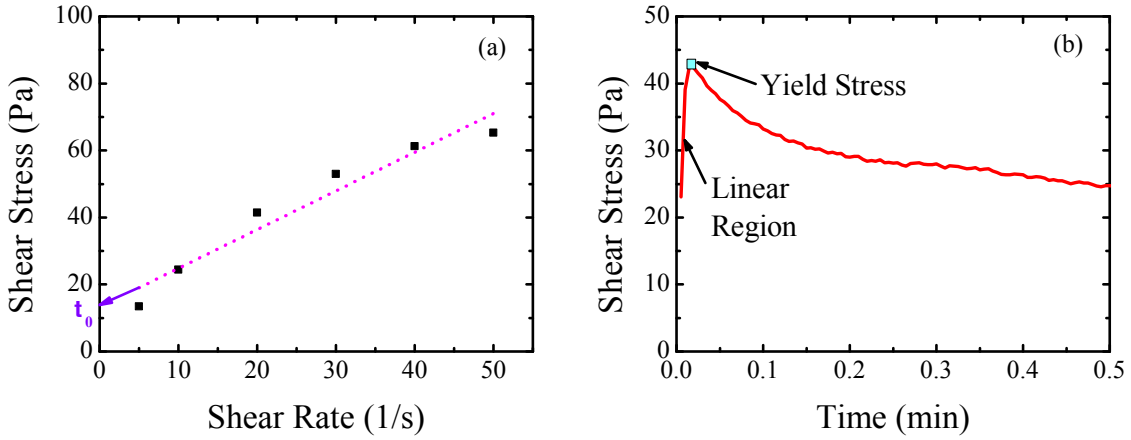

Figure 2.2 Yield stress measurement of 10 minute old cement paste through (a) Bingham fit (dotted line) for the measured data (black solid squares) and (b) stress growth technique at shear rate of 0.1 s^{-1}

yield stress of a material. In the stress growth technique, the material is sheared at a continous increasing strain that changes at a low constant rate (i.e. constant shear strain rate) and the shear stress is monitored over time (Cheng 1986; Nguyen and Boger 1992; Amziane and Ferraris 2007). As shown in Figure 2.2 (b), the shear stress response consists of an initial linear phase which is an indicator of the elastic deformation that the material is undergoing. The end of the linear region represents the end of elastic deformation where the stucture breaks down beyond which the material begins to flow. The point where the linear region ends can be used as a measure of yield stress (Nguyen and Boger 1992), but this point is difficult to determine and thus the peak stress (noted in Figure 2.2 (b)) has received importance. At the peak value, there is a complete breakdown of the fluid structure and it corresponds to start of a pure viscous flow. In this work, the peak value is used as a measure of yield stress.

The yield stress that is obtained from a flow curve test is known as a dynamic yield stress because the yield stress value is extrapolated from a material that is already in flow. Thus, the value of yield stress that is obtained is really equivalent to the minimum stress required for maintaining flow (i.e. dynamic yield stress). Whereas the yield stress obtained from the stress growth technique is known as the static yield stress. In the stress growth technique, low shear rates are used such that the material is initially at rest, and beyond the yield stress, flow is initiated, which is true to the definition of yield stress. With the development of new sensetive rheometers, the stresses much below the yield stress can be measured seamlessly.

Apart from being a tool to measure yield stress of a material, stress growth curves can also be used to obtain information regarding the nature of the fluid; in specific it can be determined if the material is a Newtonian, viscoelastic or viscoplastic fluid. Newtonian fluids are ideal fluids that flow upon application of any amount of load, thus they do not have a yield stress and the shear stress value achieved in Figure 2.3 depends on the shear rate that is applied. As Newtonian fluids have a constant viscosity, the shear stress remains at a constant value (because in the stress growth technique the shear rate is held constant). A viscoplastic material is one which has a yield stress and above the yield stress the material flows readily. Beyond the yield stress, the shear stress value decays at a fast rate and reaches an equilibrium. In contrast, in a viscoelastic material, the shear stress value decays at a slower rate (which is necessary for materials that are used as

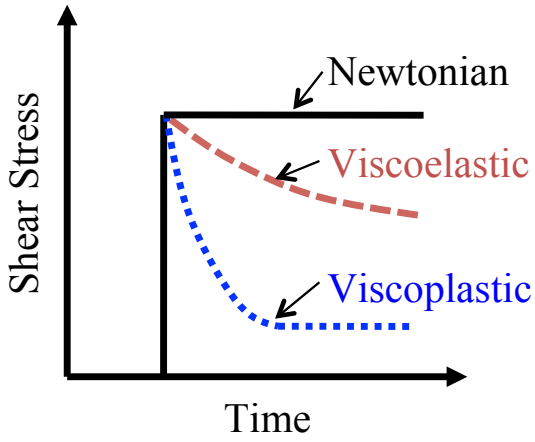

Figure 2.3 Shear stress response to a constant shear rate based on the type of the material

shock absorbers). Thus when materials are subjected to the same constant shear rate, by observing the shape of the shear stress curves, the viscous nature of the fluids can be compared.

Despite the fact that stress growth curves are ideal for measuring the true yield stress of a fluid, they cannot be used to measure the viscosity of the sample. The traditional method for measuring yield stress is to extrapolate to zero shear rate on flow curves to find the yield stress. Nevertheless there is no universal method to measure yield stress, but rather certain industries tend to favor certain methods.

2.2.3 Small angle oscillatory shear (SAOS)

Oscillatory shear testing is often used to characterize the viscoelastic behavior of materials (Gartner et al. 2002). SAOS provides insight about the fresh-state microstructure of the material at rest. SAOS testing is a dynamic method in which a sinusoidal mechanical input (shear stress or shear strain) with a fixed frequency and small amplitude is applied. SAOS is considered as a dynamic testing method because the shear strain is oscillated periodically and the value of shear strain is time-dependent. By limiting the mechanical input to small amplitudes within the linear viscoelastic region (LVER), the particles stay in close contact with one another and are able to recover elastically; thus the microstructure is not disturbed significantly (Larson 1998). Let us say that the imposed mechanical input is a shear strain (γ) given by:

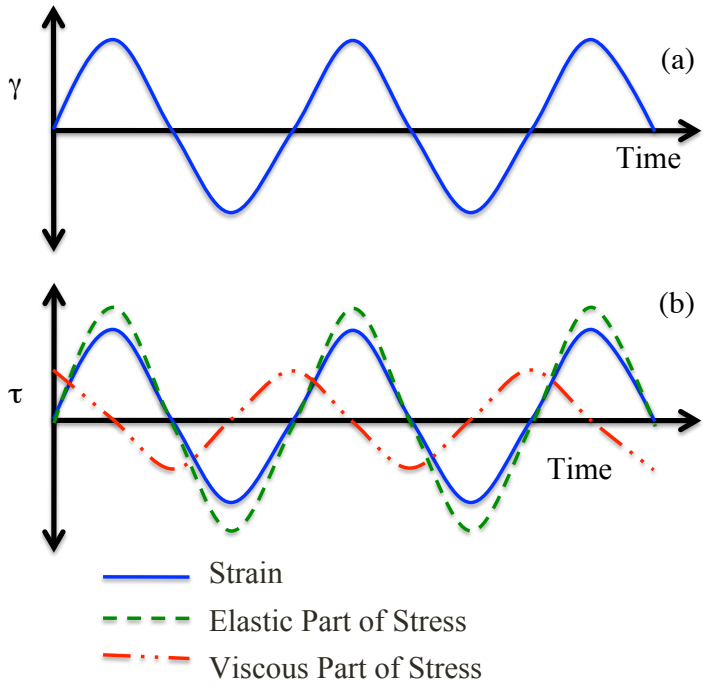

Figure 2.4 Schematic of small amplitude oscillatory shear test (a) shows an applied sinusoidal shear stress (b) response of a viscoelastic material that is split in to the elastic (in phase) component and the viscous (out of phase) component.

$$\gamma = \gamma_0 \sin(\omega t) \qquad \text{Equation 2.6}$$

where γ_0 is the constant small strain amplitude, ω is the angular frequency and t is time. A schematic of the imposed shear strain is shown in Figure 2.4 (a).

If a purely elastic material is subjected to the sinususoidal shear strain that is within its LVER, then the shear stress response would be completely in-phase with the applied shear strain (green dashed line in Figure 2.4 (b)). Similarly, the shear stress response for a

purely viscous material would be 90° out-of-phase with the input shear strain (red dash-dot-dot line in Figure 2.4 (b)). The shear stress (τ) response of a viscoelastic material can be represented by:

$$\tau = \gamma_0 \left[G'(\omega)\sin(\omega t) + G''(\omega)\cos(\omega t) \right] \qquad \text{Equation 2.7}$$

where *G'(ω)* is the storage modulus and *G''(ω)* is the loss modulus. The shear modulus, *G** is given by $G^* = G' + i\,G''$ and the loss factor is given by, tan δ = G''/G', where δ is the phase lag.

G' is the component which is in phase with the applied shear strain and is the deformation energy stored in the material during shearing and represents the elastic behavior of the material. The component that is out-of-phase with the applied strain is the loss modulus, *G''*, which is the energy dissipated from the material and represents the viscous behavior of the material. Monitoring the viscoelastic behavior of a material over time gives information regarding both the viscous and the elastic components. If *G'* is greater than *G'',* then the elastic properties are more prominent or significant than the viscous properties. Similarly if *G' < G'',* then the elastic properties are less significant than the viscous properties. When *G' = G'',* both the viscous and the elastic properties are equally significant.

2.2.4 Why study rheology of concrete?

Rheology is important for understanding the behavior of fresh concrete during different stages of construction such as mixing, pumping or consolidation of concrete. By applying the right rheological testing parameters, the shearing conditions of concrete during processing can be replicated in the lab. Observing the evolution of shear modulus with time in the linear viscoelastic region (LVER) range gives an indication regarding rate of hydration. As cement paste ages, due to flocculation and hydration mechanisms, the value of shear modulus increases over time. Yield strength can give an indication regarding the formwork pressure that is applied by concrete (Khayat and Omran 2009) as well as the green strength of concrete (Tregger 2010). Rheology has also been successfully used to understand the changes in fresh state microstructure and floc size development (Ferron et al. 2013). Fresh state rheological properties can also be helpful in predicting the long-term durability characteristics and aesthetics of concrete. Understanding the fresh state properties of concrete3 leads to better quality control which in turn reduces the need for costly repairs and reduces the need to use more materials to conduct the repairs (Kim, Ferron, and Shah 2012). Thus, in the mix design phase through quick testing, rheological results can help design a mix that is suitable for a required application. Rheology is also useful in identifying any material incompatibilities that might affect both the fresh state and long term hardened state properties of concrete (Taylor et al. 2006).

2.2.5 Measurement devices for rheology

Several rheometers have been developed for measuring the rheological properties of concrete. They include Tattersall two point device, IBB rheometer, BML viscometer, Bertta apparatus, BTRHEOM, CEMAGREF-IMG, ICAR rheometer etc (Tattersall and Banfill 1983; Ferraris and Brower 2001; Koehler and Fowler 2004). More details regarding each of the above mentioned rheometers can be found in the cited references. Most of these rheometers only give an indication about the viscosity and/or yield stress of concrete and do not give information regarding, say, the viscoelastic properties of concrete. In addition these rheometers generally require large quantity of materials for testing and are not very accurate at low shear rates or low torque measurements. The variability in aggregates also leads to a large scatter in the rheological data of concrete (Ferraris and Gaidis 1992). Due to these reasons and the development of sensitive rotational paste rheometers, many rheological research studies have been focused on cement paste (the main contributor to the rheological properties of concrete).

Commercially, both stress controlled and strain controlled rheometers are available to measure a wide range of rheological properties of viscous or viscoelastic materials. A historical evolution of these rheometers can be found elsewhere (Barnes, Schimanski, and Bell 1999; Barnes and Bell 2003). With recent advances such as fast feedback loops, modern rheometers can be operated in both modes. Because of small gap sizes, most commercial rheometers are limited to use with cement paste. Geometries that are suitable for cement paste include parallel plate, coaxial cylinders and vane. The last two are

preferable for measuring flowable pastes to prevent the sample from flowing out of the test apparatus. Care must be taken to avoid common issues such as wall slip, plug flow and sedimentation. As cement paste is a colloidal suspension with cement particles suspended in water, it is probable that a water rich layer can form at the walls leading to wall slip. Presence of slip underestimates the rheological properties and can be prevented by using serrated surfaces or a vane geometry. Plug flow occurs when a material moves as a whole without being sheared; this can be avoided by changing the proportions of the geometry or by increasing the shear rates. Particle sedimentation can occur in cement pastes with high water to cement ratios because of gravitational settling. Sedimentation can be avoided by increasing the viscosity of the suspending medium.

Researchers have found that the mixing conditions have an effect on the rheological properties of cement paste (Yang and Jennings 1995). To link the rheological properties of cement paste with those of concrete, it is important to mix and measure the properties of cement paste at the shear rates experienced by cement paste in concrete. When mixing concrete in a transit truck the shear rate experienced by cement paste (in the presence of aggregates) can increase to 2000 s^{-1} (Helmuth et al. 1995). The most common way to mix cement paste in most laboratories is by using a Hobart mixer, which only results in a shear rate of about 70 s^{-1}. To obtain a cement paste with rheological properties similar to those in concrete mixtures, it is recommended to mix it in a high shear mixer (ASTM-C1738 2011). Thus, all the rheological tests conducted in this research study have been performed on cement pastes mixed using a high shear mixer.

2.3 CEMENT HYDRATION, FLOCCULATION AND THIXOTROPY

The evolution of fresh state rheological properties of cement paste is influenced by factors such as cement hydration, particle flocculation and the thixotropic nature of cement paste. When cement is mixed with water, chemical and physical processes take place which lead to setting and hardening of concrete (Mindess, Young, and Darwin 2003). During hydration, free water is consumed and an interlocking network of hydration products is formed. This leads to a loss of workability and an increase in yield stress within the first few hours after mixing the paste.

In the fresh state, cement paste is a concentrated flocculated suspension (with micron sized cement particles dispersed in water). The stability of the suspension depends on the balance of colloidal forces such as attractive van der Waals forces and repulsive electrostatic and steric forces. van der Waals forces are weak secondary intermolecular attractive forces that are significant only when the particles are very close together (in the nanometer range). They result from the attraction between positive and negative charges without any actual transfer or sharing of electrons (Shackelford 1996) and the attraction decreases as the distance between the particles increases. When the cement particles are mixed with water, they become electrically charged, leading to electrostatic repulsive forces. Different from van der Waals forces, steric repulsion occurs from the presence of an adsorbed polymer layer (such as a high range water reducer) on the particle surface

(Mewis and Wagner 2012). Steric repulsion increases as the particle packing increases. These attractive and repulsive forces together determine the size and rate at which flocs are formed. A floc is a cohesive mass consisting of two to more particles.

Thixotropy is defined as "the continuous decrease of viscosity with time when flow is applied to a sample that has been previously at rest, and the subsequent recovery of viscosity when the flow is discontinued" (Mewis and Wagner 2012). It is a reversible phenomenon wherein cement particles floc or coagulate at rest and then breakdown during mixing because of the rupture of the interparticle bonds. This was observed by Ferron et al. (2013) through focused beam reflectance (FBRM) measurements (Ferron et al. 2013). They found that at rest (or very small stirring intensities) flocs come together to form a larger floc (thereby increasing the viscosity of the sample). These flocs are weakly bonded and a large shearing force can break down the floc sizes (Ferron et al. 2013).

In cement based materials hydration and thixotropy will affect structural rebuilding and the thixotropy is the reversible component that plays an influence on structural rebuilding at early ages (prior to set), whereas hydration is not reversible and it continues throughout the lifetime of the composite.

2.4 BASICS OF MAGNETISM

Lodestone was the first known magnetic material around 2500 years ago (Cullity and Graham 2009). Up until the 18th century placing iron next to the magnetic field lines of lodestone was the only known way of producing magnets. However, in 1825, Hans C. Oersted discovered that an electric current produced a magnetic field (Brian, Cohen, and Knudsen 2007). This invention led to the production of stronger magnets because of the stronger magnetic fields that could be generated with an electric current. In recent years, magnetic fields and magnetic materials have led to the development of many technological devices such as tape recorders, loudspeakers, radios, televisions, computers, electric motors electrical power generators and transformers (Cullity and Graham 2009).

The next part of this section gives details about commonly used units of magnetism, magnetic behavior of materials (diamagnetic, paramagnetic and ferromagnetic), magnetization curves and differences between soft and hard magnetic materials. Because of the several possible applications, magnetic fields and magnetic materials have received great interest and have been discussed in several books. The following information is a brief summary compiled from the following books: Stöhr and Siegmann 2006; Cullity and Graham 2009; Chung 2010; McCurrie 1994).

2.4.1 Magnetic field and magnetic units

When an electric current is passed through a coil, a magnetic field is generated in the direction perpendicular to the passing current. If current *I*, is passed through a cylindrical coil (or solenoid) with *N* closely spaced turns having a length *l,* then the magnetic field, *H* generated by the coil is given by:

$$H = \frac{N\ I}{l} \qquad \text{Equation 2.8}$$

The direction of *H* will be along the axis of the cylinder. The unit of *H* is Ampere/meter or Oersted (Oe). When a material is subjected to the magnetic field, *H* then the magnetic field experienced by the material is known as magnetic flux density or magnetic induction, *B*. *B* is given by:

$$B = \mu\ H \qquad \text{Equation 2.9}$$

where μ is the permeability of the material. Permeability gives an indication of how a material responds to an external magnetic field. A high value of permeability is a representation of a material that can be magnetized with ease. In vacuum, the permeability is $4\pi \times 10^{-7}$ Vs/Am. The unit of B is Tesla or Vs/m^2. In vacuum, 1 Tesla corresponds to 10,000 Oe. Equation 2.2 suggests that "B field" is an effect of which "H field" is the cause. However, in the presence of magnetic particles (or magnetic materials), the formula changes to:

$$B = \mu\ H + \mu\ M \qquad \text{Equation 2.10}$$

where M the magnetization in the sample. Magnetization is caused by the currents of electron orbitals within magnetic materials and is defined as "the total vector sum for the magnetic moments of all the atoms in a given volume of the material". M is also given by χH where the susceptibility, χ is equal to $\mu - 1$. The magnetic units are all given in Table 2.1 in both SI and cgs units. (Note: emu is electromagnetic unit.)

Table 2.1 Magnetism units

Quantity	*Symbol*	*SI unit*	*cgs unit*	*Conversion*
Magnetic field	H	A/m	Oe	10^3 Oe = 4π A/m
Magnetic flux density	B	T	G	10^4 G = 1 T
Magnetization per unit volume	M	A/m	emu/cm^3	1 emu/cm^3 = 10^3 A/m
Magnetization per unit mass	σ	Am^2/kg	emu/g	1 emu/g = 1 Am^2/kg
Volume Susceptibility	χ	-	-	χ (SI) = 4π χ (cgs)

2.4.2 Diamagnetic materials

Diamagnetic materials show a very weak negative magnetism. These materials have atoms with completely filled electron shells and they are oriented such that the net magnetization of the atom is zero. But when an external magnetic field is applied, there is an effective current produced due to the orbital motion of electrons. This current generates an extremely small magnetic moment in a direction opposite to the applied magnetic field. Therefore the weak negative magnetism of diamagnetic materials arises from the small current that is generated. Thus diamagnetic materials have a negative susceptibility and a permeability of less than 1 (but almost close to 1). Because of their

extremely small susceptibility, diamagnetic materials can also be said to be non magnetic. Diamagnetic materials could include noble gases (He, Ne, Ar, Kr etc), or polyatomic gases (H_2, N_2, etc.) or ionic solids like NaCl or covalent materials like carbon, silicon etc. All these materials have completely filled electron shells either due to transfer or sharing of electrons leading to no net magnetization (in the absence of an external magnetic field).

2.4.3 Ferromagnetic materials

Ferromagnetic materials show strong magnetic properties. Their properties arise from the presence of unpaired electrons in the outer shell of each atom. These unpaired electrons lead to a net magnetic moment in each atom. In the unmagnetized state, the moments are so oriented that the net magnetic moment of the material is zero. But when a magnetic field is applied, these moments align in the direction of the applied magnetic field. The rate at which the moments align gives an indication of the magnetic susceptibility and permeability of the material. The magnetic properties of a material depend on the direction in which they are measured, and this phenomenon is known as magnetic anisotropy. In single crystal materials, there is an "easy direction" of magnetization wherein at very small fields, the material reaches saturation. Therefore the magnetic properties of single crystalline materials are highly dependent on the direction in which they are measured. In polycrystalline materials, the net magnetization depends on the orientation; if the orientation of the different crystallites is random, then the anisotropy will average out and there will be no magnetic anisotropy (which means that the magnetic

properties will be uniform in any measured direction and thus will not depend on the direction in which they are measured). But if the crystals have a preferred orientation, then the anisotropy depends on the weighted average of the individual crystals. Thus by changing the crystal orientation, the properties of a magnetic material can be varied. In ferromagnetic alloys consisting of 2 phases, if only one phase is ferromagnetic, then the magnetization saturation of the alloy varies linearly with the percentage of the added ferromagnetic element in the alloy.

2.4.4 Magnetization curves

Magnetization is the magnetic dipole moment per unit volume. Unpaired electrons present in an element give rise to a magnetic moment. Thus conceptually, one can consider that magnetization arises from the spin of an electron. The interaction between the spins is known as the exchange interaction. When a magnetic material is heated and then cooled below its Curie temperature, magnetic domains are formed (see Figure 2.5). In each individual domain, all the magnetic moments are aligned in the same direction and each domain is spontaneously magnetized to the saturation value, M_s. This saturation value is a property of the material and is dependent on the magnetic moment per atom of the material. In its demagnetized state; the directions of magnetization (or magnetic moments) of the various domains are oriented such that the net magnetization is zero. When a magnetic field is applied, the domains with magnetic moments in the same direction of applied magnetic field grow at the expense of domains with magnetic

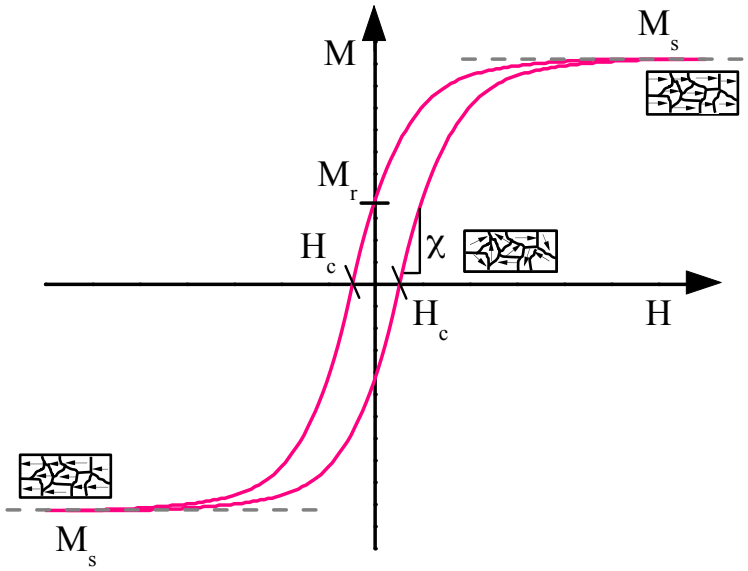

Figure 2.5 Typical magnetization curve showing saturation magnetization (M_s), remnant magnetization (M_r), coercivity (H_c) and susceptibility (χ) along with the orientation of magnetic moments in domains in the demagnetized state and at a completely magnetized state.

moments in other directions. During this process, there is only a change in the direction but not in the magnitude of the magnetization. Magnetization curves (hysteresis loops between magnetization (M) and applied magnetic field (H), see section 2.4.1 for information about M and H) give important information regarding magnetic materials. A typical magnetization curve is shown in Figure 2.5. When a large enough magnetic field is applied, the all the domains align in the direction of the applied magnetic field and the magnetization saturates and is denoted as M_s. At intermediate magnetic fields, only few domains are aligned in the direction of applied field. The level to which a material is magnetized depends on the applied magnetic field strength. At low magnetic fields, the

magnetization curve is linear and the slope of the line is called as magnetic susceptibility (χ). Magnetic permeability (μ) is defined as $1+\chi$. Susceptibility and permeability give an indication of how the material responds to an external magnetic field. A high susceptibility (or high permeability) indicates the ease with which domains can be aligned which is key for a ferromagnetic material. Table 2.2 lists susceptibility values of some common materials (Zhang et al. 2005). The first few materials listed in the table belong to the category of diamagnetic materials (discussed in Section 2.4.2) that have a negative but a very small value of susceptibility. Their value of susceptibility does not arise from domains but arises from the currents in the electron orbitals. From the table it can also be seen that the susceptibility values vary over a few orders of magnitudes. In addition it can be seen that the susceptibility of iron oxide can vary significantly based on the oxidation state of iron oxide.

Table 2.2 Volume susceptibilities of some common materials in SI units (Zhang et al. 2005)

Substance	*Formula*	χ ($\times 10^{-6}$)
Water	H_2O	- 9
D-Glucose	$C_6H_{12}O_6$	-11
Carbon (diamond)	C	- 250
Carbon (graphite)	C	- 420
Erbium oxide	Er_2O_3	21000
Hematite	α-Fe_2O_3	500 ~ 40,000
Maghemite	γ-Fe_2O_3	2,000,000 ~ 2,500,000
Magnetite	$2Fe_2O_3.FeO$	1,000,000 ~ 5,700,000

When the applied magnetic field is increased to a high value, the magnetization saturates at M_s. When the magnetic field is reversed and its magnitude is decreased, the magnetization may not follow the original path, as seen in Figure 2.5 and leads to a hysteresis loop. When the magnetic field is reversed, the domain alignment has to be reversed. But some materials show more resistance to reversal of domain walls compared to other materials. Due to this resistance, when the magnetic field is reduced to zero, there is some left over magnetization and this is called as remnant magnetization or M_r. M_r is obtained from Figure 2.5 by finding the intercept on the y-axis. It takes a magnetic field H_c known as coercivity to reduce the magnetization to zero, or in other terms to demagnetize the material. H_c is obtained from Figure 2.5 by finding the intercept on the x-axis. The area within the hysteresis loop represents a magnetic energy loss per unit volume. This energy is lost as heat in the magnetic specimen and could lead to an increase in the specimen temperature.

2.4.7 Soft vs. hard ferromagnetic magnetic materials

Ferromagnetic materials can be classified into soft and hard magnetic materials based on their magnetization curves. As shown in Figure 2.6 (a), soft magnetic materials have low coercivity (< 500 A/m), low remnant magnetization and a high permeability. Soft magnetic materials are easy to magnetize and demagnetize. The area under the hysteresis loop is smaller, which leads to low energy losses. These properties are feasible because

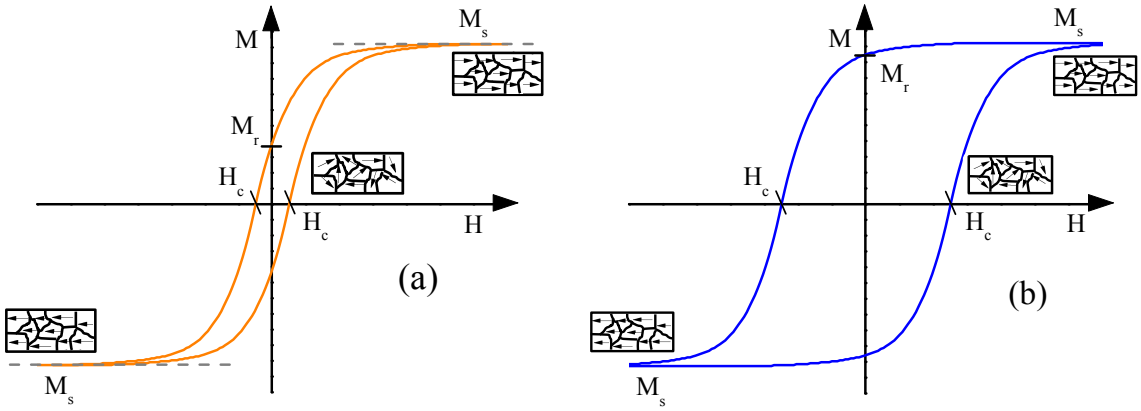

Figure 2.6 Typical magnetization curves of (a) soft magnetic materials (with low coercivity H_c and low remnant magnetization M_r) and (b) hard magnetic material (with high coerivity H_c and high remnant magnetization M_r) along with the orientation of magnetic moments in domains in the demagnetized state and at a completely magnetized state.

the domain walls of soft magnetic materials can migrate easily and align in the direction of the applied magnetic field. Examples of soft magnetic materials include iron, low carbon steel, nickel-iron alloys, soft ferrites (XO Fe_2O_3 where X stands for divalent elements such as Mn, Ni or Mg) and garnets. Because of their low coercivity, low remnant magnetization and a high permeability soft magnetic materials are useful in applications such as transformers, generators, motors and electromagnetic cores (Cullity and Graham 2009).

On the other hand, hard magnetic materials have higher coercivities and higher remnant magnetization values (see Figure 2.6 (b)) compared to those of soft magnetic materials. The high remnant magnetization makes hard-magnetic materials attractive for producing

permanent magnets, and the high coercivity (> 10,000 A/m) enables them to resist demagnetization from stray magnetic fields. As discussed in the introduction, permanent magnets have been in use for over 2500 years and the earliest known use of permanent magnets was for needles in a magnetic compass. Although an electric coil can be used to produce a magnetic field, permanent magnets provide a source of magnetic field without the constant use of electricity and also without the generation of any heat. In addition, permanent magnets can be manufactured in any desired shape and size but the maximum magnetic field strengths are limited to approximately 0.4 T whereas electric coils can be used to generate magnetic fields beyond 1 T. Examples of hard magnetic materials include quenched high carbon steels, hard ferrites (containing barium, strontium or cobalt) and rare earth materials. Apart from permanent magnets, hard magnetic materials are also used in devices such as loudspeakers, computer hard disks, floppy disks and audio or videotape.

2.4.8 Paramagnetic materials

Paramagnetic materials show weak magnetic properties. Unlike diamagnetic materials and similar to ferromagnetic materials, the magnetic properties of paramagnetic materials arise from the presence of unpaired electrons in the atoms. But the number of unpaired electrons and thus the magnetic moment per atom of a paramagnetic material is much smaller compared to those of ferromagnetic materials. For paramagnetic materials, the magnetization curves (*M vs. H)* are linear lines and they do not exhibit hysteresis. The

susceptibility values are in the order of 10^{-5} and thus the magnetic permeability is slightly greater than one. The magnetic response is extremely weak and can be detected only by sensitive instruments such as a vibrating sample magnetometer. Paramagnetic materials include elements that do not have completely filled electron shells such as Na, Cu, Pb or transition metals ions or rare earth ions.

2.4.9 Influence of temperature on ferromagnetic materials

The properties of a ferromagnetic material are affected by temperature. As temperature is increased, the disorder in domains increases thus reducing the magnetization of the material. When the disorder is at its highest, the material is no longer ferromagnetic, and the material is stated to have reached its Curie temperature (named after a French physicist Pierre Curie). Beyond the Curie temperature the materials exhibits paramagnetic behavior. Curie temperature of iron is of the order of 725 °C, which is much higher compared to the working temperatures of fresh concrete.

2.5 MAGNETORHEOLOGY

Magnetorheology is the study of flow of magnetorheological (MR) fluids. MR fluids undergo large, reversible and rapid changes in their rheological properties when subjected to an external magnetic field. Jacob Rabinow first discovered MR fluids in 1948 (Rabinow 1948). MR fluids typically consist of micron sized magnetic particles that are

suspended in a carrier fluid. As very few elements possessing ferromagnetic properties are available in abundance, the particles used are limited to iron, carbonyl iron, and iron/cobalt alloy based materials. In the presence of a magnetic field, the magnetic dipoles of these particles align along the magnetic field lines (Deshmukh 2007). The interaction between the dipoles causes the particles to form columnar structures, parallel to the applied field (see Figure 2.7). These chain-like structures restrict the motion of the fluid, thereby increasing the viscous characteristics of the suspension. The mechanical energy needed to yield these chain-like structures increases as the applied field increases resulting in a field dependent yield stress.

Although MR fluids are not common in civil engineering applications, they have been used in variety of areas, such as automotive clutches (Rabinow 1948), cancer treatment (Sheng, Flores, and Liu 1999), drilling fluids (Lee et al. 2009), body armor (Son and Fahrenthold 2012), gun recoil system (Li and Wang 2012), precision polishing (Kordonski and Jacobs 1996), prosthetic knee dampers (Carlson, Matthis, and Toscano 2001), seat dampers, fluid brakes, vibration damper (Carlson, Catanzarite, and St. Clair 1995), and seismic vibration control (Dyke et al. 1996). A detailed review of properties and applications of MR fluids has been published elsewhere (Klingenberg 2001; Bica 2006; de Vicente, Klingenberg, and Hidalgo-Alvarez 2011; Park, Fang, and Choi 2010; Kciuk and Turczyn 2006). It is envisioned that cement-based magnetorheological fluids can potentially be used in applications to act as a "set-on-demand" material, allowing the user greater control over the processing (e.g. mixing, casting, pumping, etc) of concrete.

Typically, in MR fluids, Newtonian carrier liquids such as mineral oil, synthetic oil, water or ethylene glycol are used to suspend the magnetic particles. The viscosities of these carrier liquids generally range from 0.2 to 0.3 Pa·s at 25°C (Kciuk and Turczyn 2006), which maximizes the transformation in the material from a liquid-like to a solid-like material when a magnetic field is applied. Nevertheless, the lack of yield stress and the low viscosity of the Newtonian carrier liquid, as well as the differences in density between the magnetic particles and the carrier fluid, typically make particle sedimentation a major concern in MR fluids. While reducing the size of the magnetic particles has been shown to reduce sedimentation, using smaller particles usually leads to a reduction in the yield stress of the fluid under an applied magnetic field (Lemaire et al. 1995; Genc and Phule 2002). Other approaches to increasing sedimentation resistance in MR fluids are to use additives, such as stabilizing additives, thixotropic additives (Takata et al. 2007) and nano-scale particles (Lim et al. 2004; Wereley et al. 2006; Klingenberg et al. 2010), or by choosing a carrier fluid with a yield stress (Rich, Doyle, and McKinley

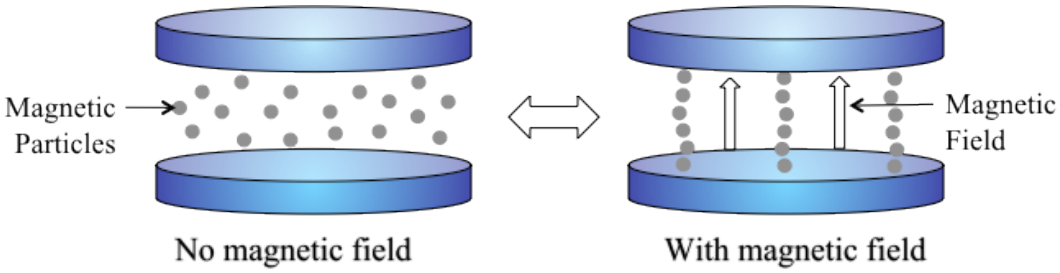

Figure 2.7 Schematic showing the response of a MR fluid to an external magnetic field.

2012). Cement paste, mortar and concrete have been characterized as being yield stress fluids (Domone 2003; Nguyen and Boger 1992; Schultz and Struble 1993), and they are typically modeled as a Bingham fluid (see Figure 2.1) (Tattersall and Banfill 1983). This inherent yield stress of cement-based suspensions can be beneficial in minimizing sedimentation of the magnetic particles.

CHAPTER 3: MATERIALS AND SAMPLE PREPARATION

This chapter gives a brief overview about the materials used to prepare the cement-based MR fluids and the sample preparation procedure. Cement-based MR fluids contain micrometer sized magnetic particles suspended in cement paste (mixture of cement and water). Section 3.1 provides general information about the materials used in this study. Section 3.2 presents the particle size distribution of all the material used, Section 3.3 presents details about the shape, Section 3.4 gives details about the composition and finally Section 3.5 gives information regarding the magnetic properties of the materials. Deionized water was used to prepare all the samples. A high-range water reducer was used for one sample to evaluate the effect of yield stress of the cement paste on the MR properties after application of magnetic field. The samples were prepared using a high shear mixer as described in Section 3.6.

3.1. GENERAL OVERVIEW OF MATERIALS EMPLOYED IN THIS RESEARCH

3.1.1 Cement

Cement is powder material comprised mainly of calcium silicates and calcium aluminates. Hydration of this material creates a binder that serves to lock aggregates together when it hardens. In the US, cement is one of the most predominantly used materials for construction (after timber) (Mindess, Young, and Darwin 2003). Approximately 3-4 billion tons of cement is produced annually around the whole world (Van Oss 2013). The first process in manufacturing cement is heating of limestone

powder and other additives such as clay or shale. Small quantities of iron oxide (~ 3%) are added to the raw materials where it acts as a fluxing agent and is added to aid in the pyroprocessing (burning) of the raw materials in the kiln. The raw materials are heated to about 1400 °C and then cooled. This process results in the formation of a clinker, which is ground to a fine powder along with gypsum (Taylor 1997). Gypsum is added to retard hydration of cement and to ensure sufficient workability time. The predominant phase in unhydrated cement is C_3S, where C stands for CaO and S stands for SiO_2. Other major phases are C_2S, C_3A and C_4AF (where A stands for Al_2O_3 and F stands for Fe_2O_3). When cement reacts with water over time these phases change to ettringite, porlandite (CH), calcium silicate hydrate (CSH) etcetera (Gartner et al. 2002). Ettringite is the first stable product that forms when the cement paste is still in its fresh state and the formation of ettringite plays a key role in the rheology of fresh cement pastes (Gartner et al. 2002).

Cement production is an energy intensive process, which leads to 5% of the global man-made CO_2 emissions (WBCSD 2012), including the emission of CO_2 from calcination of limestone ($CaCO_3 \rightarrow CaO + CO_2$). Thus it is important to improve the durability of concrete and increase the lifetime of concrete structures to reduce the amount of cement that has to be used for repairs. Cement-based MR fluids can potentially be used to improve the quality control of concreting operations at different stages of construction and thereby improve the durability of concrete.

3.1.2 Iron Oxide Powder

In 2005, 1550 million tons of iron ore was mined. From this, 1260 million tons of steel were produced. Thus, iron ore is mainly used for production of steel (Yellishetty, Ranjith, and Tharumarajah 2010). Along with a high dosage of one or more of the iron bearing minerals [such as magnetite (Fe_3O_4), hematite (α-Fe_2O_3), maghemite (γ-Fe_2O_3) etcetera], iron ores have other unwanted substances that are known as the gangue of the ore (Camp and Francis 1920). Gangue can contain silica, lime, magnesia, sodium oxide, potassium oxide, manganese, phosphorus, etc (Grant, Paul, and O'Neill 1991). Gangue has to be removed to increase the richness of iron oxide and this is done through washing, screening, heavy media separation, magnetic separation, froth floatation and/or electrostatic separation (Lepinski, Myers, and Geiger 2005). Of all the naturally occurring minerals, magnetite (Fe_3O_4) is the most magnetic (ferromagnetic) and thus low intensity magnetic separators can be used for their collection (Lepinski, Myers, and Geiger 2005). Hematite (α-Fe_2O_3) is only weakly magnetic but maghemite (γ-Fe_2O_3) exhibits strong magnetic behavior. Iron oxide powder is made up of highly pure iron oxide (in one of the above mentioned states) with less than 0.1% of impurities.

3.1.3 Iron Powder

Iron powder in its purest would contain 99.9% iron. According to the European Powder Metallurgy Association (EPMA 2013), there are several methods by which pure iron powder can be formed from iron bearing minerals. They include:

- crushing or grinding of solid metal
- precipitation from solution of a salt
- thermal decomposition of a chemical compound
- reduction of a compound, usually the oxide, in the solid state
- electrodeposition
- and the atomization of molten metal.

In this research study iron powders manufactured through thermal decomposition, electrolytic decomposition and hydrogen reduction are used, and the manufacturing processes are briefly described in sections 3.1.3.1, 3.1.3.2, and 3.1.3.3, respectively. Iron powders are used in several materials such as inductive electronic components, metal powder injection molding (Piotter et al. 2001), diamond tools (Hsieh and Lin 2001), nutritional supplements (Lynch 2005) etcetera and are used in applications such as microwave absorption (Zhang et al. 2006) and radar absorption (Feng et al. 2006). Iron powders have been the focus of many studies on traditional MR fluids (Deshmukh 2007; Sheng, Flores, and Liu 1999; Yang and Jennings 1995).

3.1.3.1 Carbonyl iron powder

Carbonyl iron powder (CIP) is one of the most commonly used magnetic particles for MR applications because of its high saturation magnetization. The process for production of CIP was invented by BASF in 1925 (BASF 2012). CIP is synthesized through thermal decomposition of purified liquid iron pentacarbonyl, $Fe(CO)_5$ (McCurrie 1994). CO_2 is produced during the thermal decomposition of $Fe(CO)_5$, but this CO_2 is captured and

reused for producing liquid $Fe(CO)_5$. In the liquid state, it is easier to remove impurities that are present in $Fe(CO)_5$, thus high purity CIP can be manufactured. According to the manufacturer (BASF 2012), a spherical shell structure is formed during the decomposition process due to deposition of layers of iron on a nucleus of iron. The conditions of the decomposition process determine the particle size distribution of the CIP particles. These CIP particles are further reduced through hydrogen annealing to increase the purity of iron. The hydrogen annealing converts the shell like structure to a polycrystalline structure. CIP might contain trace amounts of carbon, nitrogen and oxygen.

3.1.3.2 Electrolytic iron powder

The process of manufacturing iron powder through electrolytic decomposition has existed since the beginning of 1900's (Kern 1908). Electrolytic decomposition is the deposition of iron at the cathode from an aqueous solution of a suitable iron electrolyte by the action of an electric current. The deposited iron is chipped from the cathode and is then ground into a fine powder (Kern 1908). One of the most commonly used electrolytes is ferrous sulfate, which is a naturally occurring salt that dissolves easily in water. Ferrous sulfate can also be obtained by mixing iron ore with sulfuric acid. The composition of the electrolyte is optimized with additives to improve the quality and quantity of deposition and to ensure desirable grinding properties of the deposited iron (Klar and Samal). According to the European Powder Metallurgy Association, electrolytic decomposition

was at one point used in large scale to produce iron powder, but is now being replaced by cheaper processes (EPMA 2013). But the Ultra-Low Carbon Dioxide Steelmaking (ULCOS) consortium is considering electrolysis (with molten metal electrolyte) as a good option to reduce greenhouse gases produced during production of iron/steel (ULCOS 2013).

3.1.3.3 Hydrogen reduced iron powder

Iron ore can be reduced from its solid state by using reducing agents such as carbon, carbon monoxide or hydrogen (Luidold and Antrekowitsch 2007). Similar to the smelting process in blast furnaces, iron ore is crushed and mixed with the reducing agent and heated in a furnace where reduction reactions occur and a cake of sponge iron is formed. This cake is further processed through crushing and sieving to produce iron powder (EPMA 2013). Depending on the type of iron ore (or type of oxide) used, the temperature to which the ore has to be heated also changes (Jozwiak et al. 2007). Although reduction through carbon and carbon monoxide are very popular methods, they result in production of CO_2 gas thus contributing to the annual greenhouse production. Reduction through hydrogen produces steam or H_2O (Jozwiak et al. 2007) which is better than producing CO_2 gas. The steam can in turn be used to increase the temperature of iron ore. By using highly pure ore and pure H_2 gas, powder with high purity can be manufactured (Luidold and Antrekowitsch 2007). Pure H_2 gas can be produced through electrolysis of water. Iron powder produced through reduction process uses less total energy (20 MBtu/ton)

compared to the electrolytic decomposition process (36.8 MBtu/ton) described above (EPRI 2000).

3.1.4 High-range Water Reducer

High-range water reducers (***HRWR***) or superplasticizers are commonly used in cement-based materials to improve the consistency of concrete (so that concrete can be placed in heavily reinforced sections), to achieve higher strengths and to produce self consolidating concrete without the addition of extra mixing water (Mehta and Monteiro 2006). There are several types of water reducing admixtures available in the market, but polycarboxylate-based HRWR, are effective for a longer duration and help with slump retention. One side of the polycarboxylate chain is absorbed on to the surface of a cement grain and the other side causes steric repulsion thus dispersing the cement grains (Mehta and Monteiro 2006).

3.2 SPECIFIC DETAILS ABOUT MATERIALS USED IN THIS STUDY

3.2.1 Sources for materials and costs

In addition to deionized water, the following materials were used in this research: cement, iron oxide powder, carbonyl iron powder, electrolytic iron powder, hydrogen reduced iron powder and high range water reducer.

An American Petroleum Institute (API) class A oil well cement (API-10A 2011) (comparable to a ASTM Type I Portland cement (ASTM-C150 2012)) was obtained from the Texas-Lehigh Cement Company in Buda, TX. From the Texas Lehigh plant in Buda, class A cement can be purchased in bulk at $100/ton (≈ 5 cents /lb or 11 cents /kg).

Black iron oxide (magnetite) powder (with 99.9% purity) was obtained from Atlantic Equipment Engineers (AEE); a division of Micron Metals, Inc. and from here on is referred to as ***F_3O_4***. From AEE, *Fe_3O_4* can be purchased in bulk at $9.60 /lb (≈ $21.20 /kg).

Two grades of *CIP (CM, SM)* containing minimum 99.5% and 99% of iron respectively were obtained from BASF. From herein *CIP (CM* grade) will be referred to as ***CIP*** and *CIP (SM* grade) will be referred to as ***CIP(sm)***. When purchased in bulk, *CIP* costs about $8.5 /lb (or $18.5 /kg). Per pound, CIP is much more expensive than cement and the dosage of *CIP* is kept to a minimum to keep the cost of cement-based MR fluids to a minimum. The cost of *CIP* is similar to that of *Fe_3O_4*.

Electrolytic iron powder (with 99.9% purity) was obtained from Atlantic Equipment Engineers (AEE); a division of Micron Metals, Inc. and from here on is referred to as ***Fe(E)***. From AEE, *Fe(E)* can be purchased in bulk at $27.10 /lb (≈ $60 /kg). This is almost three times more expensive than *CIP* that is sold by BASF. Hydrogen reduced iron powder (with 99.8% purity) was also obtained from AEE and from here on is

referred to as ***Fe(H)***. From AEE, *Fe(H)* can be purchased in bulk at $8.50 /lb (≈ $18.70 /kg). This is similar to the cost of *CIP* obtained from BASF and is three times cheaper than *Fe(E)*.

Glenium 3400 NV (supplied by BASF) polycarboxylate-based HRWR was used in one of the samples to evaluate the effect of yield stress of the cement paste on the MR properties after application of magnetic field. The smallest recommended dosage (130 ml/100 kg of cement) of HRWR was used.

3.2.2 Particle Size Distribution

A Mastersizer 2000 particle size analyzer with a Hydro MU 2000 (Malvern, Worcestershire, United Kingdom) wet dispersion unit was used to measure the particle size distributions of the powder materials (i.e., cement and iron powders). The data are based on the average of five measurements for each material. The specific gravity, refractive index and absorption values used for each material can be found in Table 3.1. Specific gravity values were obtained from the manufacturers. The refractive index values were obtained from current literature (Chiara F. Ferraris et al. 2006; Red 2009). The absorption value was chosen such that the residual weighted particle size distribution calculated by the Mastersizer software was less than 1, indicating the proper choice of the value.

Table 3.1 Material properties

Raw material	*Specific Gravity*	*Refractive Index n (Real)*	*Absorption k (Imaginary)*
Cement	3.14	1.7	1.0
CIP, CIP(sm)	7.8	1.51	0.1
Fe(E)	7.8	2.86	1.0
Fe(H)	7.8	2.86	1.0
Fe_3O_4	5.1	2.42	1.0

In order to prevent hydration, cement particles were dispersed in isopropyl alcohol (IPA). A refractive index of 1.39 was assumed for IPA (Ferraris et al. 2006). The CIP, iron and iron oxide magnetic particles were dispersed in tap water; and a refractive index of 1.33 was used for water (Red 2009). Prior to measuring the particle size distribution, the particles were recirculated at a pump speed of 2000 rpm and sonicated with an ultrasonic probe (at 10 μm of tip displacement) for 30 seconds. During testing the sample was recirculated in the particle size analyzer at a pump speed of 2000 rpm without any sonication.

Figure 3.1 shows the particle size distribution of all the materials. It can be seen that all the materials are not of uniform size (meaning they are polysized) and have a wide distribution. From the distribution, d_{10}, d_{50} and d_{90} can be calculated. d_{10} is the size at which 10% of the total powder volume consists of particles with effective diameter less than that diameter; similarly d_{50} and d_{90} is the size at which 50% and 90%, respectively,

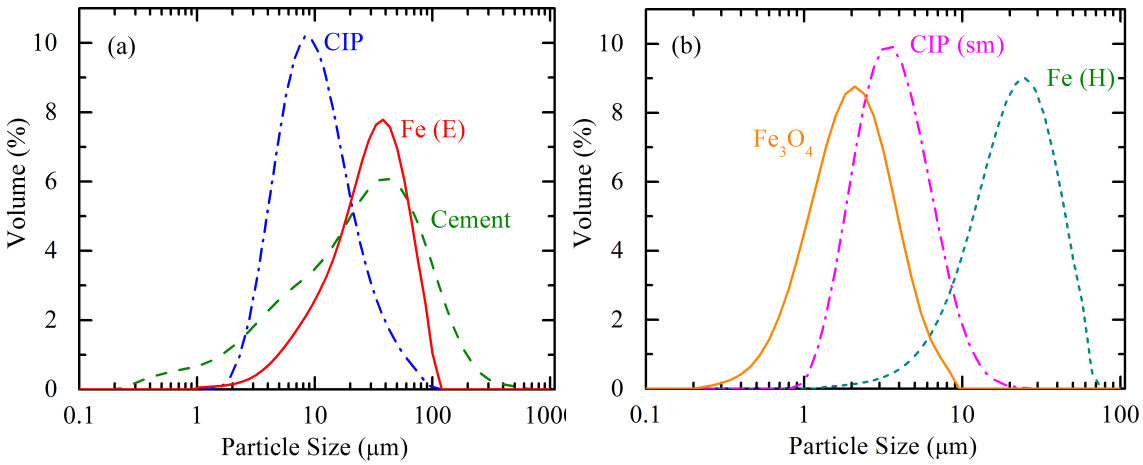

Figure 3.1 Volume weighted particle size distribution of all the particles. For the x-axis, (a) 50 size intervals were generated logarithmically between 0.1 and 1000 μm and (b) 50 size intervals were generated logarithmically between 0.1 and 100 μm. y-axis shows the volume of particles between these sizes.

of the total powder volume consists of particles with effective diameter less than that diameter. In Table 3.2, the magnetic particles are sorted based on the their particle sizes, from smallest to largest. *Fe_3O_4* and *CIP(sm)* have the smallest particle sizes and *Fe(E)* has the largest particle size among the magnetic particles. Cement has the largest distribution varying from 0.25 μm to 500 μm. All the magnetic particles fall within the particle size distribution of cement.

Table 3.2 Particle size distribution of cement and magnetic particles

Raw material	d_{10} (μm)	d_{50} (μm)	d_{90} (μm)
Cement	2.8	23.3	89.6
Fe_3O_4	0.8	1.9	4.3
CIP(sm)	1.7	3.3	6.8
CIP	3.8	8.7	24.5
Fe(H)	8.1	20.1	39.9
Fe(E)	8.1	27.9	61.0

3.2.3 Particle Shape

JSM 6490-LV Scanning Electron Microscope (Jeol Ltd., USA) was used to observe the shape of the particles. The accelerating voltage was kept at 20 kV while the working distance was held constant at 9-11 mm at various magnifications. The images were observed in secondary electron imaging (SEI) mode, which produces high-resolution images. Double-sided carbon tape was used; wherein one side was stuck to a standard stub mount and the other side was dipped into the powder that was being tested. Figure 3.2 shows the micrographs of all the materials.

Cement particles are angular and have irregular shapes (owing to the fact that cement is ground from clinker that varies in size from 1 mm to 25 mm). Fe_3O_4 has the smallest particles compared to the rest of the materials and are highly agglomerated. For Fe_3O_4, it was difficult to focus the image at a larger magnification and thus the shape of the particles is not completely perceptible.

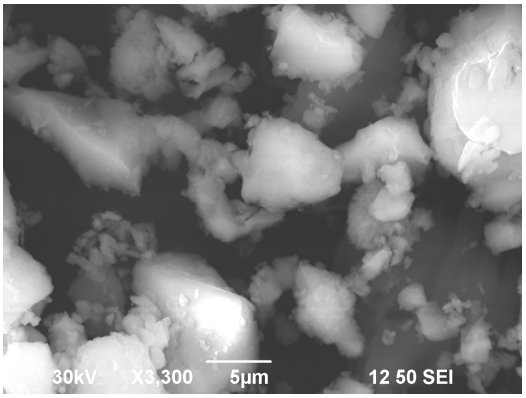

(a) Cement

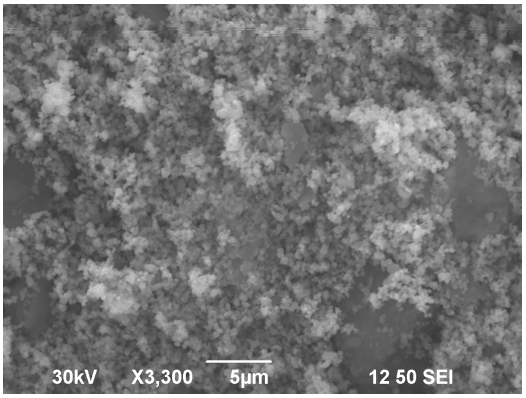

(b) Fe_3O_4

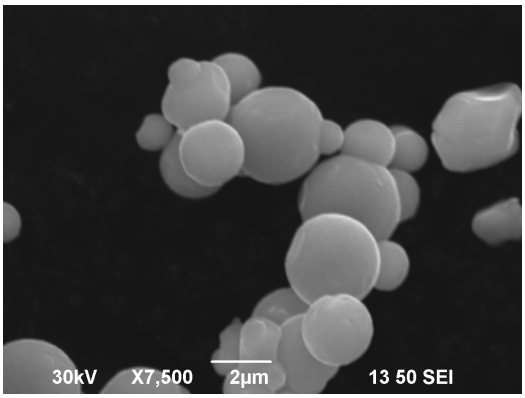

(c) CIP

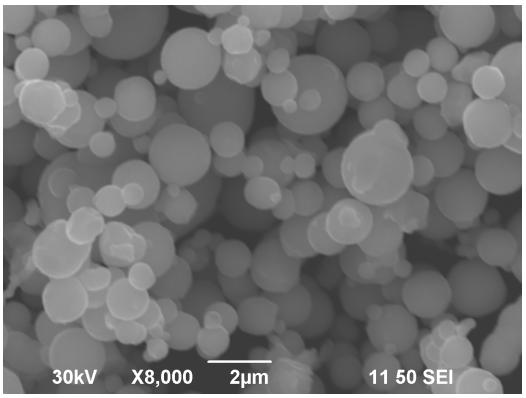

(d) CIP (sm)

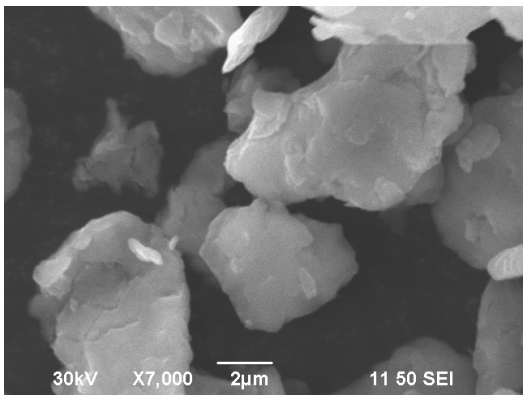

(e) Fe (E)

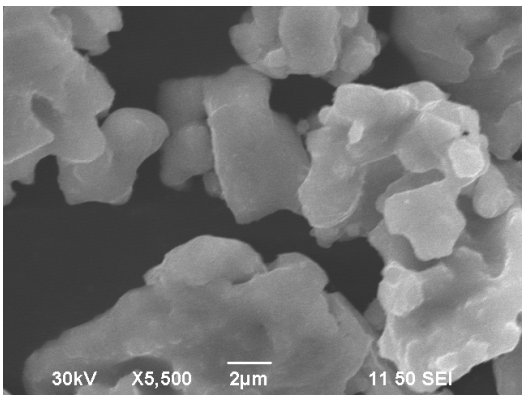

(f) Fe (H)

Figure 3.2 Particle shape of all materials obtained through a scanning electron microscope.

It can be seen that both grades of *CIP* are mostly spherical and are poly disperse (similar to the observation from Figure 3.1). The texture of the *CIP* particles appears to be smooth. Section 3.1.3.1 discusses the manufacturing process that leads to the spherical shape. It can be seen that surfaces of some larger particles are flat and not completely round which can be attributed to the finishing processes (milling) of *CIP* or it could be an artifact of the imaging process. It can also be observed that the particles do not appear to be agglomerated. Spherical particles lead to better particle packing and improve the workability of concrete based on the spherical shape of fly ash particles (Mehta and Monteiro 2006).

Both *Fe(E)* and *Fe(H)* particles are irregular in shape. Unlike *CIP, Fe(E)* does not have a smooth texture and the surface appears to be in layers. *Fe(E)* is manufactured through crushing of flaky deposits of iron, which might lead to the appearance. The *Fe(H)* particle located at the bottom of the picture on the right hand side of Figure 3.1 (f), appears to have a hollow interior which matches with the information available in literature. Due to this reason iron produced through the reduction process is also known as sponge iron.

3.2.4 Chemical Composition of Cement

The composition of the class A cement was obtained from the manufacturer. The predominant phase in raw cement is C_3S, where *C* stands for *CaO* and *S* stands for SiO_2. Other major phases are C_2S, C_3A *and* C_4AF (where *A* stands for Al_2O_3 and *F* stands for

Fe_2O_3). The Blaine fineness of the cement is 307 m^2/kg and details regarding the chemical composition of the cement can be found in Table 3.3. It can be noted that the cement has 2.7% iron oxide and through further testing it has to be determined in the iron oxide is ferromagnetic or paramagnetic in nature (see Section 3.2.6).

Table 3.3 Composition of class A oil well cement (Jarl 2012)

Chemical Composition	*Percentage by Mass*
Calcium oxide (CaO)	64.8
Silica dioxide (SiO_2)	20.2
Aluminum oxide (Al_2O_3)	5.3
Ferric oxide (Fe_2O_3)	2.7
Magnesium oxide (MgO)	1.1
Sulfur trioxide (SO_3)	3.3
Na_2O_{eq}	0.75
Loss on Ignition (LOI)	2.6
Insoluble Residue (IR)	0.6
Tricalcium silicate (C_3S)	58
Dicalcium silicate (C_2S)	13
Tricalcium aluminate (C_3A)	9

3.2.5 Phase Composition of Magnetic particles

The phase composition of the magnetic particles were identified through powder X-ray diffraction studies. Powder diffraction can be used mainly to study the crystalline phases, which produce a distinctive diffraction pattern as shown in Figure 3.3 (a). The presence of amorphous phases can be detected by the occurrence of a wide hump in the diffraction pattern as shown in Figure 3.3 (b). Identification is performed by comparison of the

diffraction pattern to a known standard or to a database. Qualitative information for phases present in the materials were obtained using the Hanawalt manual and the Jade program (MDI) (JCPDS 1989). Approximately 2 g of each sample was compacted into a plastic sample holder using a glass disc while ensuring a flat surface. Following this, the samples were measured in a powder X-ray diffractometer (Seimens D-500 Cu Kα, λ=1.5046 Å). The X-ray source was operated at 40 kV and 30 mA. A step size of 0.02° 2θ with a dwell time of 3 s was used, and the scan range was varied based on the material measured.

Figure 3.4 (a) shows the x-ray diffraction pattern of Fe_3O_4 from 20° to 70° 2-theta. The peaks (occurring at 35.5°, 62.5°, 57°, 30.1°, 43.1° and 53.4° 2-theta arranged here in the order of peak intensity) of Fe_3O_4 match with those of magnetite. The numbers shown in parenthesis next to each peak refers to the lattice plane (identified by Miller indices) indicating a crystallographic direction. It gives information regarding the atomic arrangement within the crystal.

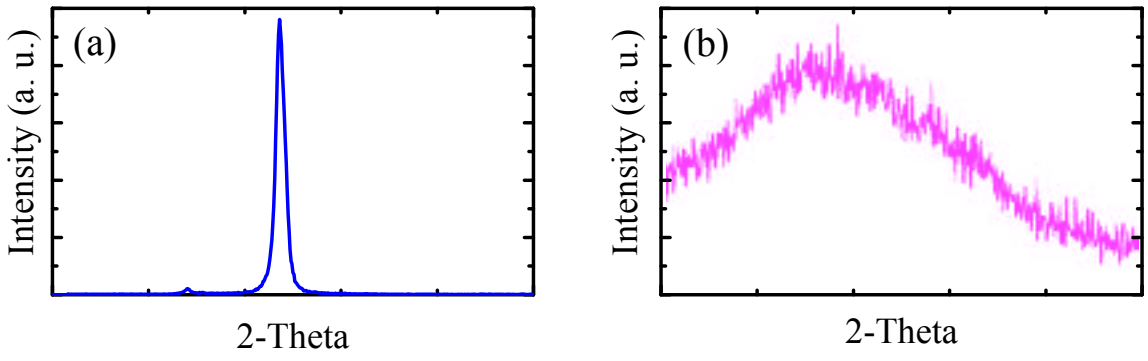

Figure 3.3 Schematic showing a typical diffraction pattern of (a) crystalline material and (b) amorphous material.

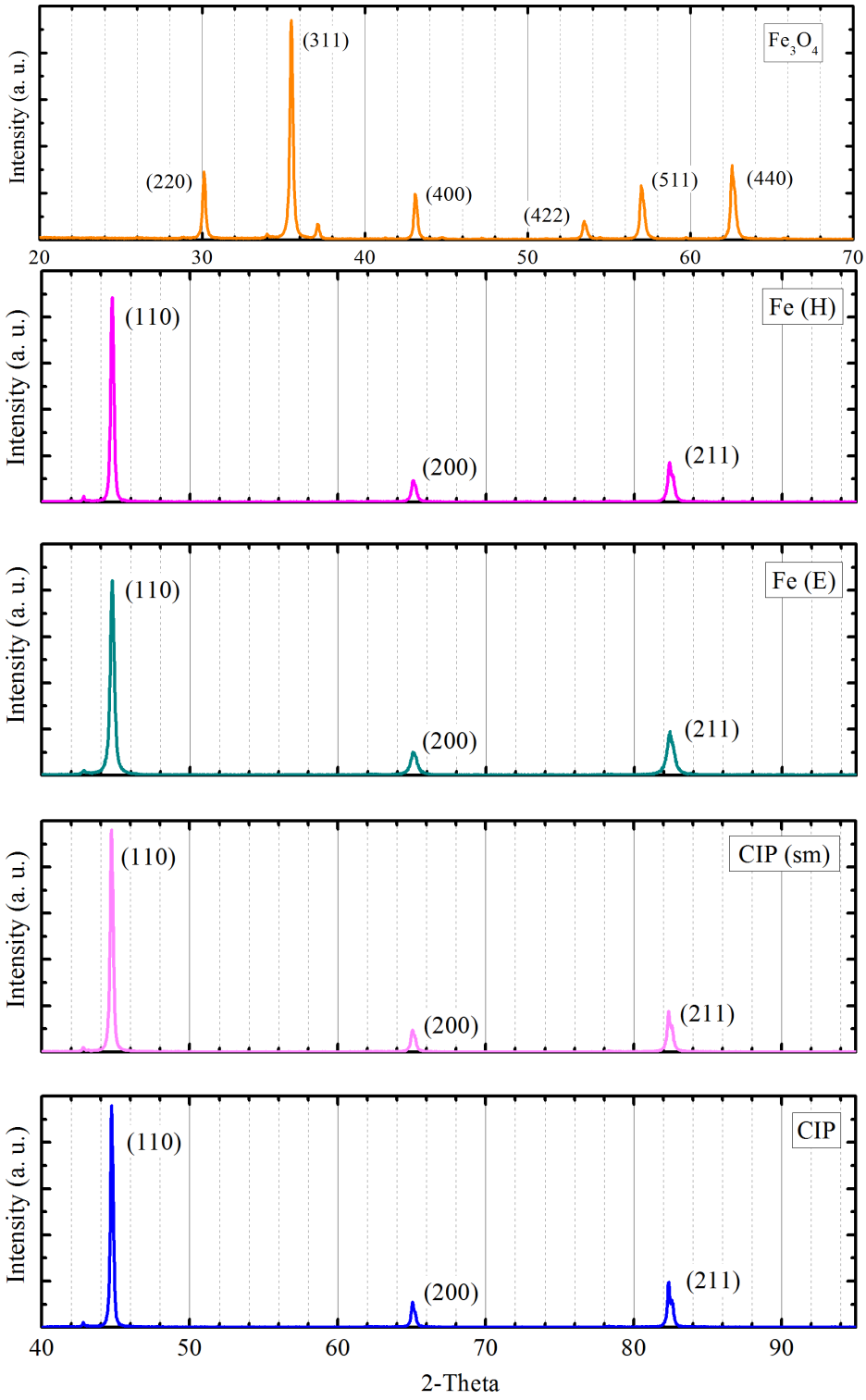

Figure 3.4 X-ray diffraction patterns of all the magnetic particles

Figure 3.4 (b-e) shows the diffraction pattern of the iron powders for a scan rage of 40° – 90° 2-theta. The iron particles (*CIP, CIP(sm), Fe(E) and Fe(H)),* have a diffraction pattern similar to that of polycrystalline α-iron (with BCC structure). For all the iron powders the peaks occur at 44.7°, 65.0° and 82.3° 2-theta. Even though all the particles were manufactured through different processes, the crystallographic structure of the end product is the same. As all the peaks are attributed for and no other elements are detected based on the analysis of the X-ray diffraction patterns and it can be concluded that all materials are of high purity.

3.2.6 Magnetic Properties of Particles

An EV7 vibrating sample magnetometer (MicroSense, USA) was used to obtain the magnetization curves of unhydrated cement and the magnetic particles at 24 $\pm$ 2 °C. A vibrating sample magnetometer (VSM) precisely measures the magnetic moment of the sample by vibrating it perpendicular to a uniform magnetic field in between a few detection coils (Foner 1959). The plot of the net magnetic moment of the material as a function of the applied magnetic field produces the magnetization curve (see Figure 2.5). Details about the interpretation of the magnetization curves can be found in Chapter 2. Approximately 0.15 g of each iron powder sample (0.06 g for cement and 0.07 g for Fe_3O_4) was carefully placed in a 6 mm diameter cup made of ULTEM™ resin and sealed with a lid. The cup was then mounted on a glass rod and then placed in the VSM. The applied magnetic field was between $\pm$15 kOe (equivalent to $\pm$1.5 T in vacuum). Volume

susceptibility (χ) was measured as the slope of the magnetization curve between $\pm$3 Oe (equivalent to $\pm$0.3 mT in vacuum).

The magnetization curves of all the materials are shown in Figure 3.5. Table 3.4 lists the important magnetic properties obtained from these magnetization curves. In the table, materials are listed in order of decreasing saturation magnetization (M_s). When the magnetic field is increased from zero, magnetization of ferromagnetic materials saturates at a certain applied magnetic field. This saturation phenomenon is not observed in paramagnetic materials and diamagnetic materials. In addition diamagnetic materials have a negative susceptibility value.

Table 3.4 Magnetic properties of materials obtained from magnetization curves shown in Figure 3.5

Raw material	M_s (emu/cm^3)	M_r (emu/cm^3)	H_c (Oe)	χ (SI)
CIP	1710.0	16	23	7.9
CIP(sm)	1680.0	15	26	5.2
Fe(E)	1650.0	26	27	6.7
Fe(H)	1530.0	12	17	6.7
Fe_3O_4	430.0	65	136	3.0
Cement	0.6	1.8×10^{-3}	11	1.6×10^{-3}

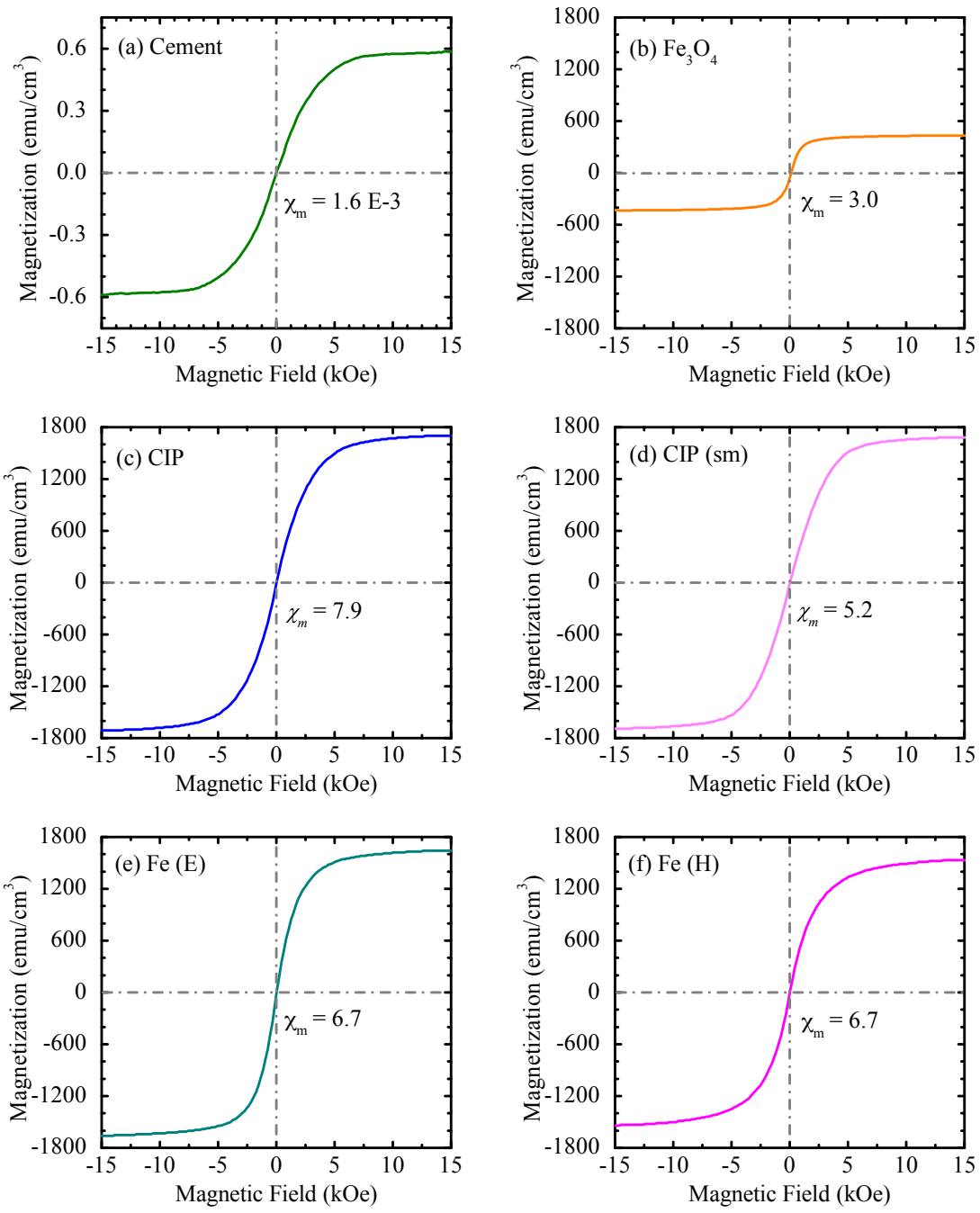

Figure 3.5 Magnetization curves of all the powders. The magnetic volume susceptibility (χ) values are also shown for each material. See text for more details.

From the shape of the curve in Figure 3.5 (a) and from the positive susceptibility value it can be concluded that cement shows ferromagnetic behavior but is only weakly magnetic because of the really small magnetic values shown in Table 3.4. From Table 3.3, it can be seen that cement has 2.7% of iron oxide and this small dosage of iron is contributing to its weak magnetic behavior. Materials exhibiting weak ferromagnetism (magnetization values in the range of 10 emu/g have been reported for $MgFe_2O_4$ (Chen and Zhang 1998)) are sometimes referred to as superparamagnetic materials; superparamagnetic materials reported in literature have a particle size in the nano-meter range (Cullity and Graham 2009). But cement particles are much larger and the particle sizes are in the micrometer range (Figure 3.1) and hence will be characterized as being weakly ferromagnetic.

Of all the particles listed in Table 3.4, *CIP* has the highest magnetization saturation and the highest volume susceptibility. Susceptibility gives the rate of change of the magnetization in the sample with respect to an applied external magnetic field. When the particle size of *CIP* (d_{50} of 8.7 μm) is reduced to *CIP(sm)* (d_{50} of 3.3 μm), there was no significant change in the value of M_s, but the volume susceptibility value was comparatively lower. In literature, it has been shown that a direct correlation exists between particle size distribution and volume susceptibility (Gorodkin, James, and Kordonski 2009). By measuring the susceptibility values of several *CIP* particles, Gorodkin et al., found the following correlation between the value of susceptibility (SI) and the d_{50} (μm) obtained from the particle size distribution:

$$\chi = 0.668 * d_{50} + 0.961 \qquad \text{Equation 6.1.}$$

Using the above empirical equation, for the *CIP* particles, the predicted value of susceptibility is 6.8 (SI), which is 16% smaller than the measured value. For the *CIP(sm)* particles, the predicted value of 3.2 (SI) is 38% smaller than the measured value. Although the empirical equation did not accurately predict the susceptibility values of *CIP* and that of *CIP(sm)* it did show a similar trend wherein a sample with larger value of d_{50} has a larger value of volume susceptibility.

Fe(E) and *Fe(H)* both have the same volume susceptibility values, which are smaller than that of *CIP*. Thus although they all have the same chemical composition, domain structure is probably dependent on the mechanism in which the particles are manufactured. Of all the iron particles, *Fe(H)* has the smallest volume susceptibility. Fe_3O_4 has smaller magnetic properties than any of the iron particles. This is probably because only a part of Fe_3O_4 is composed of iron. The saturation magnetization of Fe_3O_4 is almost 1/3rd that of the iron particles and the value of the volume susceptibility is approximately half that of the iron particles.

The remnant magnetization (intercept at y-axis) of both *CIP* and *CIP(sm)* are very small and the values are less than 1% of the saturation magnetization value. Thus they can be categorized as soft ferromagnetic materials. This also means that when the magnetic field is reduced to zero, the domains of the particles are no longer aligned with respect to each

other. *Fe(H)* and *Fe(E)* also have small M_r and H_c values and are both soft ferromagnetic materials. M_r of Fe_3O_4 is comparatively higher at 15% of M_s, but it demagnetizes very easily and its H_c value is only 136 kOe.

3.3. MIX PROPORTIONS

The water to cement ratio of all the samples was 0.4 (by mass). The magnetic particles were added on an addition basis, based on weight of cement. For the iron powders, 10% by weight addition corresponds to a volume addition of 4%. The cement-based MR fluid samples are named based on the volume percentage and the name of the magnetic particles. For example, *4CIP* corresponds to a sample, which contains 4% (by volume) addition of *CIP* particles (with respect to the volume of cement). The mix proportions are shown in Table 3.5.

Table 3.5 Mix proportions

Sample	*DI Water (g)*	*Cement (g)*	*Magnetic Particles (g)*	*HRWR (g)*	*Magnetic vol. fraction*	*Solids vol. fraction*
Control	200	500	-	-	-	0.443
2CIP	200	500	25.0	-	0.8%	0.447
4CIP	200	500	50.0	-	1.8%	0.452
4CIP_HRWR	200	500	50.0	0.715	1.8%	0.452
4CIP(sm)	200	500	50.0	-	1.8%	0.452
4Fe(E)	200	500	50.0	-	1.8%	0.452
4Fe(H)	200	500	50.0	-	1.8%	0.452
4Fe_3O_4	200	500	32.4	-	1.8%	0.452

In a traditional MR fluid, the dosage of magnetic particles generally varies from 40% to 50% of the fluid volume (Jolly, Bender, and Carlson 1999). The uniqueness of this work is the use of dilute dosages of magnetic particles (less than 5% of paste volume) to investigate the changes in rheological properties with application of magnetic field. The dosages were kept to a minimum to maximize cementitious content and to minimize cost.

The samples were prepared using a high shear mixer (Chandler Engineering, USA) in a 1-liter stainless steel container with a cooling jacket (Waring Laboratory, USA). It is important to use a high shear mixer to obtain a uniform mix, and replicate the shearing conditions of cement paste within concrete. Researchers have found that when mixing concrete in a transit truck the shear rate experienced by cement paste (in the presence of aggregates) goes up to 2000 s^{-1} (Helmuth et al. 1995). Mixing paste in a Hobart mixer results in a shear rate of approximately 70 s^{-1}; whereas the shear rate of paste prepared using a high shear mixer, such as a Chandler mixer used here, can approach 2200 s^{-1} (Helmuth et al. 1995). To obtain a paste with rheological properties similar to those in concrete mixtures, it is important to use a high shear mixer and mix at the specified speeds. A water bath was attached to the container to help minimize the frictional heating of the cement paste due to the high rotational speed of the mixer.

The dry ingredients (cement and magnetic particles) were hand mixed with a spatula for 30 seconds prior to adding them to the container. The samples were then mixed according

to ASTM C1738-11a, Standard Practice for High-Shear Mixing of Hydraulic Cement Pastes (ASTM-C1738 2011), and the procedure is summarized in this manuscript. Mixing water was placed in the container, and with the help of a water bath attached to the container, the mixing water was cooled to 17.2 $\pm$ 1 °C (63 $\pm$ 1 °F). Then, the dry materials were added within 60 seconds at 4000 $\pm$ 200 rpm using a funnel and then mixed at 12000 $\pm$ 200 rpm for 30 seconds. The sides of the container were scraped and the paste was rested for 150 seconds followed by mixing at 12000 $\pm$ 200 rpm for 30 seconds. At the end of mixing, the temperature of the paste was measured using a digital thermometer and all the pastes had a temperature within 21 – 22 °C (71 – 72 °F). For the samples containing HRWR, the HRWR was added in the beginning to the mixing water. Immediately after mixing, the samples were used for the appropriate test and a mini slump flow test was performed. Table 3.6 shows the slump flow diameters for all the samples.

The schematic of the mini-slump cone is shown in Figure 3.6. The slump test was performed on a clear sheet glass placed on a countertop. The paste was poured into the slump cone from a beaker and was rodded 15 times using a 14 mm wide, flat stainless steel spoonula. The top surface was struck and the slump cone was lifted vertically. The slump flow diameter of the samples was measured using a Vernier caliper to avoid parallax error. Table 3.6 shows the slump flow diameters for all the samples. The addition of 4% *CIP* magnetic particles does not considerably affect the slump flow diameter of the *Control* sample. Addition of *HRWR* to *4CIP* increased the slump flow

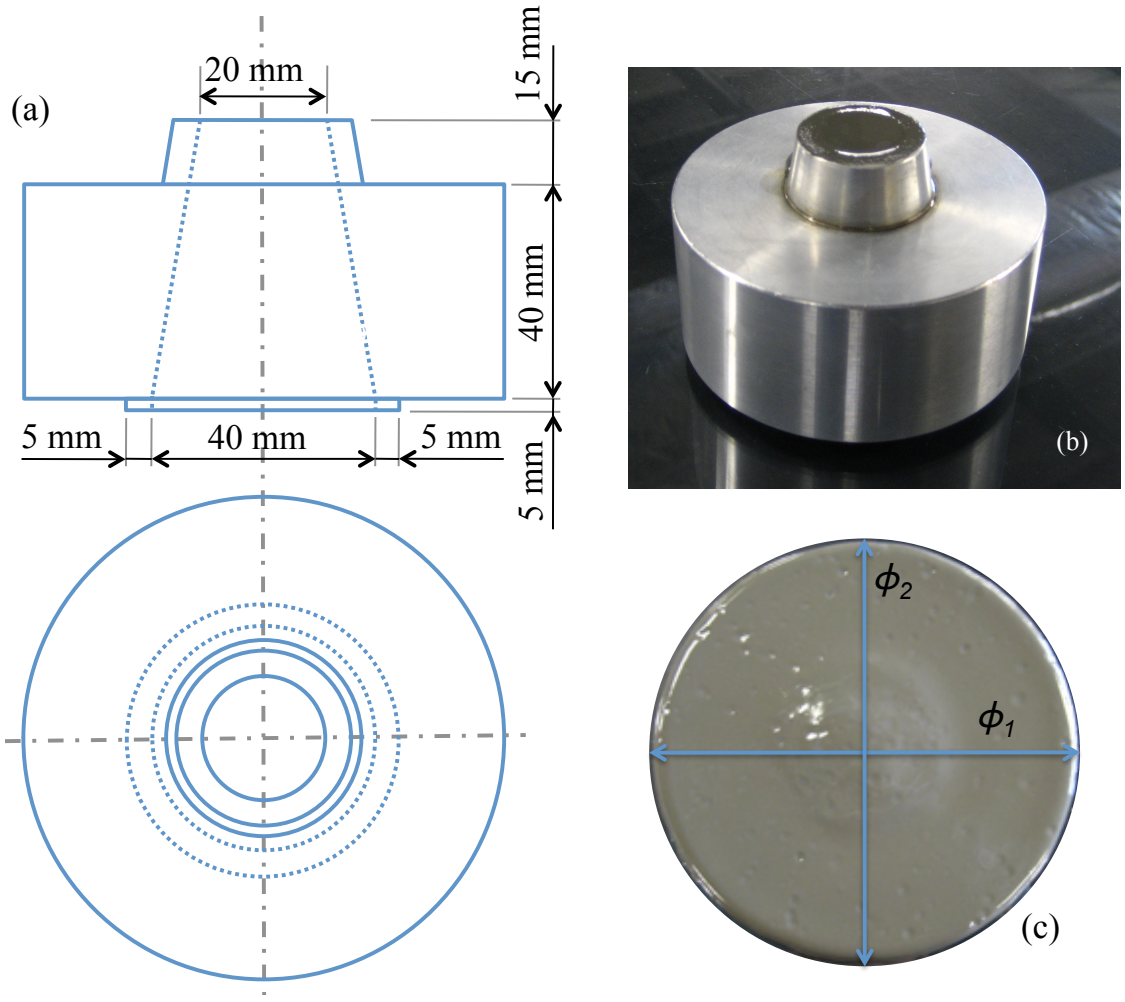

Figure 3.6 (a) Schematic of mini slump cone (not to scale) (b) image of the slump cone (c) slump flow of a sample where slump diameter = $(\phi_1 + \phi_2)/2$

diameter by 9%. *4Fe_3O_4* had the smallest slump flow diameter among all the samples, which is because of the smaller particle size distribution of *Fe_3O_4*. For the same volume, *Fe_3O_4* would have more number of particles compared to *CIP,* which has larger sized particles.

Table 3.6 Slump flow diameters

Sample	*Slump flow dia. (in.)*
Control	5.6 ± 0.1
2CIP	5.5 ± 0.1
4CIP	5.4 ± 0.1
4CIP_HRWR	5.9 ± 0.1
4CIP(sm)	5.5 ± 0.1
4Fe(E)	5.0 ± 0.1
4Fe(H)	5.1 ± 0.3
4Fe_3O_4	4.3 ± 0.2

CHAPTER 4: RHEOLOGICAL PROPERTIES OF CEMENT-BASED MAGNETORHEOLOGICAL FLUIDS

In traditional MR fluids the magnetic particles are suspended in a Newtonian fluid. But in cement-based MR fluids, magnetic particles are suspended in the cement paste. So it is imperative to first understand the rheological properties of the cement paste. The rheological tests used to characterize the samples are listed at the beginning of the chapter. *CIP* (with d_{50} of 8.7 μm) and *CIP(sm)* (with d_{50} of 3.3 μm) magnetic particles were used in this part of the study. The chapter investigates the changes in rheological properties of cement-based MR fluid (with and without external magnetic field) with changes in magnetic particle dosage, magnetic particle size and effect of changing the viscosity of the suspending medium (cement paste). All the above tests were conducted at a constant magnetic field. The final section of this chapter looks at the effect of changing the applied magnetic field strength at 30 minutes and 60 minutes after the application of magnetic field. It is being hypothesized that an MR approach can be used to manipulate the viscoelastic behavior of a sample composed of *CIP* particles dispersed in cement paste.

4.1 RHEOLOGICAL MEASUREMENTS

4.1.1 Equipment and geometry

Rheological properties of the cement paste samples were measured using a rotational rheometer (MCR 301, Anton Paar, Graz, Austria) equipped with an electromagnetic kit (MRD 70/1T) that can generate a magnetic field perpendicular to the direction of the shear flow (Figure 4.1). The picture on the right shows the bottom plate, which holds the magnetic coils and hoses for water circulation for temperature control. After the top plate is lowered to the required gap, the yoke (cover in white) that is shown as open in the figure is placed around the shaft holding the top plate and is closed during the test. This yoke ensures that the magnetic field lines form closed loops and is connected to a water

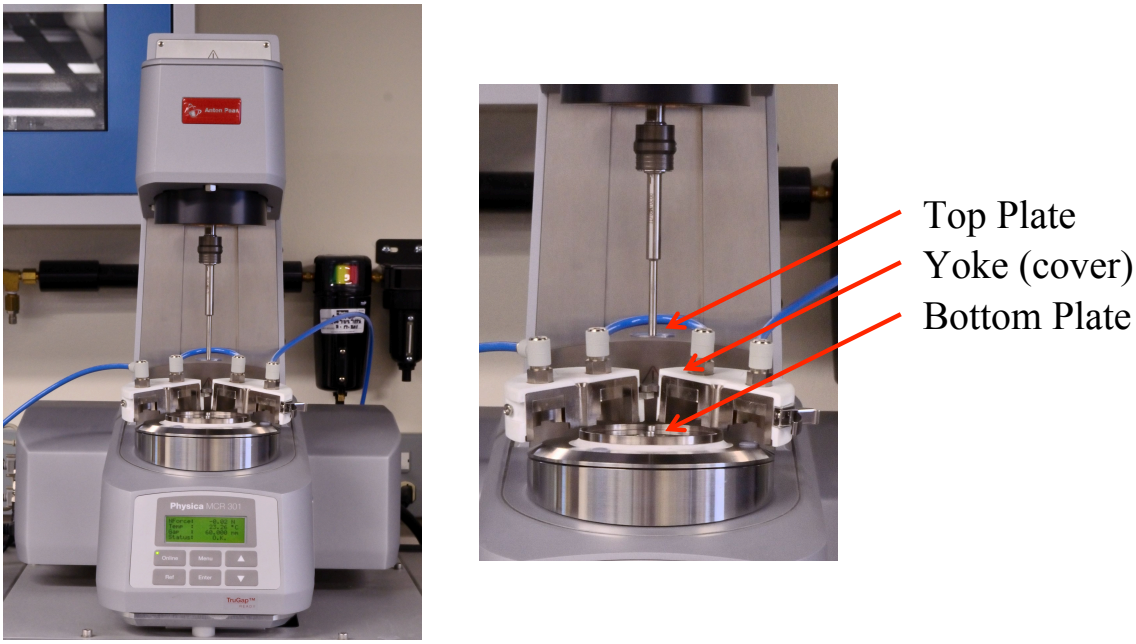

Figure 4.1 Anton Paar MCR 301 rheometer with a parallel plate attachment.

source to maintain the temperature. A 20 mm diameter (serrated titanium top plate and a smooth bottom surface) parallel plate measuring system was used for all measurements. During testing, the bottom plate remains fixed and the top plate rotates. The top plate is serrated to minimize problems that may occur due to slip. The gap between the plates was maintained at 1 mm (accurate up to $1/10^{th}$ of a micron) throughout testing. All samples were tested at 23.3 $\pm$ 0.3 °C and the temperature was maintained using a water bath. Lightweight oil (viscosity = 0.034 Pa.s) was applied (using a dropper) to the exposed sides of the cement paste to prevent drying. After mixing the sample according to the procedure described in the previous chapter, it took approximately 2 minutes to load the sample into the rheometer and start the test.

4.1.2 Pre-conditioning protocol

Prior to conducting the actual rheological tests, the samples were pre-conditioned according to the protocol detailed in Table 4.1. Pre-conditioning reduces the effects of shear history of the material and brings all the samples to a similar starting point, which aids in ensuring the reproducibility of the initial conditions of the samples (Deshmukh 2007). Applying a shear stress of zero simulates at rest condition. During interval III, a constant magnetic field was applied to align all the magnetic domains such that all the magnetic particles have the same starting point.

Table 4.1 Pre-conditioning protocol

Interval	*Duration*	*Shear Stress (Pa)*	*Shear Rate (s^{-1})*	*Magnetic Field (T)*
I	60 sec	-	50	0
II	30 sec	0	-	0
III	30 sec	0	-	0.9
IV	30 sec	0	-	0
V	120 sec	-	50	0
VI	30 sec	0	-	0

4.1.3 Flow Curve Protocols

After the pre-conditioning protocol depicted in Table 4.1, the samples were subjected to the following flow curve shearing protocol: sheared at 50 s^{-1}, 40 s^{-1}, 30 s^{-1}, 20 s^{-1}, 10 s^{-1} and 5 s^{-1} for 120 seconds each (readings were taken every 5 seconds). 120 seconds was found to be sufficient to ensure that the shear stress value reached equilibrium state. The average values for the last 10 points in each interval were used to determine the stress response of the material during that interval. The *Control* samples were subjected to the shearing test protocol at 15 minutes and 2 hours after the end of pre-conditioning protocol at 0 T; whereas the *4CIP* samples were tested at 0 T and 1 T at 15 minutes after the end of the pre-conditioning protocol. During the time interval the sample was maintained in the rheometer in a rest state (at the same magnetic field as the one it is tested and at $\tau = 0$ Pa). A new sample was used for each different time interval examined for the shearing test protocol (i.e. one sample was prepared for the shearing test protocol conducted at 15 minutes for the *Control* sample, and another sample was prepared for the shearing test

protocol that was conducted at 2 hours) and the tests were replicated twice for each sample with freshly mixed paste.

The resulting shear stress of the samples measured by the rheometer vs. the applied shear rate (only for the portion during the shearing protocol) were plotted on a x-y plot. This plot is called a flow curve, and it is a graphical representation of the shear stress versus the shear strain rate of a flowing material when the material is subjected to a varied shear strain rate. The Bingham model was fitted to the results to find the slope (an indicator for viscosity) and the intercept with shear stress axis, which is an indicator for the dynamic yield stress of the material. As stated in section 2.2.1, this yield stress is considered a dynamic yield stress because the yield stress is extrapolated from a condition in which the material was already flowing.

4.1.4 Stress Growth (Static yield stress measurement)

A stress growth technique is also used to measure the yield stress of the sample (with and without magnetic field). In this technique, the material is sheared at a low and constant shear rate and the shear stress is monitored over time (Cheng 1986; Nguyen and Boger 1992; Amziane and Ferraris 2007). The yield stress is measured based on the shear stress response and is denoted as static yield stress because the yield stress is determined from a condition in which the sample was at rest and flows only after the yield stress value is reached.

In this research, the yield stress was measured at varying levels of magnetic field up to 1 T. For each dosage of magnetic particles and each applied magnetic field strength, 2 fresh samples were tested. Following the pre-conditioning protocol, the samples were allowed to rest for 10 minutes (at $\tau = 0$) at the specified magnetic field. Then the samples were tested at a constant shear rate of 0.1 s^{-1} and at the same magnetic field that was used during the 10 minute rest period.

4.1.5 Small Amplitude Oscillatory Shear (SAOS) testing

Oscillatory shear testing is often used to characterize the viscoelastic behavior of materials (Gartner et al. 2002). Monitoring the viscoelastic behavior of a material over time gives information regarding both the elastic (*G'*) and viscous (*G"*) behavior of the sample. SAOS provides insight about the fresh-state microstructure of the material at rest. Conducting the test in the linear viscoelastic region (LVER) ensures that the particles stay in close contact with one another and are able to recover elastically, so the microstructure is not disturbed significantly (Larson 1998). To ensure that the testing parameters (strain amplitude and frequency) were within the LVER region of the sample, a strain sweep was conducted on the *Control* sample without any magnetic field. The *Control* sample has the lowest viscosity and thus should have the smallest LVER region of all the samples. The end of the LVER was determined to occur at 0.03% strain. From a frequency sweep, an angular frequency of 1 s^{-1} was determined to be in the linear region.

Based on these results, the oscillatory tests for all samples were conducted at 0.01% strain amplitude and 1 s^{-1} angular frequency.

The SAOS tests were performed at varying levels of magnetic field up to 1 T. For each dosage of magnetic particles and each applied magnetic field strength, 3 fresh samples were tested. During the first 10 minutes, readings were taken every 6 seconds following which, readings were taken every 30 seconds. Two types of results are shown here, one is timesweep (showing the evolution of elastic properties over time) and magnetosweep (a bar graph showing the effect of applied magnetic field on both the elastic and the viscous components) at a specified time period.

4.2. RESULTS: EFFECT OF MAGNETIC FIELD ON CEMENT PASTE WITHOUT ANY ADDITIONAL MAGNETIC PARTICLES

In the previous chapter, the magnetic properties of the unhydrated cement powder were presented. It was established that raw cement powder exhibited a weak ferromagnetic behavior likely due to the presence of a small quantity (2.7%) of Fe_2O_3. In this section the influence of magnetic field on cement paste (*Control* sample) is investigated.

4.2.1 SAOS Testing

Figure 4.2 shows the evolution of the elastic component of the shear modulus (also known as storage modulus or *G'*) over a span of 120 minutes. The time is reset to 0 after the end of pre-shear protocol. Note that both the axes are plotted on a $\log_{10}$-$\log_{10}$ scale. The plot shows the influence of magnetic field on the *Control* sample without any magnetic particles. The general trend of the curves is a continuous increase in the value of *G'* over time and compared to samples that contained magnetic particles (see Figure 4.5), the rheological response of the *Control* sample (without any magnetic particles) was

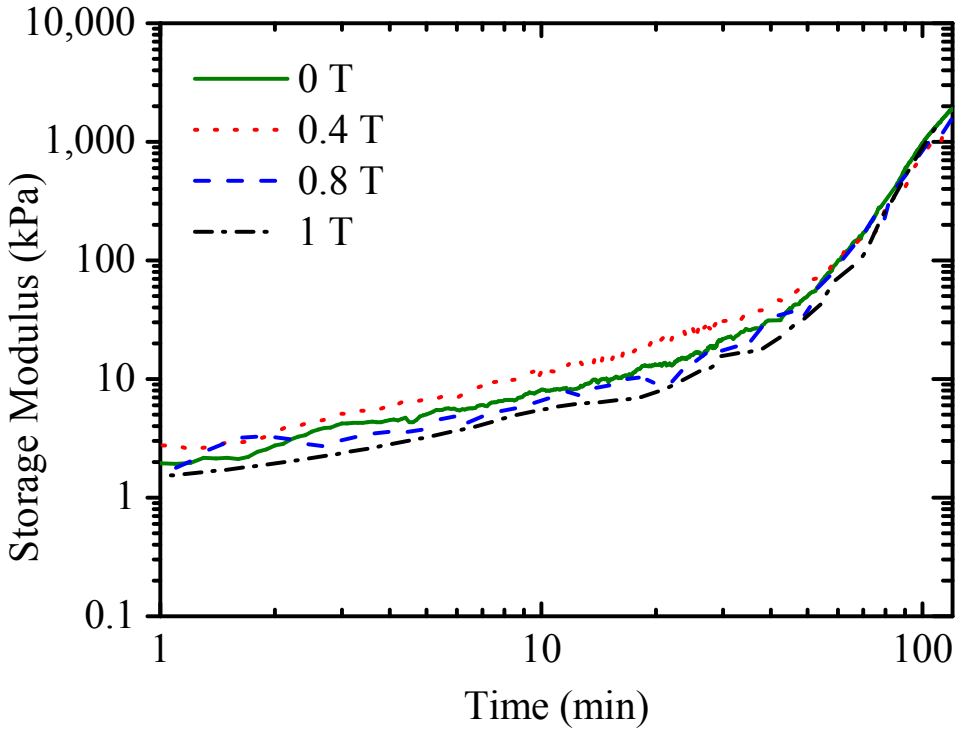

Figure 4.2 Storage modulus results for the *Control* sample for 120 minutes. By varying the magnetic field strengths the storage modulus evolution doesn't change considerably. Note: Both the axes are plotted on a $\log_{10}$-$\log_{10}$ scale.

not significantly affected by the presence of a magnetic field. At 1 minute, the values of *G'* vary between 1 and 3 kPa and at 10 minutes they vary between 3 and 6 kPa. This difference is very small and be assumed to be within the experimental error. Thus, although cement powder shows weak ferromagnetic behavior, the saturation magnetization value (0.6 emu/cm^3) is so small that there is no measurable change in its viscoleastic behavior, at least at the magnetic fields that were investigated in this study.

Over the duration of 120 minutes, the storage modulus of the *Control* sample increased from approximately 2 kPa (at t = 0 min) to 2000 kPa (at t = 120 min). The increase in *G'* is due to the structural buildup caused by particle flocculation (Ferron et al. 2013), the reversible thixotropic nature of the material (Ferron et al. 2007) and the irreversible microstructural changes due to hydration. Within the first 2 minutes, *G'* increases at a rate of approximately 0.5 kPa/min (see Table 4.2) and the increase is attributed to the formation of the weakly bonded flocs that are responsible for reversible structural build-up (i.e. thixotropy) (Ferron et al. 2007; Wallevik 2009; Roussel et al. 2012). However, towards the end of the testing duration (90-120 minutes), the rate of increase in *G'*, $\partial G'/\partial t$ increases to approximately 40 kPa/min (see Table 4.2). This increase could be an indication of acceleration in formation of hydration products (Jiang, Mutin, and Nonat 1995; Roussel et al. 2012).

Schultz and Struble (Schultz and Struble 1993) performed SAOS tests on cement pastes at a water to cement ratio of 0.4 in the LVER region. They reported *G'* values in the

range of 14 to 20 kPa right after mixing the sample. The higher values in *G'* could be because of (a) difference in measuring geometry or (b) differences in sample preparation. The samples in this study were tested using parallel plate geometry while their samples were measured using cup and bob geometry. In addition, our samples were prepared at higher shear rates using a high shear mixer leading to a paste with smaller yield stress and viscosity compared to their samples that were mixed at lower shear rates by hand. Roussel et al. (Roussel et al. 2012) also performed SAOS tests on cement pastes at w/c ratio of 0.4 in the LVER region. They loaded their samples into a rheometer with vane geometry, 20 minutes after mixing the samples (the mixing procedure was not described). They report *G'* values ranging from approximately 20 kPa right after initiating the rheological measurement to 160 kPa at 20 minutes after starting the rheological tests (which is 40 minutes after mixing the sample). Our *G'* values surpassed 150 kPa after a duration of 60 minutes.

4.2.2 Stress Growth Test

In the stress growth test, a constant shear rate is applied to the material and the shear stress response is observed over a period of time. Figure 4.3 shows the stress growth curves for the *Control* sample. It can be seen that the stress reaches a peak value within the first few seconds and then it gradually trials off to a small shear stress. The decay after the peak is a representation of the material in flow and the peak value is considered to be the static yield stress. As the applied magnetic field is varied (up to 1 T), there is no

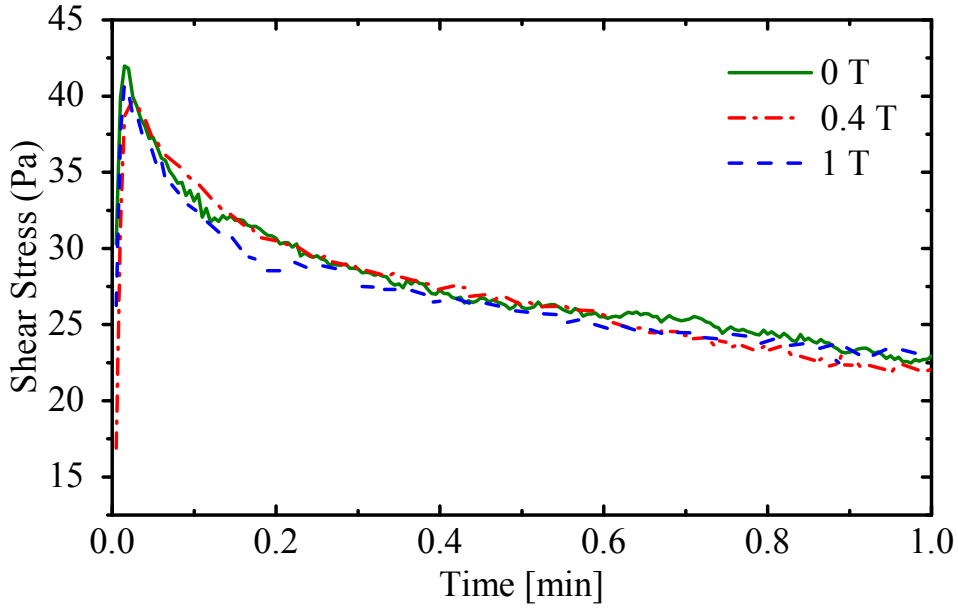

Figure 4.3 Stress growth curves for measuring the static yield stress of *Control* samples at different applied magnetic field strengths.

considerable change in the peak value (≈ 40 kPa). Thus, similar to the results from SAOS tests, it can be concluded that an external magnetic field does not have an impact on the fresh state rheological properties of the *Control* sample.

4.3 Effect Of Addition Of 4% CIP Magnetic Particles

4.3.1 Vibrating Sample Magnetometer

Similar to the principles described in Section 3.2.6, the magnetic properties of the *4CIP* sample were measured using a vibrating sample magnetometer (VSM). 40 *µl* of the sample was placed in a 6 mm ULTEM™ resin cup and was placed in the VSM 1 hr after

the mixing process. Figure 4.4 (a) shows the magnetization curve for *4CIP* between ± 15 kOe applied magnetic field. The magnetization values (shown on the y-axis) were normalized with respect to the total sample volume (40 μl = 4 × 10^{-2} cm^3). The magnetization value saturated at approximately 30 emu/cm^3 and the volume susceptibility was 0.085. But if the magnetization curves are normalized based on the volume of *CIP* particles present in the sample (≈ 7 × 10^{-4} cm^3), then the magnetization value saturates at a higher value (≈ 1690 emu/cm^3), as shown in Figure 4.4 (b). This value of M_s is within 1% of the value measured for pure *CIP* particles. Thus, it can be hypothesized that the saturation magnetization of the *4CIP* sample is based on the volume of the magnetic particles that are present in the sample. This hypothesis is similar to the one regarding ferromagnetic alloys; wherein the magnetic properties of an alloy containing one magnetic component and one non-magnetic component are based on the volume of the component containing magnetic particles (Cullity and Graham 2009)

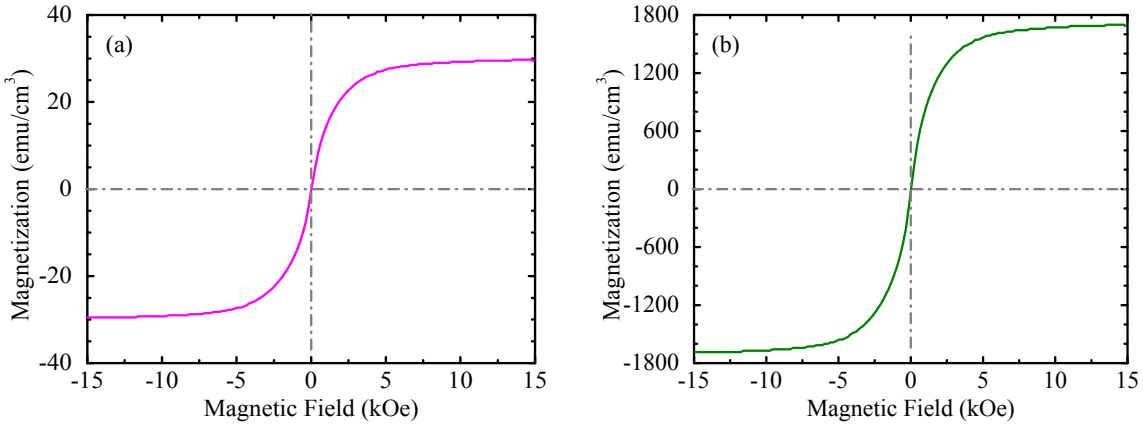

Figure 4.4 Magnetization curves for *4CIP* (a) with respect to total volume of sample and (b) with respect to the volume of *CIP* in the sample.

4.3.2 SAOS: Timesweep

Figure 4.5 shows the variation of *G'* over a duration of 120 minutes for:

- *Control* with 0 T applied magnetic field
- *4CIP* with 0 T applied magnetic field
- *2CIP* with 0.4 T applied magnetic field
- *4CIP* with 0.4 T applied magnetic field
- *4CIP* with 0.8 T applied magnetic field
- *4CIP* with 1.0 T applied magnetic field

Similar to Figure 4.2, it can be seen that the *G'* of all the samples increased over time. In general in the absence of a magnetic field, the addition of *CIP* powder influenced the evolution of *G'* (for example, compare *4CIP* and *Control* at 0 T in Figure 4.5). From Table 4.2 it can also be seen that the rate of change in *G'* of the two curves did not vary by much during the first 2 minutes, but there is an increase in $\partial G'/\partial t$ during the last 30 minutes. From Table 4.3 it is apparent that there is a clear increase in the magnitude of *G'* in the *4CIP* sample (at 0 T) compared to the *Control* and *2CIP* samples (at 0 T) and this increase is attributed to the higher total solid volume content when 4% *CIP* particles are added. As the particle volumetric concentration increases, the value of viscosity of the sample tends to increase, which could help explain the observed behavior.

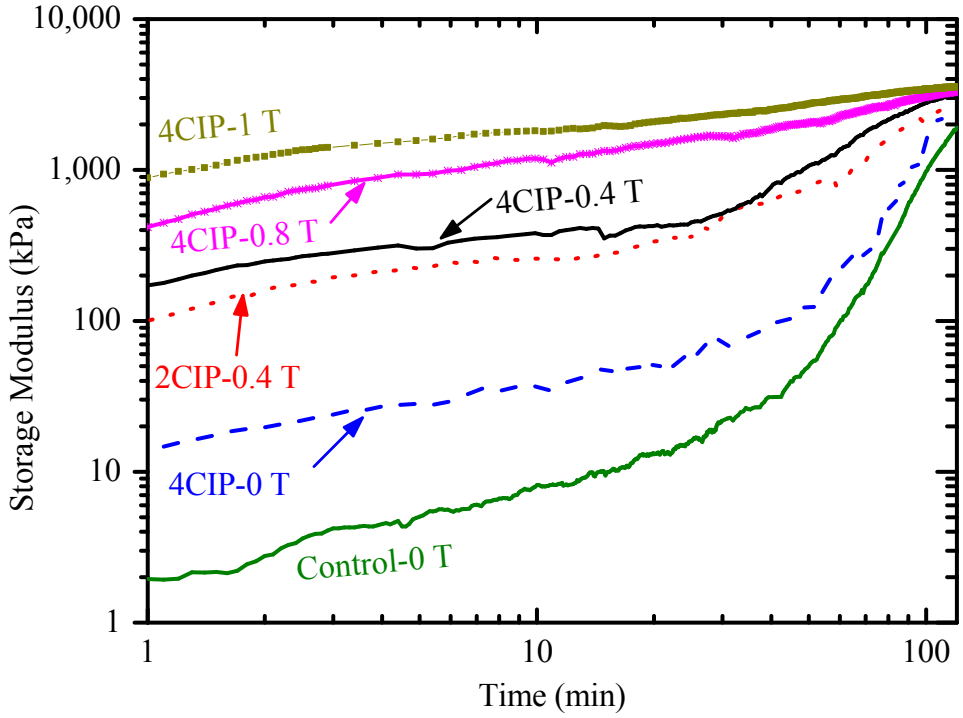

Figure 4.5 Storage modulus timesweep results with different dosages of *CIP* magnetic particles and at the specified magnetic field for 120 minutes. Notation: *4CIP-1 T* represents sample *4CIP* that is exposed to a magnetic field of 1 T. Note: Both the axes are plotted on a $\log_{10}$-$\log_{10}$ scale.

From Figure 4.5, it can be seen that at t = 1 min the storage modulus of *4CIP* increased by a factor of 300 when the sample was subjected to a magnetic field strength of 1 T compared to the value in the absence of magnetic field. This initial increase is from the alignment of field induced magnetic dipoles in the magnetic particles and the formation of chain-like structures of *CIP* particles when a magnetic field is applied (Rich, Doyle, and McKinley 2012) and is influenced by the magnetic properties of the particles. The value of *G'* is mainly dependent on the magnetic field strength and dosage of *CIP*

magnetic particles (as shown later), which is in agreement with work conducted by Klingenberg et al. (Klingenberg et al. 2010). They conducted their tests on *CIP* particles submerged in different polymers and showed that non-magnetic interparticle forces within the polymers did not have a strong influence on the field induced properties of an MR fluid. Thus the change in response observed in the values of *G'* for *4CIP* at 1 T magnetic field, compared to that at 0 T is mainly due to the alignment of the particles and there is probably no contribution from the cement-based suspending medium.

Within the first 2 minutes of being exposed to 1 T magnetic field, the *G'* value of the *4CIP* sample increased at a rate of 380 kPa/min (see Table 4.2). This is significantly higher than the 0.57 kPa/min value obtained when the sample was not exposed to a magnetic field. As seen in Table 4.2, as the magnitude of the magnetic field strength increased for the *4CIP* samples, there was an increase in the rate change of *G'*. Only 15 minutes was required for the *4CIP* sample to achieve a *G'* value of 2000 kPa when it was subjected to a 1 T magnetic field; whereas in absence of a magnetic field, it took approximately 120 minutes for a comparable *G'* value to be achieved. Thus by applying a magnetic field, the early age properties of cement paste could be changed considerably. In all cases the storage modulus for the cement-based MR fluid was significantly greater than that of the *Control* samples, which indicates the potential to create an MR mortar/concrete.

Table 4.2 Rate of change of storage modulus ($\partial G'/\partial t$) of the representative curves shown in Figure 4.2, Figure 4.5, Figure 4.9 and Figure 4.10

Sample	*Magnetic Field (T)*	*∂ G'/∂ t (kPa/min)*	
		0-2 min	*90-120 min*
Control	0	0.56	45
	0.4	0.46	37
2CIP	0	0.45	45
	0.4	85	31
4CIP	0	0.57	55
	0.2	15	35
	0.4	96	23
	0.8	320	14
	1.0	380	7.3
4CIP_HRWR	0	0.28	23
	0.4	52	42
	1.0	420	10
4CIP(sm)	0	0.46	42
	0.2	9.7	30
	0.4	56	23
	0.8	150	19
	1.0	560	7.1

Now to compare these values of *G'* with those reported in literature, it has to be first pointed out that the *4CIP* sample has a *CIP* volume fraction of 1.8%. Li et al. measured the viscoelastic properties of 10% volume fraction of iron suspended in silicone oil (Li, Chen, and Yeo 1999). By varying their magnetic field between 0.07 T to 0.25 T (at 8 Hz frequency, 0.1% strain amplitude and using a parallel plate arrangement at 1mm gap) they observed a steep increase in *G'* up to 0.2 T magnetic fields followed by a gradual increase. At 0.25 T they reported a *G'* value of 1500 kPa, which is much higher than the values reported here for a similar magnetic field (250 kPa at 0.2 T). This difference in values could be because of the higher frequency that their strains were oscillated at and also because of the higher volume fractions used in their studies.

Claracq et al. (Claracq, Sarrazin, and Montfort 2004) measured viscoelastic properties of 15% volume fraction of CIP particles suspended in silicone oil using a cone and plate geometry. At a strain of 0.01% and frequency of 6.2 rad/s (1 s^{-1}), by increasing their magnetic fields from 7.1 kA/m to 28.5 kA/m their *G'* values increased from 20 kPa to almost 180 kPa. They also found these values to be independent of the frequency. For our configuration, 0.2 T corresponds to a magnetic field strength of 42.3 kA/m and at t = 0 has a *G'* of 35 kPa. Thus, the differences in *G'* between our values and their values is mainly because of the variation in volume fractions of magnetic particles.

Table 4.3 Temporal evolution of storage modulus.

Sample	*Magnetic Field (T)*	*G' (kPa) value at*					
		15 min	*30 min*	*45 min*	*60 min*	*90 min*	*120 min*
Control	0	13	18	40	80	510	1800
	0.4	15	32	56	110	660	2000
2CIP	0	10	22	39	90	590	1800
	0.4	260	380	530	790	2000	3100
4CIP	0	27	51	99	270	1100	2500
	0.2	250	350	530	850	1900	2800
	0.4	420	630	880	1200	2200	3000
	0.8	1300	1700	2000	2400	3000	3400
	1.0	1900	2300	2500	2800	3200	3500
4CIP_HRWR	0	8	14	22	39	160	790
	0.4	310	390	460	670	1500	2700
	1.0	2100	2300	2500	2800	3200	3500
4CIP(sm)	0	11	28	59	94	620	1900
	0.2	200	300	450	710	1900	3000
	0.4	380	620	890	1300	2400	3100
	0.8	1200	1600	1900	2100	2800	3300
	1.0	1900	2200	2600	2800	3300	3500

From Table 4.2 it can also be seen that the $\partial G'/\partial t$ values for 90-120 minutes decreased as the magnetic field increases. When a higher magnetic field is applied, a higher degree of rigidity is induced early on and thereafter there is a decrease in $\partial G'/\partial t$. This could indicate a maximum degree of structure that can be reached within the time frame of the

study. As discussed earlier, during the initial phase (0-2 min), structure formation is based on the alignment of the domains in the magnetic particles whereas in the final phase, structure formation might be governed by hydration. This hypothesis is also backed by the fact that at 120 minutes all the samples reached similar *G'* values (Table 4.3).

4.3.3 SAOS: Magnetosweep

Figure 4.6 shows the influence of the magnitude of the magnetic field on the shear moduli (both storage and loss modulus) of the cement pastes (note, the moduli were measured 5 minutes after applying the magnetic field). As discussed earlier the *CIP* magnetic particle dosage had a pronounced effect on the early-age MR behavior and increasing the content of *CIP* magnetic particles resulted in an increase in the shear moduli. For *4CIP* the storage modulus increased from 18 kPa (at 0 T magnetic field) to 1600 kPa (at 1 T), whereas for the *Control* sample there was no significant change from 4 kPa.

By comparing Figure 4.6 (a) storage modulus (*G'*) with Figure 4.6 (b) loss modulus (*G"*), it can be seen that *G"* also increased with increasing magnetic field for both *2CIP* and *4CIP*, but the magnitude was smaller than that of *G'*. For *4CIP* the loss modulus increased from 3 kPa (at 0 T) to only 170 kPa (at 1.0 T) and again for *Control* sample there was no significant change from 1 kPa. Thus, for the field-induced samples

containing magnetic particles, not only was the magnitude of the shear moduli affected, but also the overall viscoelastic behavior was influenced.

In the *Control* sample, the magnitude of the storage modulus is approximately higher by a factor of four compared to that of the loss modulus (or a loss factor *G"/G'* ~ 0.25). Whereas in the samples containing *CIP* magnetic particles (both *4CIP* and *2CIP*), the storage modulus was found to be higher by a factor of 6.5 when compared to the loss modulus when a field was applied. The loss factor *(G"/G')* decreases from 0.2 (at 0 T) to 0.1 (at 1.0 T) for both *2CIP* and *4CIP*. The higher value of loss factor is an indicator of higher fluidity or viscosity of the sample.

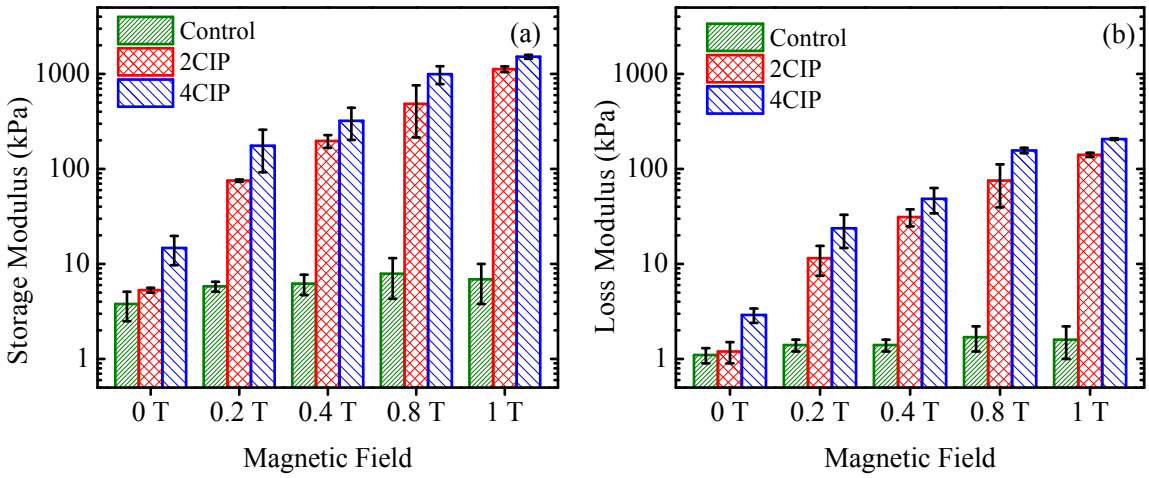

Figure 4.6 (a) Storage modulus and (b) loss modulus results at different dosages of *CIP* (magnetic particles) and at varying magnitudes of applied magnetic field at 5 minutes after application of magnetic field. Note that the y-axis is on a $\log_{10}$ scale.

4.3.4 Flow Curve: Dynamic Yield Stress

Bingham yield stress values (herein referred to as dynamic yield stress) were extrapolated from flow curves using Bingham model as show in Figure 4.7 (a) and the values are shown in Table 4.4. At 15 minutes after mixing the sample, the yield stress of the *Control* sample was determined to be 3 Pa. A yield stress around 500 Pa was reported for a cement paste with a lower water to cement ratio of 0.3 (Amziane and Ferraris 2007). From the graph shown by the authors (Amziane and Ferraris 2007) for 0.4 w/c ratio, the yield stress appears to be significantly less than 100 Pa. Thus, the yield stress (3 Pa) measured for the *Control* sample in this present study is comparatively less than the value reported in literature. The R^2 value comparing the actual curve and the Bingham fit of the *Control* sample at 15 minutes was 0.99, but at 120 minutes, the R^2 fit dropped to 0.88. This can be attributed to the fact that as cement hydrates, there is an increase in the solid-solid contacts and decrease in the free water which leads to an increase in the frictional forces (Amziane and Ferraris 2007). Because of this, there is an increase in the elastic properties of the material and, at low shear rates, the material is not completely broken down and thus does not give an accurate reading of shear stress. Therefore it can be concluded that Bingham model does not represent cement paste at later stages. As stated by Banfill and Frias (2007), to find the consistency index and power exponent for using the Herschel-Bulkley model (see Equation 2.4), a regression model has to be used. But the yield stress results obtained using these regression models were extremely dependent on the values used to conduct the regression analysis (Banfill and Frias 2007), and, thus, in this study the flow curve values were fit to a Bingham model to calculate the yield

stress of the samples. Using a Bingham fit, in the absence of a magnetic field a yield stress of approximately 40 Pa was obtained at 2 hours in the *Control* sample and is almost 13 times higher than the value of the *Control* sample at 15 minutes.

Table 4.4 Dynamic yield stress (calculated using Bingham model)

Sample	*Magnetic Field (T)*	*Time*	*Shear Yield Stress (Pa)*	R^2
Control	0	15 min.	3.2	0.99
Control	0	2 hr.	39	0.88
4CIP	0	15 min.	13	0.97
4CIP	1	15 min.	8400	0.87

When a 1 T magnetic field is applied to the *4CIP,* as explained in the previous section the elastic response of the sample is significantly higher compared to the *4CIP* sample without any magnetic field. Because of which, at low shear rates, the sample cannot be broken down and the shear stress values are higher at lower shear rates. When a Bingham model is fit to these data, it yields a negative slope and the plastic viscosity cannot be calculated. A similar behavior has been reported in literature when a flow curve was conducted on cement pastes at later ages close to initial set (Amziane and Ferraris 2007). Because of all the issues with accurately determining the yield stress based on flow curves, after this section yield stress of all the samples are measured using the stress growth technique.

At 1 T magnetic field strength, for the *4CIP* sample a yield stress of 8370 Pa was obtained at 15 minutes using a Bingham fit. This value is substantially higher (approximately 215 times the yield strength of the *Control* sample at 2 hours without any magnetic field) and supports SAOS results discussed earlier that showed that the elastic properties of the cement based MR fluid (*4CIP* at *1 T* magnetic field) are noticeably higher with magnetic field compared to the *Control* sample at 0 T. Rankin et al. (Rankin, Horvath, and Klingenberg 1999) reported yield stresses of field induced MR fluid in the range of 2 kPa (at 0.1 T) to 6 kPa (at 0.4 T) for 10% volume fraction of *CIP* in a silicone oil plus grease based carrier fluid. These values are within the range of yield stresses reported here (8.4 kPa at 1 T magnetic field) for only 1.8% volume fraction of *CIP*. Hence, it can be concluded that by adding magnetic particles and applying a magnetic field, that the energy loss due to viscous flow is reduced and that the mechanical response of the sample to stresses became significantly more solid-like.

4.3.5 Stress Growth: Static Yield Stress

Figure 4.7 shows three stress growth curves for the *4CIP* sample with varying magnitudes of magnetic field. With no magnetic field, the shape of the curve is similar to that of *Control* sample that was shown in Figure 4.3. The yield stress is approximately 40 Pa, which is almost 10 times higher than the value measured using a flow curve. The yield stress measured through flow curves is dependent on the shear rate range that it is measured at and in this case it underestimates the yield stress compared to the value

found from stress growth curves (similar to the observation by Amziane and Ferraris 2007). When a small magnetic field is applied, the stress value peaks at approximately 0.2 min (12 seconds) and the value gradually decreases in value. But the percentage decrease in shear stress value as shown in Figure 4.7 (c) is much smaller than the decrease in value as shown in Figure 4.7 (b). Comparing Figure 4.7 (b) and (c), the *4CIP* sample at *0 T* can be classified as a viscoplastic fluid whereas the *4CIP* sample at *0.1 T* can be classified as a viscoelastic fluid. At a magnetic field strength value of 0.1 T, the yield stress is *4CIP* is approximately 250 Pa. This is higher by a factor of 6 when compared to the yield stress of *4CIP* without any magnetic field.

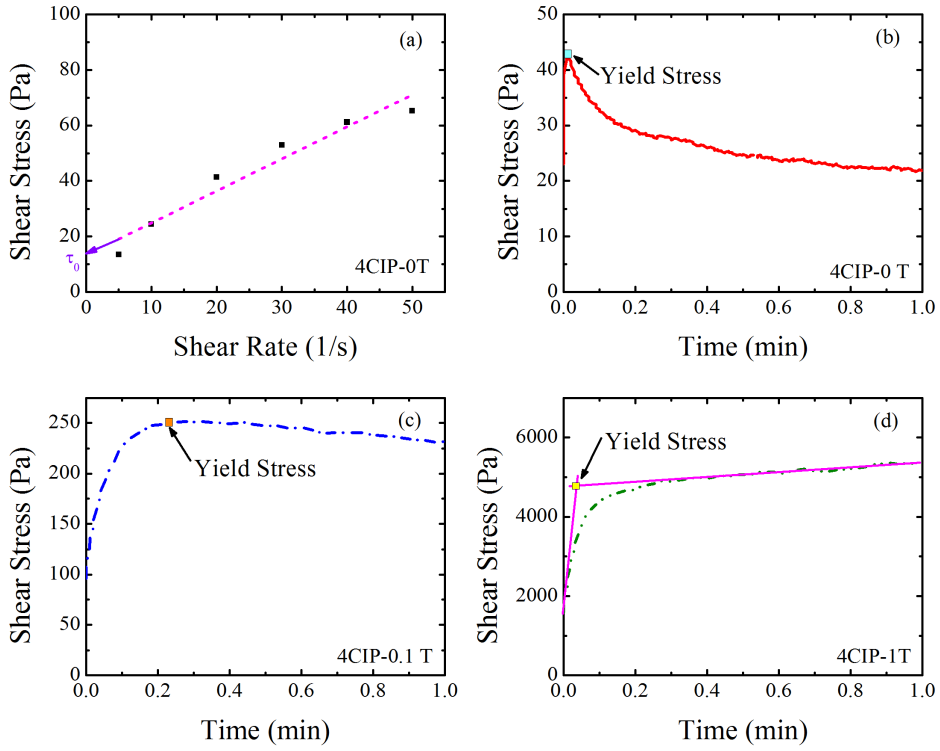

Figure 4.7 (a) Bingham fit for measuring dynamic yield stress (b-d) Stress growth curves at specified magnetic field strengths.

When a magnetic field of large magnitude is applied, as shown in Figure 4.7 (d), the shear stress value continuously increases and it can be classified as a viscoelastic solid. As it is difficult to exactly determine the end of the linear portion in the first few seconds and therefore the yield stress is calculated based on the intersection of two lines. The first line is the slope of linear region during the first few seconds and the second line is the slope within the last 0.5 minute. At 1 T magnetic field, the yield stress of *4CIP* was found to be 4900 Pa, which is higher by a factor of 120 compared to the value without any magnetic field.

4.4 EFFECT OF MAGNETIC PARTICLE DOSAGE

4.4.1 SAOS Testing

From Table 4.3, it can be seen that during the first 60 minutes, the *G'* value of the *4CIP* sample at *0.4 T* is almost twice that of the *2CIP* sample at *0.4 T*. According to the results reported in the literature, the *G'* (and yield stress) of field induced MR fluids increases with increase in the volume fraction of magnetic particles (De Vicente, Klingenberg, and Hidalgo-Alvarez 2011; Li, Chen, and Yeo 1999) which is in fact the trend observed in this study.

However, cement-paste is an aging MR fluid and it can be seen that beyond the first 60 minutes, the *G'* values are very similar for both the *2CIP* and *4CIP* samples that are subjected to 0.4 T, and this may be because of the hydration forces are starting to play a

more dominant role in the formation of the internal structure. This suggests that CIP magnetic particle concentration plays a minor role on the magnitude of the later age (> 60 min) rheological response, and leads to the possibility of optimizing the magnetic particle dosage for a certain response requirement, especially at earlier ages.

4.4.2 Stress Growth: Static Yield Stress

Figure 4.8 shows the static yield stress values of *Control, 2CIP* and *4CIP* measured using the stress growth technique. As discussed, there is no substantial change in the yield stress of the *Control* sample at varying levels of magnetic field strength. When magnetic particles are added to the cement paste, there isn't much change in the yield stress value

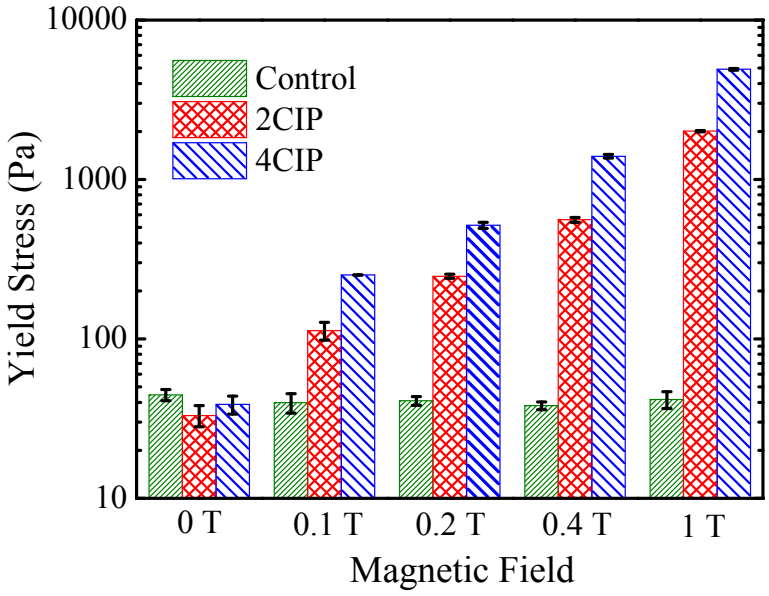

Figure 4.8 Static yield stress results with different dosages of *CIP* and at several magnetic field strengths. Note that the y-axis is on a $\log_{10}$ scale.

at 0 T, but when the magnetic field is increased, the yield stress also increases. For all the magnetic fields (0.1 T to 1 T), as the dosage of magnetic particles is doubled, the yield stress value also doubles. This trend matches with the results reported in literature (De Vicente, Klingenberg, and Hidalgo-Alvarez 2011; Li, Chen, and Yeo 1999).

4.5 EFFECT OF SUSPENDING MEDIUM RHEOLOGICAL PROPERTIES

4.5.1 SAOS Testing: Timesweep

Figure 4.9 shows the impact of varying the yield stress and viscosity of the cement paste matrix. A *HRWR* was used to reduce the yield stress and viscosity of the cement paste matrix, without changing either the solid content volume or the water to cement ratio. As expected, in absence of a magnetic field, the storage modulus of *4CIP_HRWR* sample was lower than that of *4CIP*. During the entire testing duration, the storage modulus of the sample with *HRWR* was at least 4 times lower than the sample that did not contain *HRWR* (see Table 4.2). Furthermore, the rate at which the storage modulus increased was also influenced; both the initial 2 min. and the 90-120 min. rate of change were decreased approximately by 50% compared those of *4CIP* (Table 4.3).

Papo et al. studied the influence of superplasticizers (or HRWR) on the rheological properties of cement paste at a w/c ratio of 0.32 (Papo and Piani 2004). For both melamine based and lignosulfonate based HRWR, they saw a decrease in values of *G'* with increasing dosage of HRWR. By changing the dosage from 0.5 ml/100 g to 5 ml/100

g they saw a decrease in *G'* from 60 to 2 Pa at t = 0 min. In the current research, when dosage of HRWR was changed from 0 ml/100 g to 0.13 ml/100 g and the value of *G'* dropped by a factor of 4.

Comparing *4CIP_HRWR* at 0.4 T and *4CIP* at 0.4 T it can be seen that with the application of a 0.4 T field, the storage modulus of both samples were very similar and that the reduction in the G' value of the *4CIP_HRWR* sample was now approximately

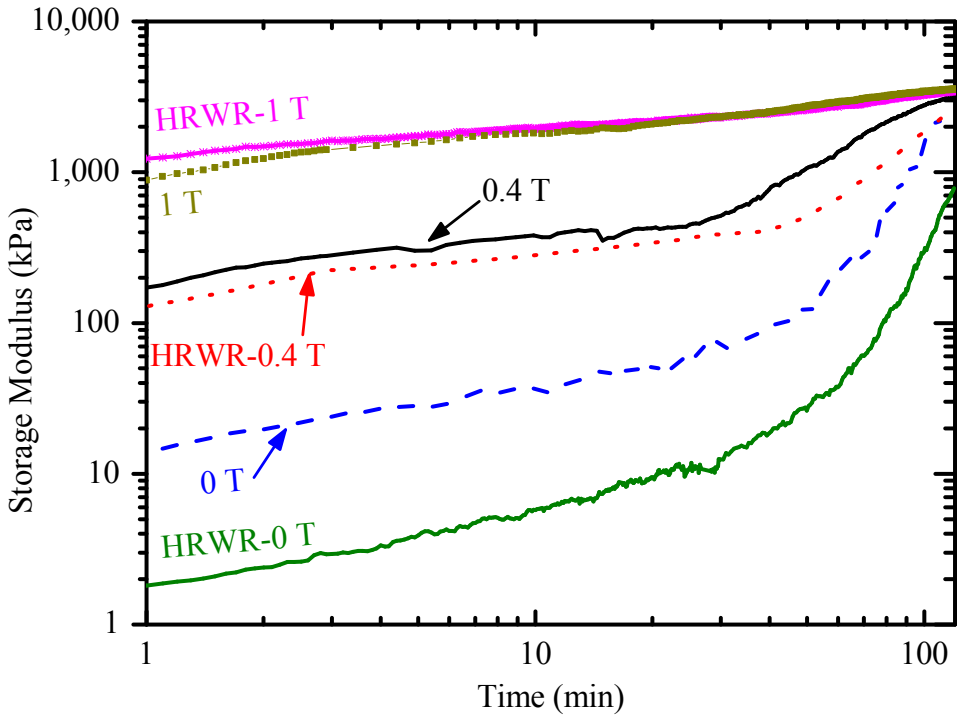

Figure 4.9 Storage modulus timesweep results for *4CIP sample* with and without *HRWR* over a period of time to show the effect of suspending medium rheological properties on the response of the MR fluid. *4CIP* notation has been omitted in the figure for the sake of clarity Note: Both the axes are plotted on a $\log_{10}$-$\log_{10}$ scale.

half of that of the *4CIP* sample compared to the 4-fold decrease that was seen when no magnetic field was applied (Figure 4.9). Hence, the structure induced by the magnetic dipoles is able to compensate for some of the reduction in structure caused by the dispersing nature of the *HRWR*. However, when a magnetic field of 1 T was applied, both the samples with and without *HRWR* followed a similar trend, and the initial yield stress of cement paste did not affect the rheological properties of the MR fluid upon application of a large magnetic field.

These results are consistent with those of Rankin et al. (Rankin, Horvath, and Klingenberg 1999) who studied the influence of 10% volume fraction of CIP particles suspended in an oil-grease medium, in which the yield stress of the oil-grease medium was varied from 0.1 Pa to 39 Pa. Upon the application of a magnetic field of 0.36 T, no changes in the yield stress of MR fluid was found when the yield stress of the suspending medium changed. It is interesting to note that while Rankin et. al used 10% volume fraction of CIP in the oil-grease medium, in this work, with only 1.8% volume of CIP, enough of a structure was induced in the cement-based suspension to compensate for the initial reduction of the storage modulus of the cement paste when HRWR was incorporated.

4.6 EFFECT OF MAGNETIC PARTICLE SIZE DISTRIBUTION

The next phase of this study is to understand the influence of the magnetic particle size distribution on the rheological response of a field induced cement-based MR fluid. The particle size distribution of *CIP* and *CIP(sm)* are shown in Section 3.2 of the previous chapter. Recall, *CIP* has a d_{50} of 8.7 μm whereas *CIP(sm)* has a d_{50} of 3.3 μm. The largest particle of *CIP* has a diameter of 90 μm whereas for *CIP(sm)* the largest particle has a diameter of 25 μm. Thus, *CIP(sm)* has smaller particle sizes but according to the manufacturer, both *CIP* and *CIP(sm)* have the same density. Both *CIP* and *CIP(sm)* have similar magnetization saturation values, but *CIP* has a higher volume susceptibility (7.9 in SI) compared to that of *CIP(sm)* (5.2 in SI).

4.6.1 SAOS results

Figure 4.10 shows a representative curve depicting the storage modulus evolution of *4CIP* and *4CIP(sm)* over a span of 120 minutes. Table 4.3 shows the average storage modulus for the samples; each value reported in the table is the average of 3 specimens. It can be seen that in absence of a magnetic field (i.e., at 0 T) the magnitude of *G'* of the *4CIP(sm)* sample was consistently smaller that the *G'* magnitude of the *4CIP* sample. The lower values of *G'* can potentially be explained based on the particle size distribution of the *CIP* and *CIP(sm)* particles. Ideally, since *CIP* and *CIP(sm)* have the same density and *CIP(sm)* has a smaller d_{50}, for a given volume *4CIP(sm)* has more number of

particles than *4CIP*; this increase in number of particles would increase the solid-solid interactions thus lead to a reduction in the viscosity (or fluidity) of the cement paste. If this were the case, then the *G'* values of *4CIP(sm)* should have been higher (less fluidity → higher stiffness), but the trend observed here is the opposite. This is most likely because apart from the d_{50} values having an influence on the fluidity of the sample, there might also be an influence from the extent of poly-dispersity (range of particle sizes) (Chong, Christiansen, and Baer 1971) and total surface area (Bentz et al. 2012) of the *CIP* and *CIP(sm)* particles.

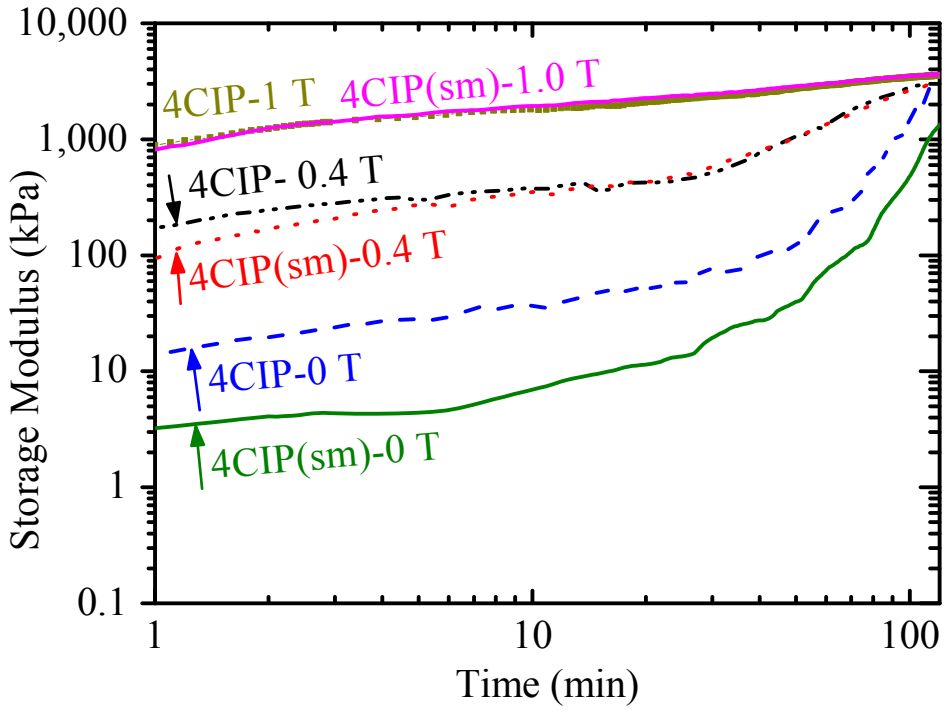

Figure 4.10 Storage modulus timesweep results with *CIP* and *CIP(sm)* magnetic particles at magnetic field strengths over a period of time. Note: Both the axes are plotted on a $\log_{10}$-$\log_{10}$ scale.

When a magnetic field is applied, even as low as 0.2 T, the *G'* values are all very similar (Table 4.3), which could be because both *CIP* and *CIP(sm)* have similar saturation magnetization values. As explained in Chapter 2, when a magnetic field is applied, the magnetic moments in a domain align in the direction of the magnetic field, which translates into magnetization in a sample. So it can be assumed that the saturation magnetization of the magnetic particles has an impact on the *G'* values. However, there was a considerable difference in the values of $\partial G'/\partial t$ for *4CIP* and *4CIP(sm)* during the initial time period of 2 minutes. The rate of change of *G'* was higher for *4CIP* at all magnetic field strengths, which might be because *CIP* particles have a higher volume susceptibility compared to that of *CIP(sm)*. Susceptibility determines how a magnetic material responds to an applied field and a sample with a higher value of susceptibility responds at a faster rate.

Figure 4.11 shows the influence of magnetic field strength on the shear moduli of *Control, 4CIP* and *4CIP(sm)* samples. These results are based on the values obtained, at 5 mins after the start of SAOS testing. Comparison of Figure 4.11 (a) with Figure 4.11 (b) shows that at all magnitudes of magnetic field strengths, for all the samples, the storage modulus (see Figure 4.11 (a)) is almost an order of magnitude higher than the loss modulus (see Figure 4.11 (b)). In the absence of magnetic field, *4CIP* has a higher value of both *G'* and *G''* compared to those of *4CIP(sm)*. Without any magnetic field, the average loss factor (*G''/G'*) for *4CIP* is 0.2 (≈ phase lag 11°) and that of *4CIP(sm)* is 0.25 (≈ phase lag 14°), thus *4CIP* comparatively has a higher elastic response (a pure

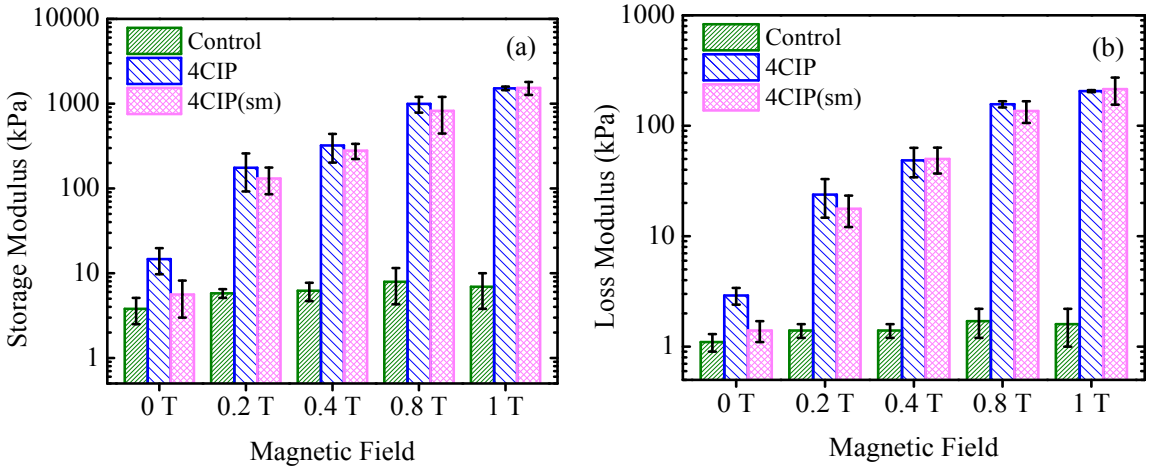

Figure 4.11 (a) Storage modulus and (b) loss modulus results with *CIP* and *CIP(sm)* magnetic particles at varying magnitudes of magnetic field (at 5 minutes after application of magnetic field).

elastic material has a phase lag of 0° and a pure viscous material has a phase lag of 90°). But when a magnetic field is applied, both the *4CIP* and *4CIP(sm)* samples have similar shear moduli values and at 1 T the loss factor decreases to 0.14 (≈ phase lag 8°).

At 120 min for all the samples, (shown in Figure 4.12) values of *G'* are almost 2 orders of magnitude higher than those of *G''*. For the *Control* sample the value of loss factor at all the magnetic field strengths is approximately 0.04 (≈ phase lag 2°), because of hydration the cement paste has stiffened and has more elastic properties compared to the sample at 5 minutes. At 120 minutes although the *G'* of the *4CIP* and *4CIP(sm)* samples reach similar values at all magnetic field strengths, the *G''* values decreases with increasing magnetic field strength. At 0 T, similar to the *Control* sample, the value of loss factor for

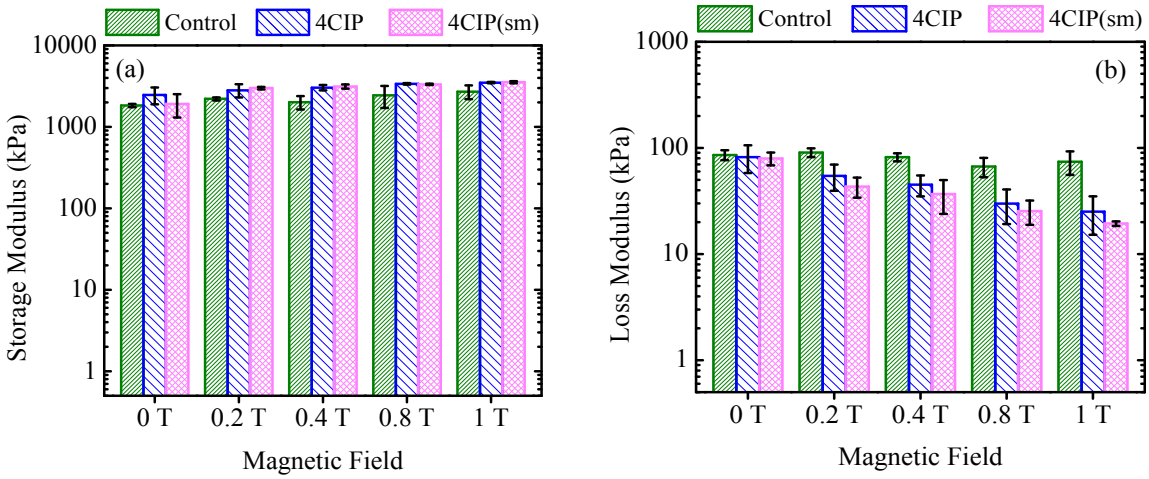

Figure 4.12 (a) Storage modulus and (b) loss modulus results with *CIP* and *CIP(sm)* magnetic particles at varying magnitudes of magnetic field (at 120 minutes after application of magnetic field).

4CIP and *4CIP(sm)* is approximately 0.04 (≈ phase lag 2°). But at a magnetic field strength of 1 T, the loss factor of both the *4CIP* and *4CIP(sm)* samples decreases to 0.06 (≈ phase lag 0.3°). Thus, when a larger magnetic field is applied to a cement-based MR fluid, at 120 minutes the viscoelastic response is very close to that of a pure elastic material. A higher magnetic field is potentially inducing a higher rigidity and thus resulting in a smaller viscous component. Thus the MR effect is not only seen in the early fresh state properties but is also apparent in the viscoelastic nature of the cement paste at later ages.

4.6.2 Stress Growth: Static Yield Stress

Figure 4.13 shows the static yield stress values of *Control*, *4CIP*, and *4CIP(sm)* at different magnitudes of applied magnetic field. It can be seen that within the error bars shown on the plot, both *4CIP* and *4CIP(sm)* have identical values (similar to the response observed in the SAOS results). When the magnetic field strength was increased from 0 T to 0.2 T, the value of yield stress for both *4CIP* and *4CIP(sm)* increased by a factor of 12 and when the magnetic field strength was increased from 0 T to 1 T, the value increased by a factor of 120. Thus, it can be concluded that although *4CIP* and *4CIP(sm)* have different particle size distribution and although *4CIP(sm)* has smaller particle sizes, the field induced rheological properties of both the samples are very similar.

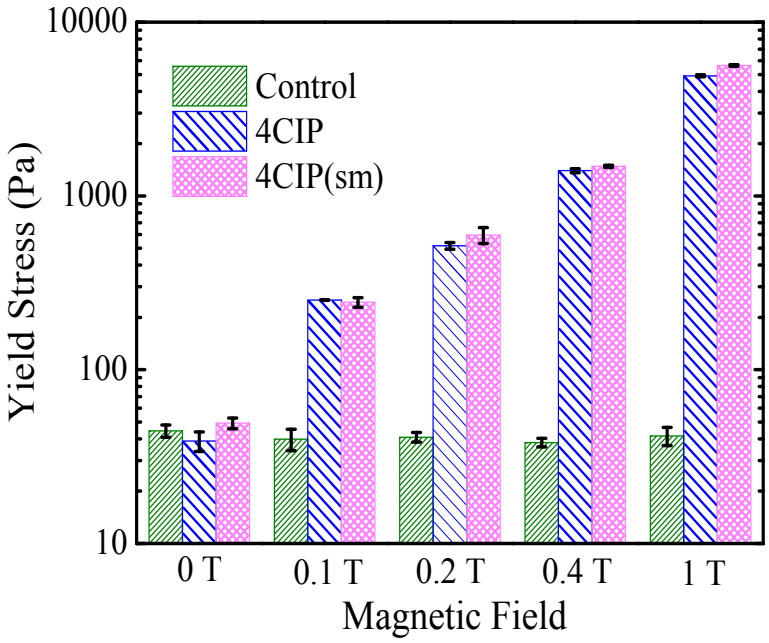

Figure 4.13 Static yield stress variation with changes in magnetic particle size at varying magnetic field strengths (The values were obtained from a stress growth curve)

4.7 EFFECT OF CYCLIC VARIATION OF APPLIED MAGNETIC FIELD

Up until this point, all the results shown were for samples subjected to a continuous constant applied magnetic field of a single strength. It was shown that when a certain magnetic field is applied, due to a combination of domain alignment in the magnetic particles, flocculation, thixotropy and cement hydration, the elastic component of the shear modulus increases over time. If this magnetic field were to be changed (increased or decreased) at a certain period of time, it would be interesting to observe the change in response of the sample. If the magnetic field were to be removed, would the cement paste retain some/all of the structure that was induced in the cement paste? If the structure is retained then it has a significant consequence in the curing of self-leveling or self-consolidating concrete, wherein it would lead to a reduction in the formwork pressures. Thus, a change in magnetic field could be applicable during construction, wherein different magnetic fields can potentially be useful for different operations and thus the cement paste would be subjected to different magnetic field strengths. In order to answer the question posed above, different combinations of magnetic fields tested in which the magnetic field was cycled from low-high-low and high-low-high. These cyclic combinations are listed below:

- *0 T – 0.4 T – 0 T*
- *0.4 T – 1 T – 0.4 T*
- *1 T – 0 T – 1 T*
- *1 T – 0.4 T – 1 T*
- *0.4 T – 0 T – 0.4 T*

Each magnetic field strength was applied for a duration of 30 minutes; thus the total test duration was 90 minutes. For example, for *0 T – 0.4 T – 0 T,* the sample was not exposed to any magnetic field for the first 30 minutes (i.e. B = *0 T),* then the magnetic field strength was increased to *0.4 T* for 30 minutes and finally it was decreased back to *0 T* for another 30 minutes. In this section SAOS tests were conducted during the entire 90-minute duration with *4CIP(sm)*. For the sake of brevity, in this section *4CIP(sm)* is omitted from the sample names and the samples are instead referred by the applied magnetic field strength. For example, *4CIP(sm)* subjected to a magnetic field strength of 0.4 T would be referred to as *0.4 T.* Fresh samples were prepared for each combination of magnetic fields and the tests were replicated three times.

Figure 4.14 shows the effect when the magnetic field is cycled from low-high-low values. The figure also shows the evolution of *G'* when the magnetic field is not cycled, but rather is maintained at a constant applied level for the 90 min duration. The samples shown are based on a representative curve from one of the replicates.

4.7.1 SAOS: Field strength cycled from 0 T – 0.4 T – 0 T

0 T – 0.4 T – 0 T follows a similar path as *0 T* for the first 30 min (see Figure 4.14). During this duration, a continuous increase in *G'* is observed which could be due to a combination of several factors such as: the structural buildup caused by particle

flocculation (Ferron et al. 2013), the reversible thixotropic nature of the material (Ferron et al. 2007) and/or the irreversible microstructural changes due to hydration.

At t = 30 minutes, when the magnetic field was increased from 0 T to 0.4 T for *0 T – 0.4 T – 0 T*, *G'* increased by twice the value. This increase is because of the alignment of field induced magnetic dipoles in the magnetic particles and formation of a chain like structure when the magnetic field is applied (Rich, Doyle, and McKinley 2012). At t = 35 min, sample *0 T – 0.4 T – 0 T* reached a *G'* value that is similar to *0.4 T* applied

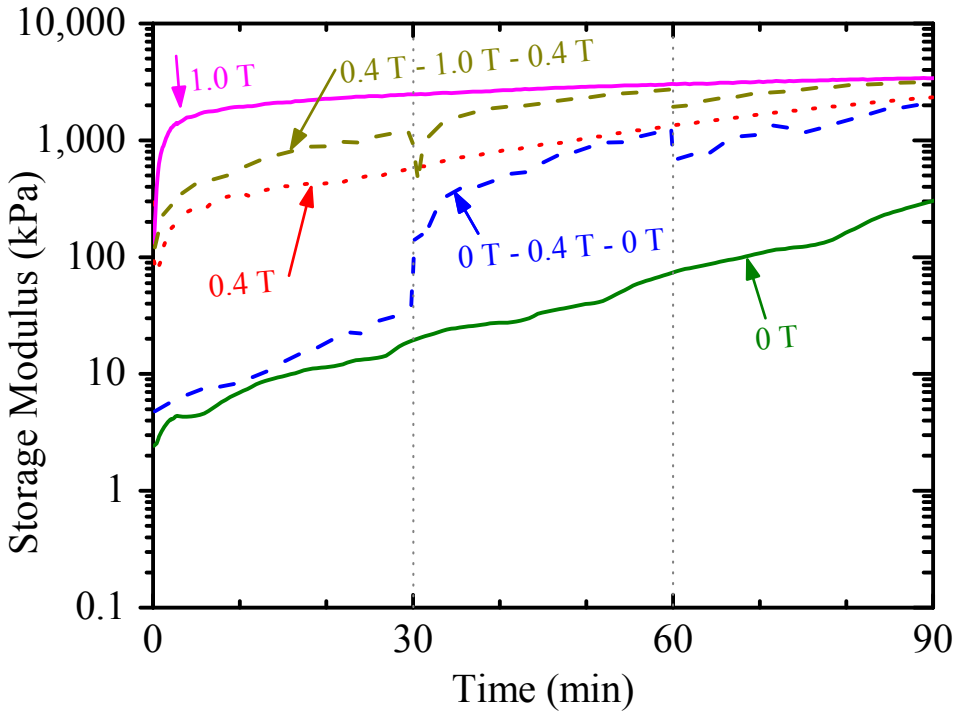

Figure 4.14 Storage modulus timesweep results of *4CIP(sm)* sample with cyclic variation (low – high – low) of magnetic field strength every 30 minutes. Note that the y-axis is on a $\log_{10}$ scale.

continuously for t = 5 min. This shows that when a magnetic field of *0.4 T* is applied (either at t = 0 min. for *0.4 T*, or at t = 30 min. for *0 T – 0.4 T – 0 T*), that the rheological properties appear to be less dependent on the time frame at which the magnetic field is applied (i.e. immediately after mixing or at 30 minutes after mixing) and more influenced by the actual magnitude of the field strength. Around t = 55 min, *G'* of *0 T – 0.4 T – 0 T* is similar to *0.4 T* (at 55 min). Even though *0.4 T* (at t = 5) and *0 T – 0.4 T – 0 T* (at t = 35 min) have a similar *G'* value, it takes *0 T – 0.4 T – 0 T* a smaller duration to match up with the evolution of *0.4 T* applied continuously.

Right after a magnetic field is applied, the value of *G'* appears to be dependent on the applied magnetic field strength, but as time progresses, there is a continuous increase in the value of *G'*. At early stages this increase in *G'* could be dependent on flocculation but at later stages there appears to be a strong dependence on hydration. Through powder-x-ray diffraction patterns (shown in Chapter 5), it was concluded that samples exposed to magnetic field for 4 hours did not exhibit any changes in hydration products compared to the sample subjected to 0 T magnetic field. Although the viscoelastic properties of the sample are being modified through the MR approach, hydration of cement is a continuous process that's occurring in parallel and is not affected by the applied magnetic field strength.

At t = 60 min, when the magnetic field is removed for the *0 T – 0.4 T – 0 T* sample, the domains of the magnetic particles are no longer aligned and the average value of *G'* decreases from 140 kPa to 70 kPa. But this value of *G'* is 7 times higher than the value of the *0 T* sample at t = 60 minutes. Thus, the structural rigidity induced in the sample is not completely reversible when the magnetic field is removed; this behavior could be beneficial in reducing the formwork pressures of self-consolidating concrete or to avoid sloughing or slumping of shotcrete from its receiving surface (e.g. wall or other vertical element) after the shotcrete is sprayed. As time progresses, as shown in Figure 4.15 the

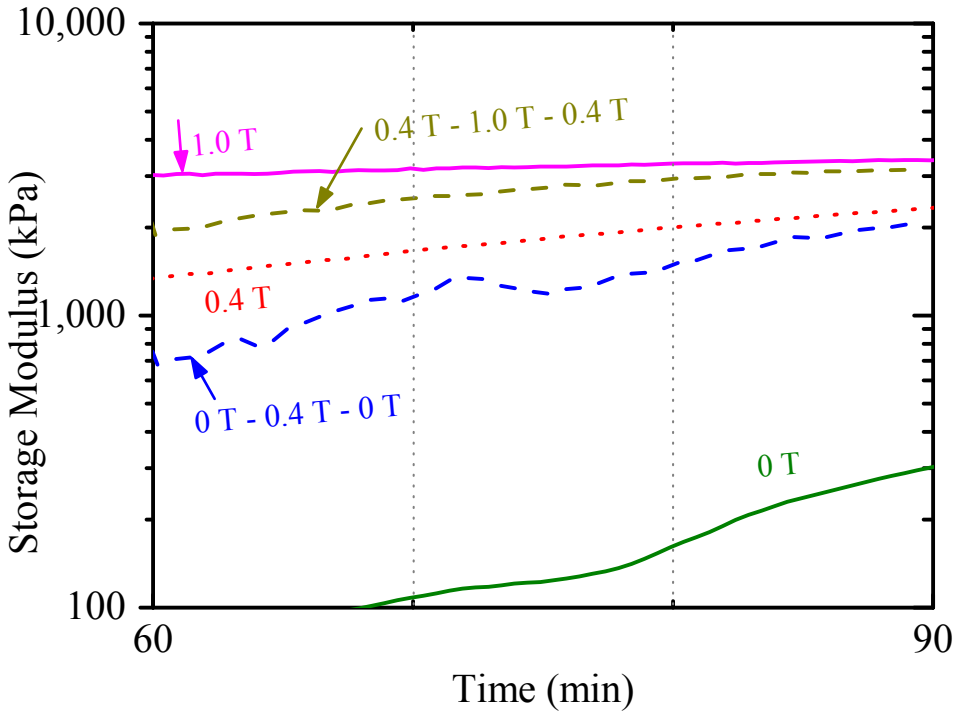

Figure 4.15 Storage modulus timesweep results during the last 30 minutes of *4CIP(sm)* sample with cyclic variation (low – high – low) of magnetic field strength every 30 minutes. Note that the y-axis is on a $\log_{10}$ scale.

value of *G'* continues to increase and at the end of the 90-minute duration, the average value of *G'* of the *0 T – 0.4 T – 0 T* sample is approximately 80% of the average value for sample *0.4 T* (applied continuously for 90 minutes), and it is almost 4 times the average value for sample *0 T* (applied continuously for 90 minutes).

Thus to summarize, for the *0 T – 0.4 T – 0 T* sample, when the magnetic field strength is increased from 0 T to 0.4 T at 30 minutes, the value of *G'* is dependent on the strength of the chains formed by the magnetic particles. Beyond this the *G'* value increases due to flocculation, thixotropy and cement hydration and matches up with the evolution of *0.4 T* applied continuously. When the magnetic field is removed at 60 minutes, the structure is not completely reversed to the state of *0 T* applied continuously but the value of *G'* is almost 7 times higher. A similar trend is observed in the evolution of *G"* and the values of *G"* were almost an order of magnitude smaller than those of *G'*.

4.7.2 SAOS: Field strength cycled from 0.4 T – 1 T – 0.4 T

At 30 minutes, for *0.4 T – 1 T – 0.4 T* when the level of magnetic field was increased from *0.4 T* to *1 T*, the value of *G'* decreased by a factor of 7 from an average value of 1100 kPa to 150 kPa. At t = 35 minutes, the value of *G'* for the *0.4 T – 1 T – 0.4 T* sample corresponds to the value of *1 T* exposed continuously for 5 minutes. (see Figure 4.14). Similar to the explanation given in the previous section, when the level of magnetic field

was increased, the elastic properties in the early stages are mainly due to the structure induced by the magnetic particle chains. When the magnetic particles move/rotate to form the chains, they could potentially break up the flocs and disturb some of the structure that was previously formed in the cement paste. At t = 30 minutes although there could have been a breakdown in flocs, beyond t = 30 minutes, the value of *G'* increases (probably because of a stronger influence of hydration) and by t = 59 minutes, *0.4 T – 1 T – 0.4 T* reaches a *G'* value that is similar to that of *1 T* applied continuously for 59 minutes.

At 60 minutes, when the magnetic field is reversed back to *0.4 T,* the value of *G'* drops by 30%. This drop in value is because of the break-up of some of the chains formed by the magnetic particles. The value of *G'* at t = 65 minutes is 1.5 times that of *0.4 T* applied continuously and it is 8 times higher than the value of *0.4 T* applied continuously at t = 5 minutes. Thus at t = 65 minutes, the structural rigidity in *0.4 T – 1 T – 0.4 T* is not only from the magnetic particle chains, but there is also a contribution from the flocculated structure. This leads to two hypotheses; first hypothesis being that the level to which the flocs are broken depends on the intensity of the applied magnetic field. This is because at t = 30 minutes when the magnetic field was changed from 0.4 T to 1 T, the value of *G'* was mainly dependent on the structure induced from the alignment of the particles. But at 60 minutes, when the magnetic field was changed from 1 T to 0.4 T, the value of *G'* was higher than the *G'* value from the alignment of the magnetic particles. This leads to the first hypothesis that there is a contribution from the suspending medium and that the level

to which the flocs are broken depends on the intensity of the applied magnetic field. The second hypothesis is that the flocs at t = 60 minutes have stronger bonds than those at t = 30 minutes and thus not all flocs are broken down at later stages. The second hypothesis can be verified by measuring the thixotropic properties of the sample at different durations. Thixotropy is a reversible phenomenon wherein cement particles floc or coagulate at rest and then breakdown during mixing because of the rupture of the interparticle bonds. But if the sample were not completely thixotropic (and if all the flocs cannot be broken down to reach the original state of the sample) then it would indicate an increase in floc strength. This was not examined here but would be an interesting test for future work.

Beyond t = 60 minutes, as time progresses, the value of *G'* continues to increase (see Figure 4.15) and at the end of the 90-minute duration, *G'* of *0.4 T – 1 T – 0.4 T* reaches a value similar to that of *1* T applied continuously, which is almost 1.5 times higher than the value of *0.4 T* applied continuously.

4.7.3 SAOS: Field strength cycled from 0.4 T – 0 T – 0.4 T

The *0.4 T – 1 T – 0.4 T* sample discussed in the Section 4.7.2 was subjected to a magnetic field strength of 0.4 T during the first 30 minutes and then the magnetic field was increased to 1 T. In the sample discussed here, the influence of reducing the magnetic field at 30 minutes is analyzed. For the *0.4 T – 0 T – 0.4 T* sample, the magnetic field

strength was decreased to *0 T* at 30 minutes. At t = 30 minutes, the value of *G'* instantaneously decreased by a factor of 4 (see Figure 4.16). When the magnetic field is removed, the magnetic particles are no longer linked, which leads to a reduction in the value of *G'*. At t = 35 minutes this value was still 11 times higher than the sample with *0 T* applied continuously for 35 minutes. Thus not all the structural rigidity is lost. This is consistent with the results discussed in sections 4.7.1 – 4.7.2 and further supports the premise that the microstructural arrangement of a cement-based MR fluid that has been subjected to the presence of a magnetic field is in a more flocculated state than a sample that has not been subjected to a magnetic field. Furthermore, this difference in the microstructural states can persist even if the magnetic field is removed. In addition, as time evolves the value of *G'* gradually increases and at t = 59 minutes, the value of *G'* for *0.4 T – 0 T – 0.4 T* was 6 times higher than the value for *0 T* applied continuously (at t = 59 minutes).

At 60 minutes, when the magnetic field is increased from 0 T to 0.4 T, the instantaneous change in the value of *G'* for the *0.4 T – 0 T – 0.4 T* sample doubles and almost reaches the *G'* value of the *0.4 T* sample. Similar to the results discussed in Sections 4.7.1 and 4.7.2, the value of *G'* at 60 minutes for *0.4 T – 0 T – 0.4 T* is not only because of the structural rigidity imparted by the magnetic chains but there is a contribution from the flocculated network of particles that are not completely broken down either due to the magnitude of applied magnetic field or due to an increase in the floc strength.

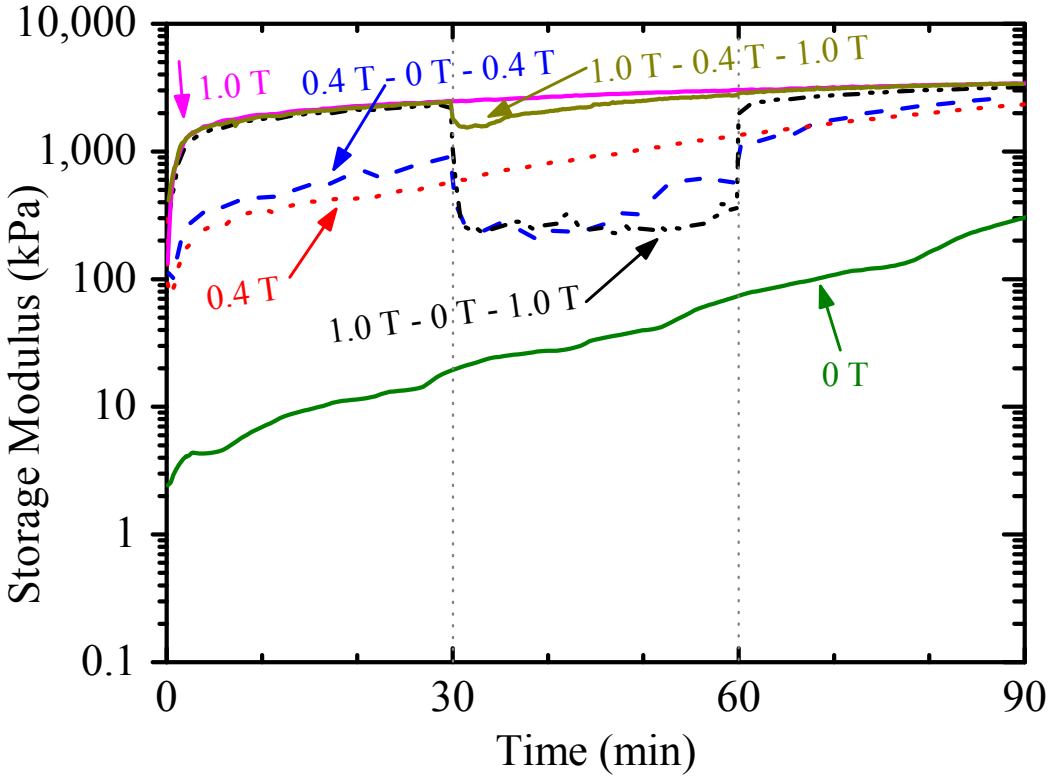

Figure 4.16 Storage modulus timesweep results of *4CIP(sm)* samples with cyclic variation (high – low – high) of magnetic field strength at every 30 minutes. Note that the y-axis is on a $\log_{10}$ scale.

Beyond t = 60 minutes, as time progresses, *G'* value of *0.4 T – 0 T – 0.4 T* continues to increase (see Figure 4.17) and follows a similar path to that of *0.4 T* applied continuously for the entire duration.

4.7.4 SAOS: Field strength cycled from 1 T to a low magnetic field and back to 1 T.

The evolution of the *1 T – 0 T – 1 T* sample is shown in Figure 4.16. At 30 minutes, when the magnetic field is removed, the value of G' decreases to 1100 kPa, but this value is 40 times higher than that of the *0 T* applied continuously for 30 minutes. Just before the change in magnetic field (at t = 29 minutes) the *1 T – 0 T – 1 T* sample is in a highly flocculated state since a high magnetic field (1 T) was applied to it. But when the magnetic field is removed, the magnetic chains relax leading to loss of structure in the sample, but the sample appears to retain a significant portion of the structure. The *1 T – 0 T – 1 T* sample appears to maintain its structure between t = 30 minutes and t = 60 minutes as there isn't a significant difference in the evolution of *G'* which leads to the hypothesis that at t = 30 minutes with 1 T magnetic field applied, the paste is in a highly flocculated state and that there is no further occurrence of flocculation. At 60 minutes when the magnetic field is increased back to *1 T,* the *G'* value of the *1 T – 0 T – 1 T* sample increases by 5 times to 1700 kPa. This value of G' is approximately half that of *1 T* applied continuously for 60 minutes. As shown in Figure 4.17, *1 T – 0 T – 1 T* trails behind the evolution of *1 T* applied continuously and matches up by 90 minutes.

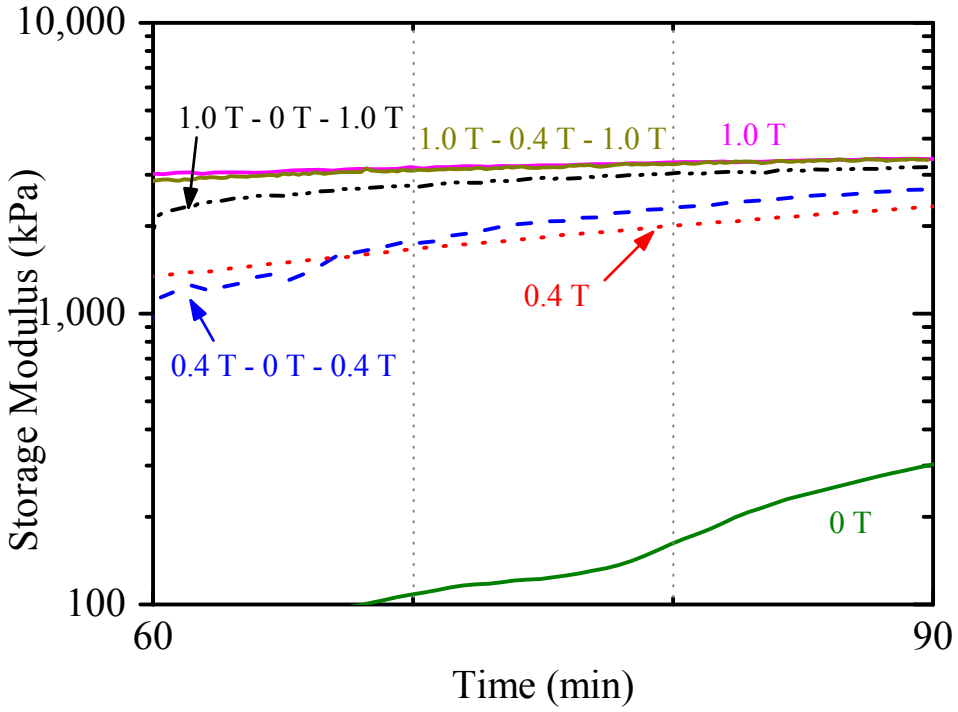

Figure 4.17 Storage modulus timesweep results during the last 30 minutes of *4CIP(sm)* sample with cyclic variation (high – low – high) of magnetic field strength every 30 minutes. Note that the y-axis is on a $\log_{10}$ scale.

The evolution of *1 T – 0.4 T – 1 T* is shown in Figure 4.16. At 30 minutes when the magnetic field is reduced to *0.4 T*, the value of *G'* drops by 1.5 times to 1700 kPa, but this value is 3 times higher than that of *0.4 T* applied continuously for 30 minutes. This follows the hypothesis (from *0.4 T – 1 T – 0.4 T)* that the level to which the flocs are broken may depend on the intensity of the applied magnetic field. Thus, for *1 T – 0.4 T – 1 T,* at t = 30 minutes, there is a major contribution from both the magnetic particle alignment and from flocculation. At 60 minutes when the magnetic field is increased to *1 T,* the evolution of *G'* follows the path of the *1 T* sample. This is different than the

evolution of *1 T – 0 T – 1 T* where the values of *G'* during the last 30 minutes were smaller than those of the *1 T* sample. This leads to the conclusion that the magnitude of the applied field has an influence on the microstructural development in the sample.

4.8 CONCLUSIONS

A smart cement-based material has been developed whose fresh-state rheological properties can be controlled in real-time. It has been shown that by incorporating magnetic particles and by applying a magnetic field, the rheological behavior of cement paste can be controlled. It has been shown that although unhydrated cement is a weak ferromagnetic material, the rheological response of cement paste does not vary with the level of applied magnetic field strength. But, by incorporating *CIP* particles, the fresh state properties of cement paste were altered significantly. By varying the level of applied magnetic field, the response of the paste can be custom tailored to the required behavior. By extension, similar behavior can potentially be obtained from mortar/concrete.

The response of the cement-based MR fluid can also be tweaked by varying the dosage of the magnetic particles. Within the first 30 minutes, by doubling the quantity of magnetic particles, the shear moduli values doubled in value. At 90 minutes, they reach similar values suggesting that *CIP* magnetic particle concentration plays a minor role on the magnitude of the later age (> 90 min) rheological response, and leads to the possibility of optimizing the magnetic particle dosage to tailor the rheological response, especially at

earlier ages. The suspending medium rheological properties only had an effect at low magnetic fields (up to ~ 0.4 T). At larger magnetic field strengths, the rheological response was similar. By varying the particle sizes from a d_{50} of 8.7 μm to d_{50} of 3.3 μm, neither the shear moduli nor the yield stress values were significantly affected.

Through cyclic variation of applied magnetic field, it was found that the structural rigidity of the sample depends on the initial magnitude of the applied field, the magnitude to which it is changed and the age of the sample. It was found that by removing the magnetic field, the elastic properties of cement paste are not completely lost and that there is some structural integrity left in the sample. This is could be beneficial in reducing the formwork pressures of self-consolidating concrete or for avoiding slumping/sloughing of shotcrete.

CHAPTER 5: EFFECT OF MAGNETIC PARTICLES AND MAGNETIC FIELD ON CEMENT HYDRATION

Cement hydration is a complex process that starts when cement comes in contact with water. Several studies have been conducted to understand the chemical reactions that occur during hydration and to understand the composition and the different phases of compounds present in cement paste. A few of the techniques used to understand hydration kinetics are to: monitor the strength development in cement paste, observe the heat evolved during the exothermic hydration process and examine the hydration products through X-ray diffraction. These techniques were used in the work presented in this chapter to study the influence of *CIP* magnetic particles and magnitude of magnetic field strength on hydration of cement-based MR fluids. Based on current literature it has been shown that 5% additions of mineral additives did not have an impact of the time of appearance of the main heat evolution peak (Barker 1990). However addition of crystalline materials at higher dosage (20-40%) of particles has been shown to improve pozzalonic activity (Rahhal et al. 2012). Based on the small dosage of magnetic particles used in this study (4% by volume of cement) it was hypothesized that the presence of the particles and the application of magnetic field would not affect the hydrations kinetics and would not influence the morphology of the hydrates.

5.1 COMPRESSIVE STRENGTH

5.1.1 Description of Experimental Method for Compressive Strength Evaluation

The *Control, 2CIP* and *4CIP* samples were prepared according to the procedure stated in Section 3.3 and were placed in 2 in. × 2 in. cubes metal molds. The specimens were maintained at 73 $\pm$ 2 °F temperature and 100% relative humidity for 24 hours after casting without any magnetic field. Then, the specimens were de-molded and placed in a limewater bath (3g of lime for 1 liter of water) at room temperature (74 ± 2 °F) until they were tested without any magnetic field. Triplicates of samples were tested at 1 day, 7 days, 28 days and 90 days for each of the samples (*Control, 2CIP* and *4CIP)* using a compression-testing machine.

5.1.2 Results and Discussion

Figure 5.1 shows the compressive strength of *Control*, *2CIP* and *4CIP* at 1 day, 7 days, 28 days and 90 days after mixing. None of the samples were subjected to a magnetic field. At 1 day the compressive strengths of the *2CIP* and *4CIP* samples were slightly higher than that of the *Control* sample. At 7 days, the compressive strengths of all the samples evaluated were similar in value. However, at later ages there appears to be a larger effect on compressive strength when 4% CIP particles were added. At 90 days the average compressive strength of the *4CIP* sample was higher by 10% compared to that of

the *Control* sample. This increase in compressive strength could be due to the higher specific gravity of *CIP* (7.8) compared to the specific gravity of cement (3.15). However, overall the general trend was that the CIP particles have a negligible effect or slightly increase the strength.

5.2 HEAT OF HYDRATION

5.2.1 Basics

Right after cement is mixed with water, complex hydration reactions start to occur. These reactions are exothermic and the heat generated can be correlated with important properties such as initial set and final set ((Bentz and Ferraris 2010), marked on Figure

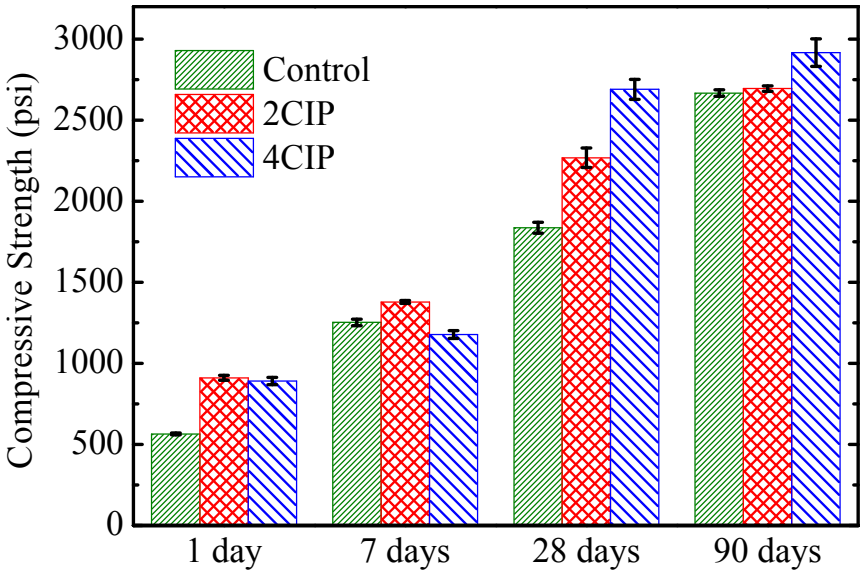

Figure 5.1 Influence of *CIP* dosage on compressive strength. The error bars are based on three samples.

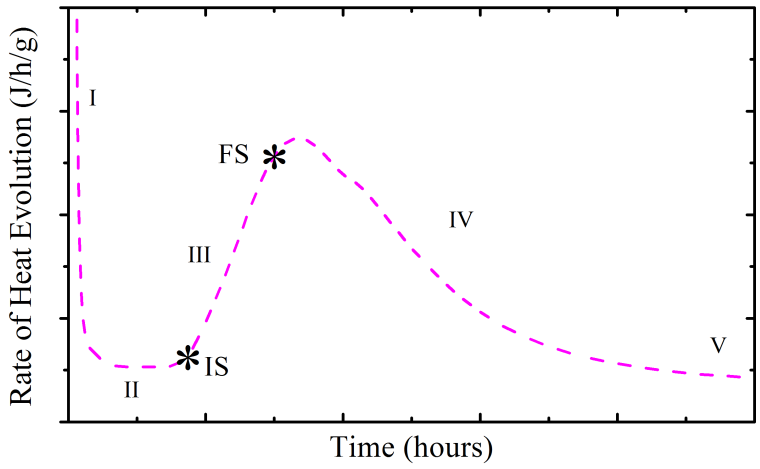

Figure 5.2 Typical heat of hydration curve for a cement paste measured using an isothermal calorimeter. Onset of Stage III is an indicator for initial set (IS) and the end of Stage III is an indicator for final set (FS)

5.2); which have a direct impact on the pumping, placing and finishing processes of concrete. Figure 5.2 shows a typical rate of heat evolution of a cement paste measured using an isothermal calorimeter. There are five significant stages in the plot (Mindess, Young, and Darwin 2003; Gartner et al. 2002).

The five stages are:

I. Initial hydrolysis: This stage is marked by a rapid evolution of heat, which is caused from the initial heat of wetting. During this stage dissolution of the ions occurs from the different cement phases (such as C_3S, C_2S, C_3S, C_4AF, gypsum). This leads to rapid formation of ettringite (AFt and AFm phases), which have an influence on the rheological properties and the microstructure development of the cement paste. The initial peak due to dissolution is typically not fully captured in

Stage 1 due to the fact that it occurs very early on and a lot of heat is released in the time frame that it takes to load a freshly prepared sample into the calorimeter.

II. Induction period: The rate of heat evolution slows down compared to that of Stage I. During this stage, ions of some phases continue to dissolve, ettringite continues to form and nucleation and precipitation of early C-S-H occurs, all of which affects the rheological properties of the sample. During the induction period (time duration before occurrence of initial set), it has been shown that there is a moderate increase in the yield stress (approximately 500 Pa to 1000 Pa at w/c of 3.0) along with an increase in the viscosity of the paste (Amziane and Ferraris 2007). As shown in Section 4.3.5, moderate increases in yield stress can be achieved instantaneously by using the MR approach by applying a small magnitude of magnetic field (up to 0.2 T). The stiffening behavior of the cement paste can be altered to any required degree by using the MR approach.

III. Acceleration phase: Stage III indicates the acceleration in growth of hydration products and the consistency of the paste changes from a viscous fluid to a viscous solid. The time at onset of Stage III is used as an indicator for initial set (actual value can be measured through penetration testing). Similarly, the time at the end of Stage III has been linked to the final set of cement paste. Beyond initial set, Amziane and Ferraris (2007) have reported an increase in yield stress (at a higher rate compared to those of Stage II) from approximately 1000 Pa to 3000 Pa. This range of changes in values of yield stress can be brought about

instantaneously with the application of a larger magnetic field (see Sections 4.3.5 and 4.4.2 for more details).

IV. Deceleration phase: This stage is indicated by a continuous decrease in the rate of heat evolved. The hydration products continue to form in this stage but the rate of heat evolution begins to slow down because of continuous reduction in available space and ions.

V. Steady state: The rate of heat evolved stabilizes to a very low rate of heat evolved which is an indicator of a slow down in the formation of hydration products.

Thus, stages II and III have a significant impact on the rheological properties of cement paste and determine the stiffening behavior of the paste from a fluid to a rigid solid.

In the previous chapter it was shown that major changes in the rheological properties could occur from the use of an MR approach. Traditionally in order to obtain such large differences a chemical admixture would have to be used, and these chemical admixtures may predominantly affect the rate of heat evolution of Stages II and III. On similar lines, the results from this section and the next section (5.3) are used to determine whether the large changes observed in the rheological properties through an MR approach are accompanied with any changes in hydration kinetics and morphology of the hydrates.

5.2.2 Description of Experimental Methods for Heat of Hydration Analysis

After preparing the cement-based MR paste using the procedure mentioned in Section 3.3, approximately 10 g of each sample was weighed into glass bottles and placed in a calorimeter. A multichannel isothermal calorimeter (3114/3236 TAM Air, Thermometric AB, Sweden) was used to measure heat flow from the sample to a heat sensor. All the channels were in a temperature controlled environment at 23 °C. PicoLog software was used to collect data and the data was collected for 72 hours. The sample was placed in the calorimeter approximately 7 minutes after the cement and water first came in to contact, thus the main peak due to dissolution was not completely captured. Each sample was replicated three times with freshly mixed paste. The hydration graphs shown are based on a representative curve from one of the replicates.

5.2.3 Results and Discussion

Figure 5.3 shows heat evolution during hydration of the *Control*, *2CIP* and *4CIP* samples without any magnetic field for a duration of 24 hours. Any retardation of the hydration reactions could cause delays in setting, thus it is important that the addition of magnetic particles does not cause significant retardation. Indeed it can be seen that the presence of particles does not affect the rate of heat evolution significantly and it also does not affect the shape of the curve expect for the peak values occurring at the end of stage III. For example, in all the samples Stage III begins at around 1 hour (which is an indicator of initial set) and stage III ends around 5 hours (which is an indicator of final set) which

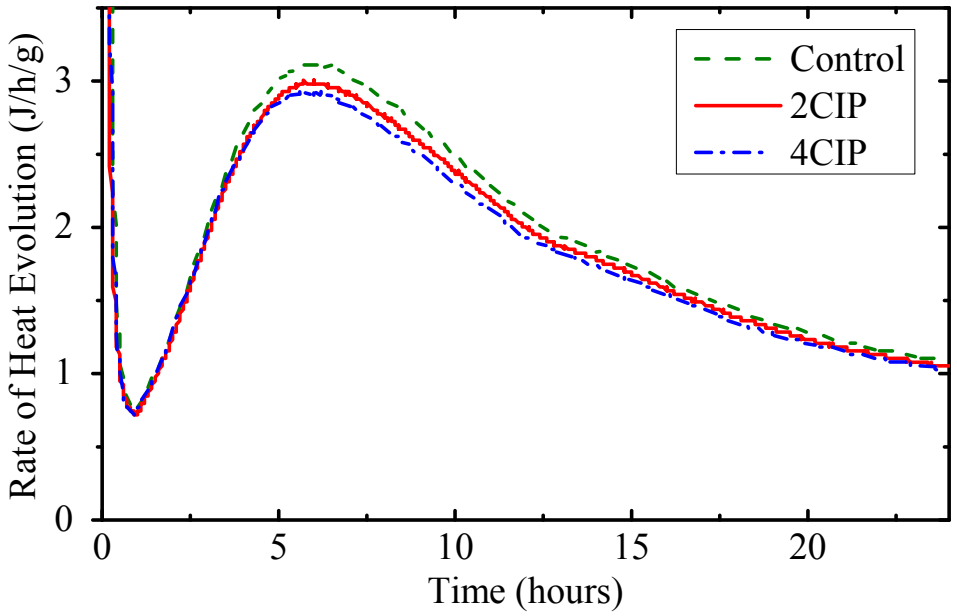

Figure 5.3 Heat of evolution curve (based on weight of total paste; cement + water + specified dosage of CIP), with varying dosages of CIP magnetic particles without any magnetic field for 24 hours. The curves are a representative of 3 samples. For all the samples, onset of Stage III occurred around 1 hr.

shows that the presence of the magnetic particles does not affect the hydration reactions of the cement paste and thus will not have an influence on construction times. As neither the end of induction period (beginning of Stage III) nor the rate of heat evolved during Stage III is affected by the particles it can be postulated that the presence of magnetic particles are not affecting the stiffening and hardening behavior of the sample.

As stated earlier, although there is no effect of the particles on the shape of the curve for all the samples, there is a difference in the peak value occurring at the end of Stage III.

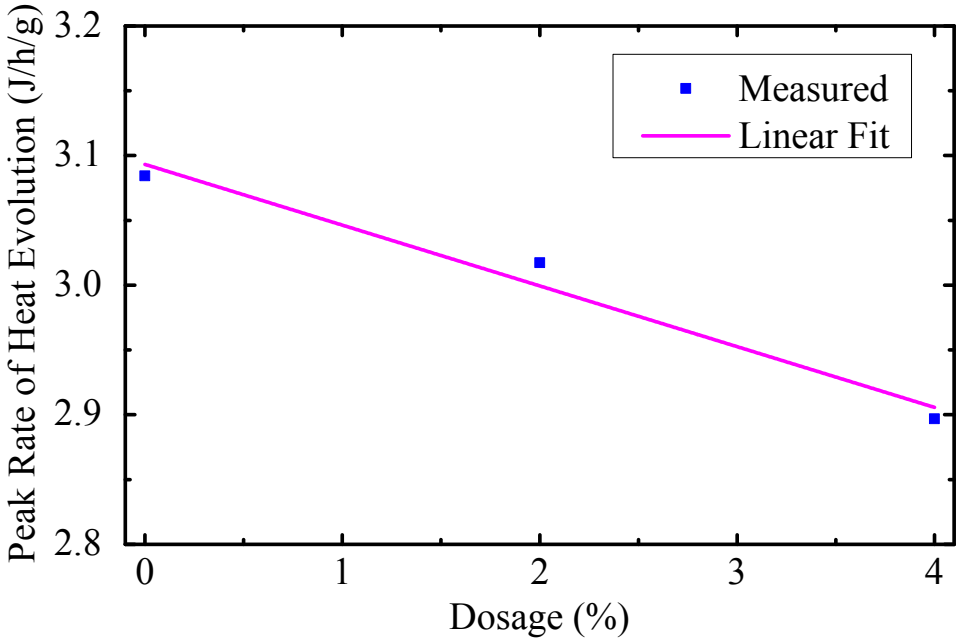

Figure 5.4 Maximum peak rate of heat evolution from Figure 5.3 for samples *Control*, *2CIP* and *4CIP* in the absence of magnetic field.

Figure 5.4 shows the changes in the peak values (occurring after 5 hours) in the rate of heat evolution. It can be seen that the peaks vary linearly based on the dosage of *CIP* magnetic particles. This decrease in peak value with increasing dosage of *CIP* particles can be explained through the dilution effect where, in a given volume, a certain percentage of cement is replaced by the *CIP* magnetic particles effectively reducing the amount of cementitious material. Thus, it can be concluded that the *CIP* magnetic particles do not have cementitious properties and do not affect early age hydration of cement paste.

5.3 HYDRATION PRODUCTS

5.3.1 Basics

Evolution of hydration products were monitored though powder X-ray diffraction studies. Powder diffraction can be used mainly to study the crystalline phases, which produce a distinctive diffraction pattern. Identification is performed by comparison of the diffraction pattern to a known standard or to a database. Qualitative information for the phases present in the hydrated pastes were obtained using the Hanawalt manual and the Jade program (MDI) (JCPDS 1989)

As mentioned in Chapter 2, the main phases in a non-hydrated cement powder are C_3S, C_2S), C_3A and C_4AF. When cement comes in to contact with water, over time these phases change to ettringite, porlandite (CH), calcium silicate hydrate (C-S-H) etc. The first five major peaks of the crystalline phases were obtained from the Jade program (MDI) and are shown in Table 5.1. For a qualitatively analysis it can be assumed that the presence of five major peaks for a specific phase at the specified 2-theta angles indicates the presence of that phase in a sample.

Table 5.1: 2θ angles (along with the standard relative intensities) for the major peaks of ZnO (internal standard), different phases in unhydrated and hydrated cement paste.

	1st Peak		2nd Peak		3rd Peak		4th Peak		5th Peak	
	2θ	*Rel. Int.*	*2θ*	*Rel. Int*	*2θ*	*Rel. Int*	*2θ*	*Rel. Int*	*2θ*	*Rel. Int*
ZnO	36.3	100	31.8	57	34.4	44	56.6	32	62.9	29
C_3S	34.4	100	32.3	85	32.7	75	29.5	75	41.4	60
C_2S	32.8	100	29.6	80	32.5	70	47.6	60	23.3	50
Fe	44.7	100	65	20	82.3	30	99	10		
Ettringite	9.1	100	15.8	76	22.9	31	35	29	32.3	25
Calcite	29.4	100	39.4	18	43.2	18	47.5	17	48.5	17
CH	34.1	100	18.1	74	47.1	42	50.8	36	28.7	23

5.3.2 Description of Experimental Method for Cement Hydration Phase Analysis

After compression testing, approximately 10 g of hardened cement paste samples were collected from the center of the cubes (at 1 day and 90 days). Then, the paste sample was ground in ethanol using a mortar and pestle. Grinding in ethanol ensures that the pore water in the paste will be exchanged with ethanol (thus stopping hydration) and will preserve the chemical composition of the paste sample (Zhang and Scherer 2011). The ground paste was placed in a vacuum desiccator for at least one day to ensure drying. Then, the ground paste powder was passed through a 100 μm sieve and 2 g of the sieved paste powder was mixed with 0.2 g of zincite (ZnO). ZnO serves as an internal standard

for the XRD analysis, and 0.2 g gram was mixed with the paste powder since this is equates to 10% of the mass of the paste powder. ZnO is used as an internal standard because ZnO does not interfere with any of the major peaks from the phases present in both unhydrated and hydrated cement paste. This adds an additional benefit for Rietveld analysis. The sieved powder paste and the zincite were mixed together using ethanol in an agate mortar and pestle and were left to air dry. Then, the paste-zincite sample was compacted into a plastic sample holder using a glass slide. A razor blade was used to remove excess powder to ensure a flat surface. Following this, the samples were run in a powder X-ray diffractometer (XRD, Seimens D-500 Cu K_α, λ=1.5046 Å). The diffractometer was operated at 40 keV and 30 mA, at a step size of 0.02° 2θ, a dwell time of 6 s, and a scan range of 5°-70° 2-theta.

In order to examine whether subjecting paste to a magnetic field will influence the hydration products, specimens were prepared from magnetorheological cement paste samples that were subjected to 4 hours of a constant magnetic field. To achieve this, cement paste was placed in the rheometer between the parallel plates and a magnetic field was applied without any other loading parameters for the specified period of time. At the end of the time frame the sample was removed from the rheometer and the entire sample was then ground in ethanol using an agate mortar and pestle. The samples were then placed in a vacuum desiccator for at least one day to ensure drying, after which the samples were passed through a 100 μm sieve, mixed with zincite (to serve as internal standard), and the paste-zincite sample was compacted into the sample holder. The

samples were run in a powder XRD with the same parameters mentioned in the previous paragraph.

5.3.3 Results and Discussion

Figure 5.5 (a) shows the X-ray diffraction patterns of the *Control* sample at 0 T magnetic field and Figure 5.5 (b-d) shows the pattern for *4CIP* at 0 T, 0.4 T and 1 T magnetic field strengths at 4 hours after mixing the samples. The y-axis shows the relative intensity with respect to the 1st peak of ZnO at 36.3° (2θ). In the figure the location of the peaks (shown in Table 5.1) for the different phases in both hydrated and unhydrated cement are identified. The relative intensity of iron occurring at 44.7° (2θ) is 0.09 for the *Control* sample at 0 T, this is in fact so weak that the peak is not even noticed in the plot. Whereas the relative intensity for the *4CIP* sample at 0 T is 0.8, which is comparatively higher because of the presence of 4% CIP particles by volume of cement.

The influence of a magnetic field on the cement hydrates can be evaluated by comparing Figure 5.5 (b-c). With an increase in magnetic field strength there is a slight increase in the relative intensity peak at 32.1° (2θ) which has contributions from C_2S, C_3S (unhydrated cement phases) and ettringite (hydrated cement phase). The peak value increases from 0.8 for *4CIP* at *0 T* to 1.2 for *4CIP* at *1 T*, but through a qualitative analysis there is no way to identify the percentage contribution of the different phases to the peak value. However, these differences are quite small and it can be concluded that

the presence of particles and the applied magnetic field does not affect majority of the peaks of early age hydration products.

Figure 5.6 shows the X-ray diffraction patterns of *Control* and *4CIP* at 1 day and 90 days. Apart from differences in the relative intensities of iron mentioned above, no major changes were observed between the *Control* and *4CIP* samples at both 1 day and 90 days. By this it can be concluded that the particles do not affect long-term hydration products and that the use of magnetic particles for the MR approach does not influence the quantity of cement hydrates.

5.4 SUMMARY

It was found that *CIP* particles did not affect the rate of strength gain in compressive strength up to 90 days (the longest duration considered in this study). From heat of hydration curves it has been found that *CIP* magnetic particles do not have cementitious properties and do not affect early age hydration of cement paste (measured up to 72 hours). Through crystalline phases detected using X-ray diffraction it was also found that *CIP* particles do have an effect on the evolution of hydration products up to 90 days (the longest duration considered in this study). There was also no significant change in the early age hydration products when different magnetic fields strengths were applied to the cement-based MR fluid for 4 hours.

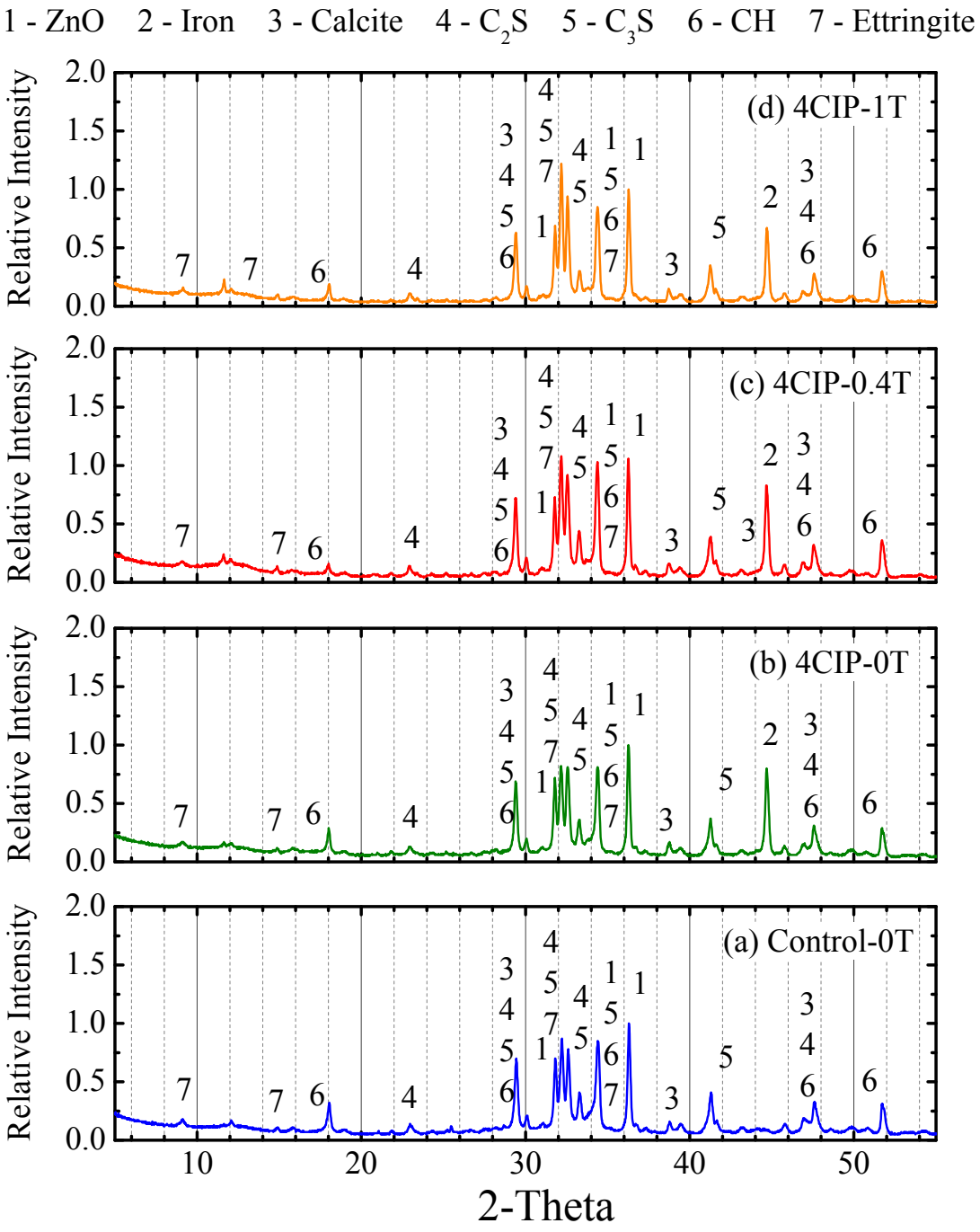

Figure 5.5 XRD qualitative analysis of samples with 0% and 4% CIP particles at 4 hours after applying the specified magnetic field. Y-axis is relative intensity (ratio of intensity with ZnO major peak intensity)

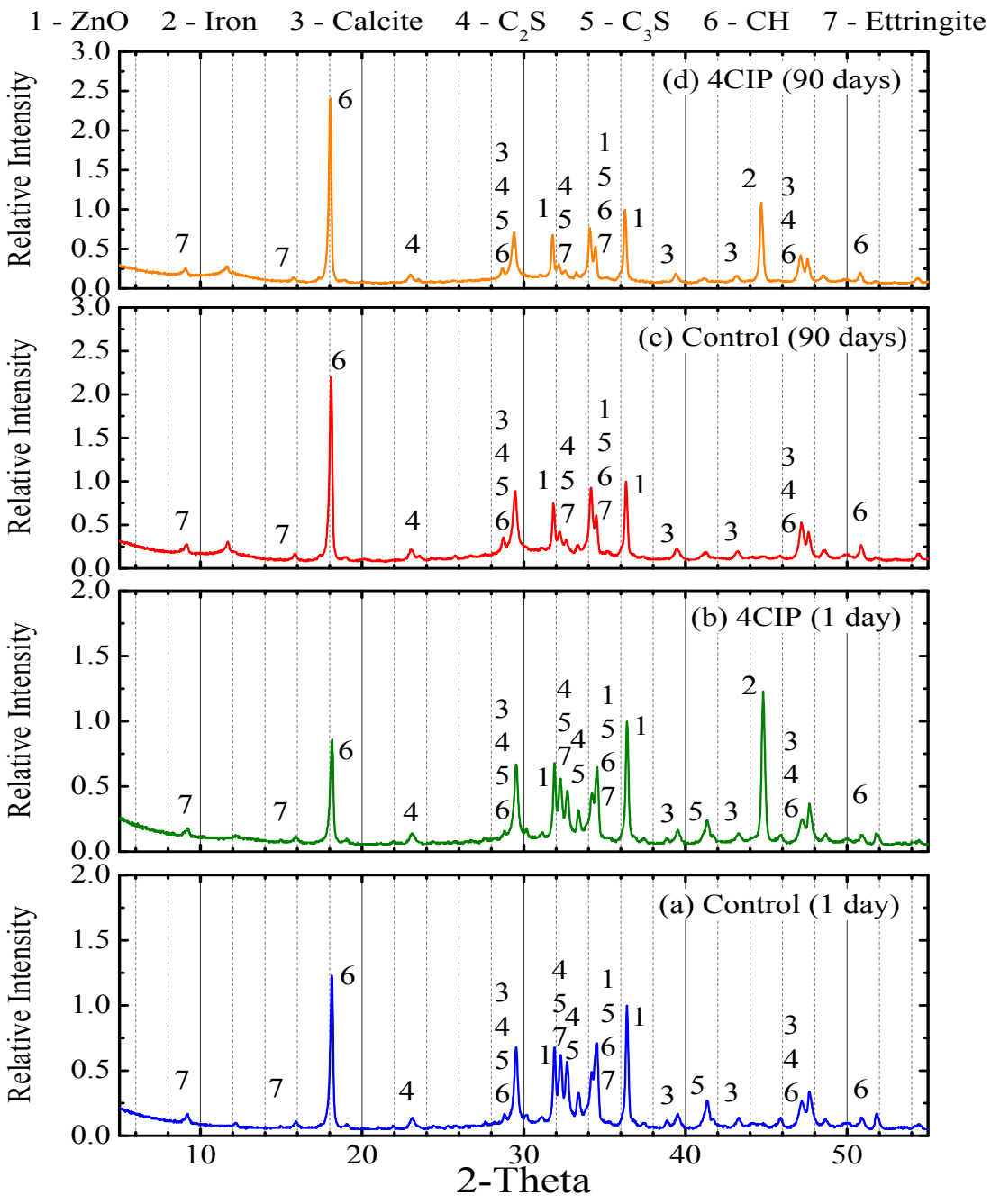

Figure 5.6 XRD qualitative analysis of samples with 0% and 4% CIP particles at 1 day and 90 days after casting the samples without any magnetic field. Y-axis is relative intensity (ratio ZnO major peak intensity)

In this chapter through compressive strength tests, heat of hydration curves and by examining the hydration products through power X-ray diffraction it has been established that the magnetic particles used for the MR approach and the applied magnetic field do not affect the hydration kinetics and morphology of the hydrates. Thus the predominant rheological changes observed in Chapter 4 using the MR approach are not accompanied by any significant changes in the hydration of cement paste.

CHAPTER 6: EFFECT OF TYPE OF MAGNETIC PARTICLES ON THE RHEOLOGICAL PROPERTIES OF CEMENT-BASED MR FLUID

To understand the effect of type of iron particles rheological properties of cement paste containing electrolytic iron powder, *Fe(E)* or hydrogen reduced iron powder, *Fe(H)* are compared with those containing carbonyl iron powder, *CIP*. The properties of cement-based MR fluids containing iron oxide (Fe_3O_4), (which has almost 1/3rd the magnetic properties of *CIP* and a particle size distribution that is smaller than that of *CIP*) . *4CIP, 4Fe(E), 4Fe(H) and* $4Fe_3O_4$ cement-based MR fluids were prepared with same dosages of magnetic particles by volume. The mix proportions are shown in Table 3.5, and the samples were prepared according to Section 3.3. Rheological tests such as small amplitude oscillatory shear (SAOS) tests and stress growth tests (see section 2.2 for description of these tests) were performed for all the cement pastes containing the above-mentioned particles. The samples were subjected to different magnitudes of magnetic field strength in order to determine the effect of iron particle type on the viscoelastic properties of the field induced cement-based MR fluid. The rheological tests were performed according to the procedures outlined in Section 4.1.

6.1. SAOS: Results and Discussion

6.1.1 Timesweep SAOS: Electrolytic Iron Powder

As discussed in Chapter 3, *Fe(E)* particles (d_{50} = 27.9 μm) are almost three times larger in size than those of *CIP* (d_{50} = 8.7 μm) (even the d_{10} and d_{90} values are three times larger). While *CIP* particles are almost spherical, *Fe(E)* particles have an irregular shape because they are ground into smaller particles from large chunks of iron deposited on the

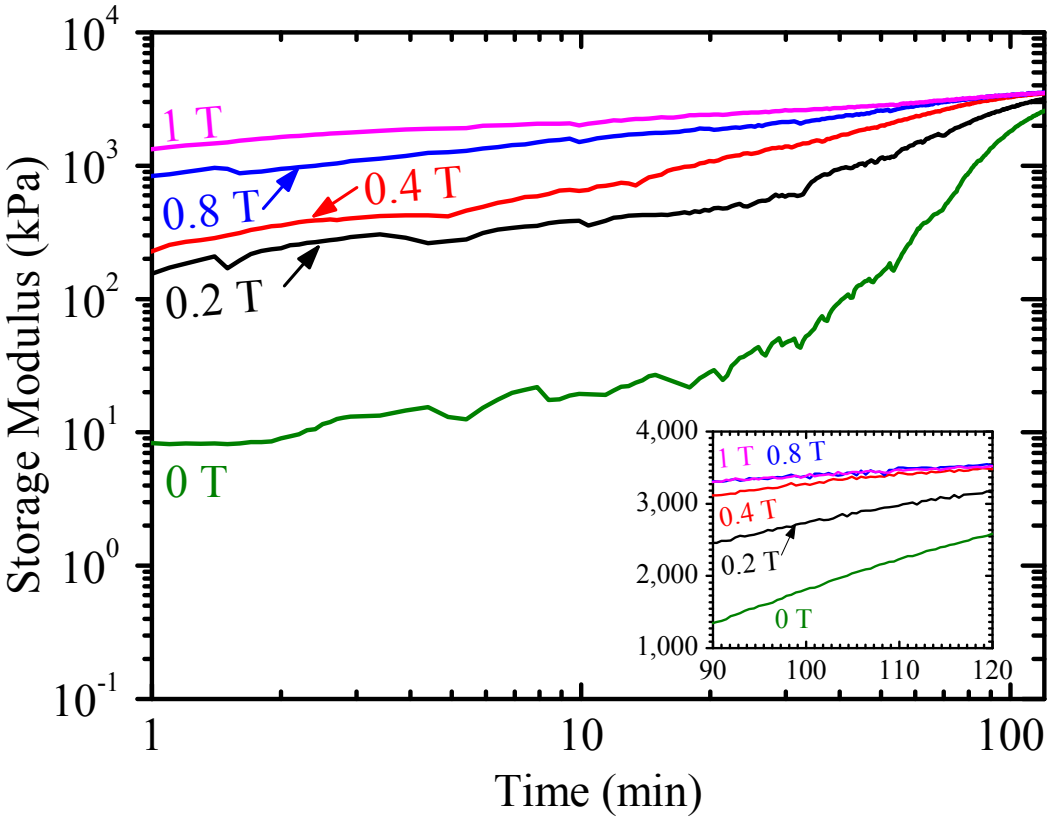

Figure 6.1 Influence of applied magnetic field strength on the storage modulus evolution of *4Fe(E)* over duration of 120 minutes. Note that both the axes are plotted on a $\log_{10} - \log_{10}$ scale. Inset shows the evolution for the last 30 minutes on a linear-linear plot.

electrodes. Both *Fe(E)* and *CIP* particles used in this study are composed of high purity iron. Both have similar magnetization saturation values, but *Fe(E)* has a volume susceptibility (6.7) that is almost 30% higher compared to that of *CIP* (5.2).

Figure 6.1 shows the evolution of *G'* (storage modulus or elastic component) of *4Fe(E),* at different magnetic field strengths over a span of 120 minutes. It can be seen that as the magnitude of the magnetic field strength was increased, there was a substantial increase in the values of *G'*. The inset in Figure 6.1 shows the evolution of *G'* during the last 30 minutes of *4Fe(E)* wherein it can be seen that beyond 90 minutes, both the evolutions at

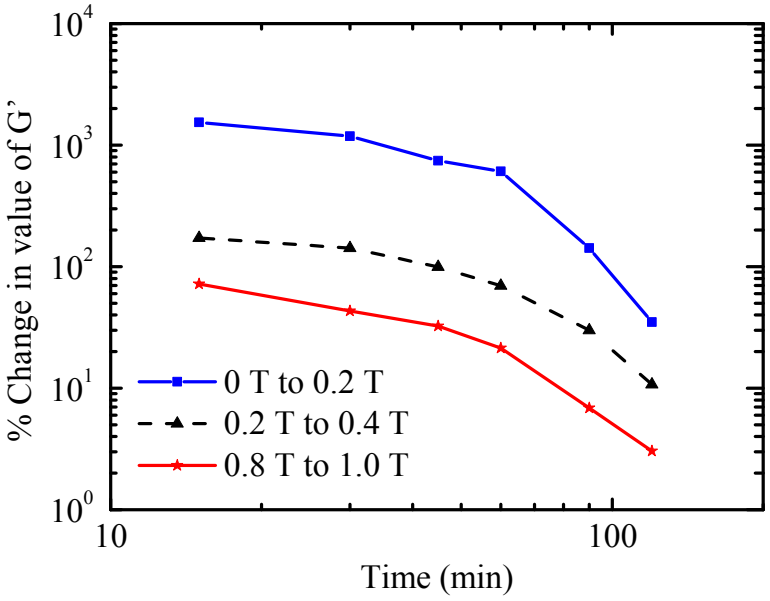

Figure 6.2 Percentage change in the values of *G'* when the magnetic field was increased by 0.2 T (values shown for a duration of 15 – 120 minutes). Note: when the magnetic filed was increased from 0.2 T to 0.4 T, the % change in the value of G' was calculated based on the 0.2 T value at the specified time period. Both axes are plotted on a $\log_{10}$-$\log_{10}$ scale.

0.8 T and 1 T were very similar. As shown in Figure 6.2, for *4Fe(E)* at 15 minutes when the magnetic field was increased from 0 T to 0.2 T, there was approximately an 1500% increase in the value of *G'*; at 45 minutes the increase was 740% and at 120 minutes, there was still an increase in value by 35%. However, when the magnetic field was increased from 0.2 T to 0.4 T, the % increase in values of *G'* were lower compared to those when magnetic field was increased from 0 to 0.2 T and along the similar lines, the percent increase was the lowest in the case when the magnetic field was increased from 0.8 T to 1.0. In all these cases, although the change in magnetic field strength was held constant (0.2 T), at any given point of time the percent change in values of *G'* for the *4Fe(E)* sample appears to be dependent on the magnitudes of the magnetic field strengths and the percentage change in the value of *G'* decreases with increasing magnitude of the field strengths.

Now comparing the evolution of *G'* for *4Fe(E)* with that of *4CIP* (shown in Figure 4.5 and summarized in Table 6.2) it can be seen that there is a considerable difference in the values of *G'* based on the level of the applied magnetic field. In the absence of magnetic field (0 T), both *4CIP* and *4Fe(E)* have a similar evolution (see Table 6.2 for average values of *G'*). As stated in Section 4.2.1, in the absence of magnetic field, the continuous increase in the values of *G'* are attributed to mechanisms such as flocculation and cement hydration. But when a magnetic field is applied, there is a significant increase in the value of *G'* right after the application of field. As stated in Section 4.3.2 this initial increase is from the alignment of field induced magnetic dipoles in the magnetic particles

and the formation of chain-like structures of magnetic particles when a magnetic field is applied. Beyond the initial stages, due to cement hydration and flocculation, there is a continuous increase in the value of *G'* over the testing duration.

When a magnetic field was applied, the *4Fe(E)* sample consistently displayed higher values for shear moduli compared to those displayed by *4CIP*. As shown in Table 6.2, during the first 60 minutes when a 0.2 T magnetic field was applied, the *G'* of *4Fe(E)* was higher by a factor of 1.5 compared to the value of *4CIP;* but by 120 minutes they reached similar values. A similar trend occurred when the *4Fe(E)* and *4CIP* samples were exposed to magnetic fields of 0.4 T. However, at 0.8 T and 1 T applied fields, the *G'* evolution of samples *4Fe(E)* and *4CIP* were similar. This leads to the first conclusion that at higher magnitudes of magnetic fields (> 0.4 T) the particle type does not seem to be playing a significant role.

This trend can be explained with the help of Figure 6.3, which shows the magnetization curves of *Fe(E)* and *CIP* raw powders. From the figure it can be seen that at 0 kOe, i.e. in the absence of magnetic field, both the particles are completely demagnetized and have zero magnetization. As the applied magnetic field was increased from 0 kOe, the difference between the magnetization values of *Fe(E)* and *CIP* grew larger and at 0.6 kOe the difference was maximum with the value of magnetization for the *Fe(E)* powder being 25% higher than that of *CIP*. By 5 kOe applied field (= 0.5 T in vacuum), the magnetization values of *Fe(E)* were similar to those of *CIP*. Thus, it can be concluded

that up to a magnetic field of 5 kOe (= 0.5 T in vacuum), compared to *CIP* the higher magnetization values of *Fe(E)* resulted in a higher rigidity in the *4Fe(E)* compared to those of *4CIP*. Beyond 5 kOe, the magnetization values for *Fe(E)* and *CIP* are within a range of 3% of each other because of which at 0.8 T and at 1T, *4Fe(E)* and *4CIP* have similar evolutions in the values of *G'*.

The second conclusion from the evolution of *4Fe(E)* compared to that of *4CIP* is that at longer durations of time (beyond 60 minutes) the particle type does not seem to have a significant effect on the field induced elastic properties of the MR fluid, which may be because the hydration forces are starting to play a more dominant role in the formation of

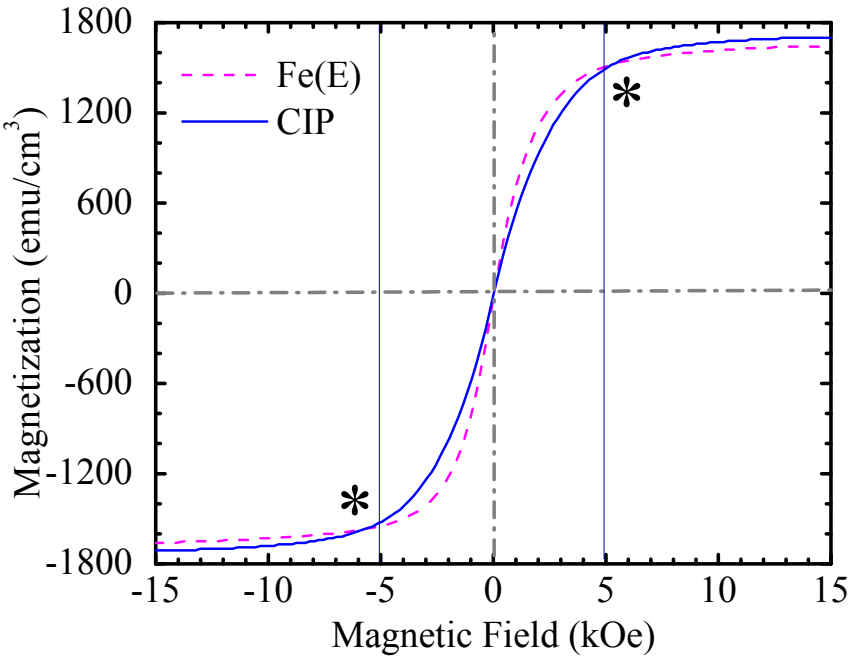

Figure 6.3 Magnetization curves of *Fe(E)* and *CIP* powders. *5 kOe (= 0.5 T in vacuum).

the internal structure.

Table 6.1 Rate of change of storage modulus ($\partial G'/\partial t$) of the representative curves

Sample	*Magnetic Field (T)*	*∂G'/∂t (kPa/min)*	
		0-2 min	*90-120 min*
4CIP	0	0.6	55
	0.2	15	35
	0.4	96	23
	0.8	320	14
	1.0	380	7
4Fe(E)	0	1.3	35
	0.2	100	24
	0.4	180	11
	0.8	480	8
	1.0	800	7
4Fe(H)	0	0.9	51
	0.2	40	35
	0.4	100	23
	0.8	330	14
	1.0	630	10
$4Fe_3O_4$	0	5	34
	0.2	35	29
	0.4	120	21
	0.8	200	13
	1.0	440	8

Table 6.2 Temporal evolution of storage modulus of different iron particles. Values shown are an average of 3 samples.

Sample	*Magnetic Field (T)*	*G' (kPa) value at*					
		15 min	*30 min*	*45 min*	*60 min*	*90 min*	*120 min*
4CIP	0	30	50	100	270	1100	2500
	0.2	250	350	530	850	1900	2800
	0.4	420	630	880	1200	2200	3000
	0.8	1300	1700	2000	2400	3000	3400
	1.0	1900	2300	2500	2800	3200	3500
4Fe(E)	0	40	45	100	180	950	2300
	0.2	370	590	890	1300	2300	3100
	0.4	1000	1500	1800	2200	3000	3400
	0.8	1700	2000	2300	2700	3200	3500
	1.0	2300	2600	2900	3100	3400	3600
4Fe(H)	0	15	36	70	140	670	2100
	0.2	140	210	250	390	1200	2300
	0.4	450	840	1100	1500	2300	2900
	0.8	1500	1800	2100	2300	3000	3300
	1.0	1800	2200	2500	2800	3300	3500
$4Fe_3O_4$	0	50	120	220	500	1500	2700
	0.2	270	500	800	1200	2300	3100
	0.4	570	900	1200	1600	2600	3200
	0.8	790	1300	1700	2100	3000	3400
	1.0	1500	2000	2300	2600	3200	3500

Table 6.1 shows the rate of change of *G' (∂G'/∂t),* during the initial period (first 2 minutes) after the application of the magnetic field as well as the rate of change of *G'* during the final time period (last 30 minutes) of the sample being exposed to the magnetic field. *∂G'/∂t* values are also presented for samples in the absence of a magnetic field. For *4Fe(E)* when the applied magnetic field strength was increased from 0.2 T to 0.4 T, the value of *∂G'/∂t* over the first 2 minutes increased by a factor of 1.8. When the magnetic field was increased from 0.2 to 0.8 T, *∂G'/∂t* increased by a factor of 4.5. However, when increased from 0.2 T to 1 T, *∂G'/∂t* increases by almost a factor of 8. Thus during the initial period the values of *∂G'/∂t* for *4Fe(E)* are not linearly related to the magnetic field strength, but have a strong dependence on the magnitude of the field strength.

Now by comparing the values of *∂G'/∂t* for *4Fe(E)* with those of *4CIP* (first 2 minutes), it can be seen that at all magnetic field strengths, the *∂G'/∂t* values of *4Fe(E)* are significantly higher (at most 2 times higher) than that of *4CIP,* which is potentially due to the higher volume susceptibility of *Fe(E)* particles. Susceptibility values indicate rate of response of a magnetic material and thus might be influencing the initial values of *∂G'/∂t*.

Because a higher initial rigidity is induced in the *4Fe(E)* sample when it is exposed to an 1 T magnetic field versus when it is exposed to no magnetic field, the *∂G'/∂t* of *4Fe(E)* during the final stages (90-120 minutes) decreases with increasing level of magnetic field

strength. As stated in Section 4.3.2, this could indicate a maximum degree of structure that can be reached within the time frame of the study and that in the final phase, structure formation might be governed by hydration.

Up to a magnetic field strength of 0.4 T, the *G'* values of *4Fe(E)* were higher by a factor of 1.5 (for a duration of 60 minutes) compared to those of *4CIP*. Similar to the trend seen above, because of the higher rigidity induced in the *4Fe(E)* sample, the $\partial G'/\partial t$ of *4Fe(E)* up to 0.4 T during the final stages (90-120 minutes) was smaller than that of *4CIP*. At 0.8 T and 1 T, both *4CIP* and *4Fe(E)* have similar values of *G'* (thus have similar rigidity) due to which the $\partial G'/\partial t$ values during the final stages (90-120 minutes) were similar.

6.1.2 Timesweep SAOS: Hydrogen Reduced Iron Powder

Fe(H) particles (d_{50} = 20.1 μm) are larger than those of *CIP* (d_{50} = 8.7 μm). d_{90} of *Fe(H)* is almost 1.5 times higher than *CIP*. Additionally *Fe(H)* particles are smaller than those of *Fe(E)* which is three times the size of *CIP*. While *CIP* particles are spherical, *Fe(H)* particles have an irregular shape and the particles appear to be like a sponge and not completely solid. Notice the particle on the bottom right of Figure 3.2 (f), where it appears that the iron is on the circumference and the interior is hollow. *Fe(H)* particles used in this study are also composed of high purity iron similar to those of *CIP*. *Fe(H)* particles have a 10% smaller magnetization saturation value compared to that of *CIP*.

Figure 6.4 shows the evolution of *G'* of *4Fe(H)* over a span of 120 minutes with varying magnitudes of applied magnetic field. Similar to the response observed in the *G'* evolution of the *4Fe(E)* sample (Figure 6.1) the following remarks can be made regarding the *4Fe(H)* samples:

- In the absence of magnetic field the values of *G'* increased over time.
- Throughout the entire testing duration, the values of *G'* were higher at higher levels of applied magnetic field.

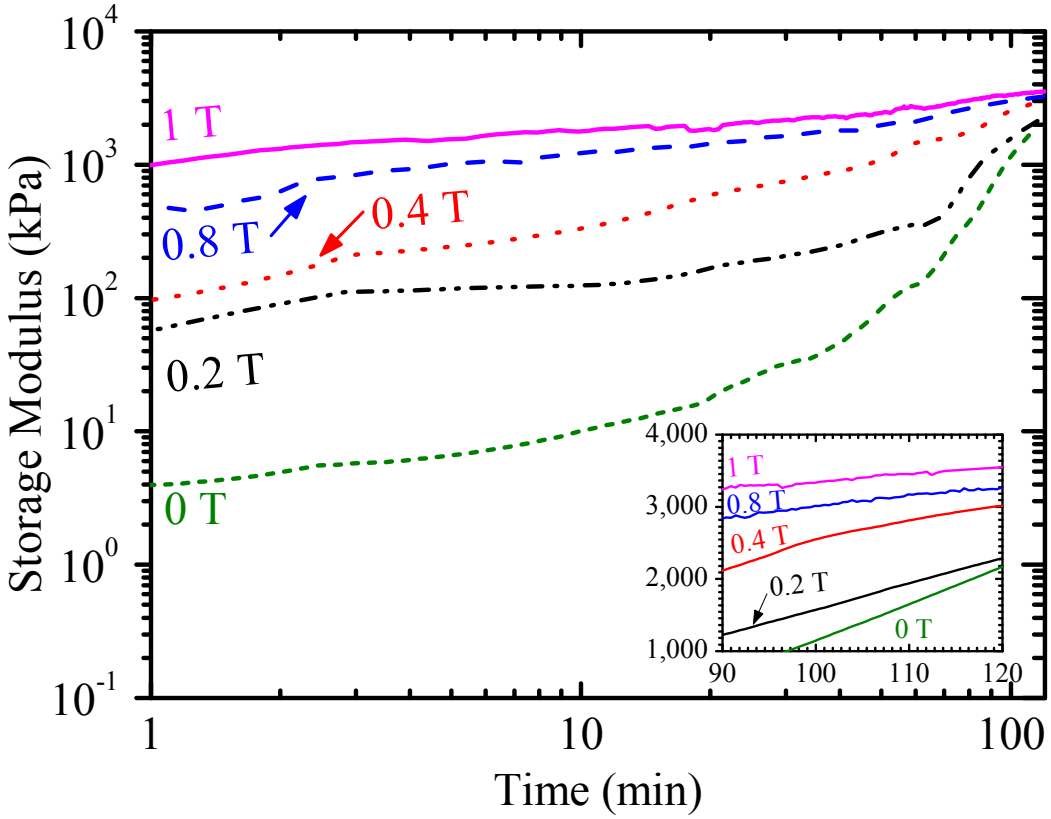

Figure 6.4 Influence of applied magnetic field strength on the storage modulus evolution of *4Fe(H)* over a durtion of 120 minutes. Note that both the axes are plotted on a $\log_{10} - \log_{10}$ scale. Inset shows the evolution for the last 30 minutes on a linear-linear plot.

- At any given point of time the percent change in values of *G'* with increasing levels of magnetic field appears to be dependent on the magnitudes of the magnetic field strengths. In addition it was found that the percent change in value of *G'* decreases with increasing magnitude of the field strengths.

The reasons behind the trends observed in these remarks (for *4Fe(H))* are similar to those that have already been discussed in Section 6.1.1 for the *4Fe(E)* sample. There is one main difference that can be observed from the *G'* evolution curves of *4Fe(E)* and *4Fe(H).* Unlike the response of *4Fe(E)* (see inset in Figure 6.1), where at high levels of magnetic field the evolution of *G'* was similar at 0.8 T and 1 T for the duration of 90-120 minutes, the response of *4Fe(H)* (see inset in Figure 6.4) was higher at higher levels of magnetic field (*G'* at 1 T was higher by 10% when compared to the *G'* value at 0.8 T). This could probably be because the magnetization values of *Fe(E)* reach up to 5% of its saturation magnetization at around 0.5 T, but it takes *Fe(H)* almost 0.8 T magnetic field strength to reach up to 5% of its saturation magnetization. Thus, magnetization values probably have an influence on the evolution of *G'.*

Now by comparing the evolution in values of *G'* for *4Fe(H)* with those of *4CIP,* it can be inferred from Table 6.2 that in the absence of magnetic field, the values of *G'* for *4Fe(H)* (up to 90 minutes) were almost 50% smaller than those of *4CIP.* The *G'* values of *4Fe(H)* were 10% smaller than those of *4CIP* at 120 minutes. This decrease in the *G'* component in the absence of the magnetic field for *4Fe(H)* compared to that of *4CIP*, could be due to

a multitude of reasons such as: the spongy nature of the *Fe(H)* particles; the total surface area of the particles (Bentz et al. 2012) and the particle size range (or extent of poly dispersity (Chong, Christiansen, and Baer 1971)) in comparison to those of *CIP*.

When a magnetic field of 0.2 T was applied, the *G'* values of *4Fe(H)* were almost 50% smaller than those of *4CIP* (up to 60 minutes) and at 120 minutes, the value of G' for 4Fe*(H)* was 10% smaller than that of *4CIP*. Beyond 0.2 T, the response of both the *4Fe(H)* and *4CIP* were similar. As explained in Section 6.1.1, when a magnetic field is applied, samples containing magnetic particles with higher magnetization values have a higher value of *G'*.

Table 6.1 shows the rate of change of *G' (∂G'/∂t)* of *4Fe(H),* during the initial period (first 2 minutes) after the application of the magnetic field as well as the *∂G'/∂t* values during the final time period (last 30 minutes) of the sample being exposed to the magnetic field. *∂G'/∂t* values are also presented for samples in the absence of a magnetic field. In the absence of the magnetic field for *4Fe(H)*, during the initial 2-minutes, *G'* increased at a slow rate of 0.85 kPa/min and during the last 30 minutes, *G'* increased at a faster rate of 51 kPa/min, the faster rate at later stages potentially be due to an increase in the rate formation of hydration products. In the presence of a magnetic field, the response of the field induced properties are much higher than that at 0 T. When the applied magnetic field strength was increased from 0.2 T to 0.4 T, the value of *∂G'/∂t* over the first 2 minutes increased by a factor of 2.5 and when the magnetic field was increased

from 0.2 T to 0.8 T, $\partial G'/\partial t$ increased by a factor of 8. When increased from 0.2 T to 1 T, $\partial G'/\partial t$ increased by almost 15 times (refer to Table 6.1). Thus similar to the evolution of *4Fe(E),* the rate of increase in *G'* of *Fe(H)* is not linearly related to the magnetic field strength, but has a strong dependence on the magnitude of the field strength. Similar to the *4Fe(E)* sample*,* the value of $\partial G'/\partial t$ at later ages for *Fe(H)* decreased with increasing magnitudes of applied field because the higher rigidity induced early on is affecting the viscoelastic properties of the material. Furthermore the initial rate of increase of *G'* for *4Fe(H)* was more or less similar to that of *4CIP* and so were the values during the final stages (90-120 minutes).

6.1.3 Timesweep SAOS: Iron Oxide (Magnetite)

In sections 6.1.1 and 6.1.2 it has been shown that the evolution of *G'* for a field induced cement paste is dependent on the magnitude of the magnetic field strength and the magnetization values of the magnetic particles. It was seen that at a specific magnetic field strength, a higher magnetization value of the magnetic particles lead to a higher value of *G'* for the corresponding paste sample. Using this theory, it can be hypothesized that when a magnetic field is applied to $4Fe_3O_4$, Fe_3O_4 particles with significantly smaller magnetization value (M_s of Fe_3O_4 particles is almost one-fourth the value of *CIP.)* compared to that of *CIP* particles would result in $4Fe_3O_4$ having significantly lower values of *G'* compared to those of *4CIP*. In this section the hypothesis will be verified.

Figure 6.5 shows the evolution of *G'* over a span of 120 minutes at different applied magnetic field strengths for the *4Fe₃O₄* sample. It can be seen that as the value of magnetic field strength was increased, the values of *G'* also increased in value. At 0 T, *G'* values of the *4Fe₃O₄* sample were almost twice the values of the *4CIP* sample for the first 60 minutes and beyond that the values are closer (Table 6.2). Furthermore at 0 T, during the initial 2 minutes, the value of *G'* increased at a rate of 5 kPa/min (Table 6.1). This is

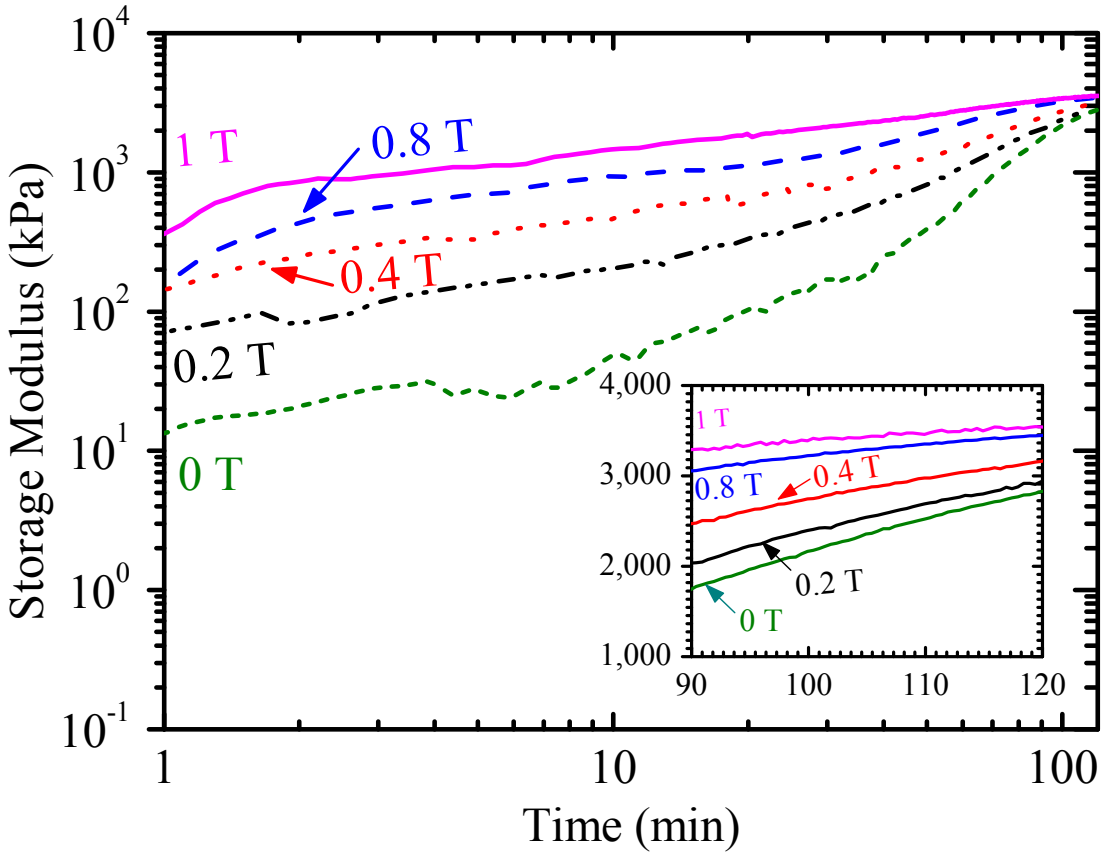

Figure 6.5 Influence of applied magnetic field strength on the storage modulus evolution of *4Fe₃O₄* over a duration of 120 minutes. Note that both the axes are plotted on a $\log_{10} - \log_{10}$ scale. Inset shows the evolution for the last 30 minutes on a linear-linear plot.

the highest rate that has been observed for all the materials that were analyzed in this chapter. In addition from Table 3.6, it can be seen that *$4Fe_3O_4$* also has the smallest slump flow diameter, which can probably be attributed to its smallest particle size distribution (*d_{50} = 1.9 μm).* Although *CIP(sm)* also has a smaller particle size distribution (*d_{50} = 3.3 μm)* compared to that of *CIP* (*d_{50} = 8.7 μm)*, the slump flow diameter of *4CIP(sm)* is not significantly different than that of *4CIP.* Thus either the presence of sub-micrometer particles in *Fe_3O_4* or a difference in the particle surface chemistry appears to have an influence on behavior of the *$4Fe_3O_4$* sample in the absence of magnetic field. The particle surface chemistry and its interaction with the cement paste can be measured using a zeta potential analyzer. This was not examined here but would be an interesting test for future work.

By comparing the values of *G'* for the *$4Fe_3O_4$* sample with those of the *4CIP* sample (see Table 6.2), it can be seen that at 0.2 T and 0.4 T magnetic field strengths, the values of *G'* for *$4Fe_3O_4$* are higher (by a factor of 1.5) than the values of *4CIP* during the first 60 minutes. But according to the hypothesis stated above, when a magnetic field is applied, a sample containing magnetic particles with significantly lower magnetization values (M_s of *$Fe_3O_4 \approx 0.25\ M_s$ of CIP*) should have significantly lower *G'* values, which is not the case when comparing *$4Fe_3O_4$* and *4CIP.* Thus the higher flocculated state of *$4Fe_3O_4$* (observed even at 0 T) along with its magnetized chains of particles leads to a better elastic response than the *4CIP* sample at low magnetic field strengths (< 0.4 T). But as the magnetic field is increased beyond 0.4 T, the *4CIP* sample (with a higher *M_s*) has *G'*

values that are higher by a factor of 1.5 compared to that of *$4Fe_3O_4$* during the first 30 minutes, beyond which the values gradually become closer.

Thus, the hypothesis that field induced MR paste containing magnetic particles with higher magnetization values will have higher values of *G'* is valid only at high magnitudes of applied field (> 0.4 T). At lower field strengths, in the case of *$4Fe_3O_4$* there was an influence of its highly flocculated nature that resulted in the *$4Fe_3O_4$* sample having higher *G'* values compared to those of the *4CIP* sample.

6.2 STATIC YIELD STRESS

Figure 6.6 shows the static yield sterss values of *4CIP, 4Fe(E), 4Fe(H)* and *$4Fe_3O_4$* at various magnetic field strengths measured using a stress growth test. In the absence of magnetic fiield (i.e. at 0 T), the yield stresses of the samples in increasing order of magnitide were 40 Pa (*4CIP*), 50 Pa (*4Fe(H)),* 70 Pa *(4Fe(E))* and finally 125 Pa (*$4Fe_3O_4$)*. To understand the significance of these values, typical yield stresses (Banfill 2003) of different cement based systems are shown in Table 6.3. Comparing the values from the table with the observed yield stress values it can be seen that *4CIP, 4Fe(H)* and *4Fe(E)* are in the range of typical yield stress values for cement pastes, but the yield stress of *4Fe(E)* is almost 1.5 times higher than that of *4CIP* which is a considerable difference. Furthermore, in the case of *$4Fe_3O_4$* the yield stress is significantly higher than

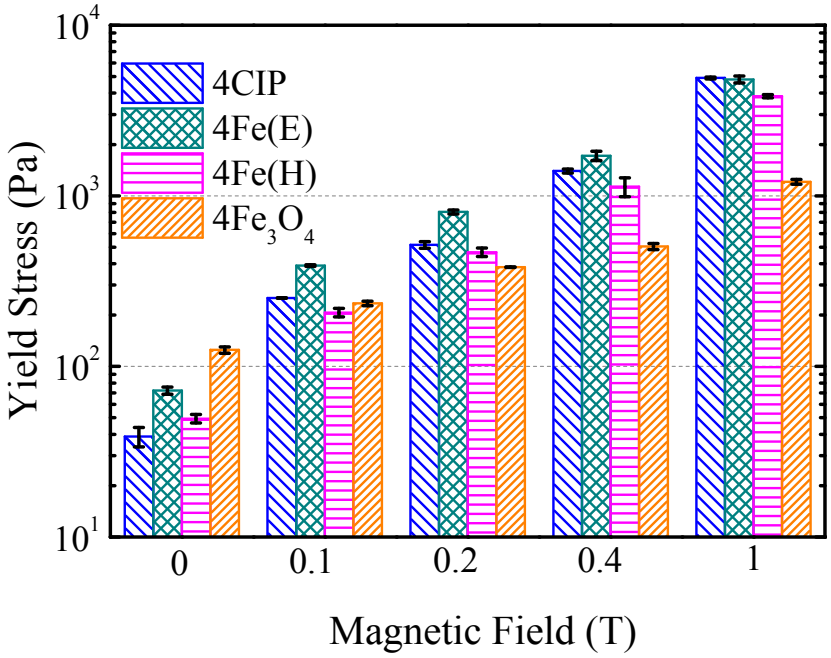

Figure 6.6 Static yield stress results of *4CIP*, *4Fe(E) 4Fe(H)* and *$4Fe_3O_4$;* 10 minutes after the application of magnetic field. Note that the y-axis is on a $\log_{10}$ scale. The error bars are based on standard deviation from three samples.

the other three samples and its value of yield stress, and in fact falls within the typical range for a mortar.

Yield stress is the amount of shear stress that is required to initiate flow and has an influence on the workability of concrete. In the absence of magnetic field, the *4CIP* sample with the smallest yield stress would be the most workable of all the samples measured here, which can be attributed to the spherical shape of the *CIP* particles. Additionally it can be assumed that the differences in the yield stress values (without any

magnetic field) are potentially due to the differences in: particle size range, extent of polydispersity, particle angularity and/or the ionic interaction of the magnetic particles with cement paste (which could be measured using a zeta potential analyzer).

Table 6.3 Yield stress values of cement-based material systems (Banfill 2003)

Sample	*Yield Stress (Pa)*
Cement paste, grout	10-100
Mortar	80-400
Flowing Concrete	400
Self Consolidating Concrete	50-200
Concrete	500-2000

In general, when the magnetic field strength was increased from 0 T to 1 T, the values of yield stresses (for all samples) increased with increasing levels of field strength. At each magnetic field strength to understand the reason behind the differences between all the four samples, the yield stress values were plotted against the magnetization value of the magnetic particles Figure 6.7. Magnetization values were obtained from the magnetization curves (shown in Figure 3.5) and it was assumed that 10 kOe was equal to 1 T. As shown in Figure 6.7, there appears to be a good correlation between the yield stress values of the field induced paste and the corresponsing magnetization values of the particles. Except for the case at 0.1 T (Figure 6.7 (a)), the data follows the an expoential increase in the values of yield stress (with incresing magnetization of the particles). Thus

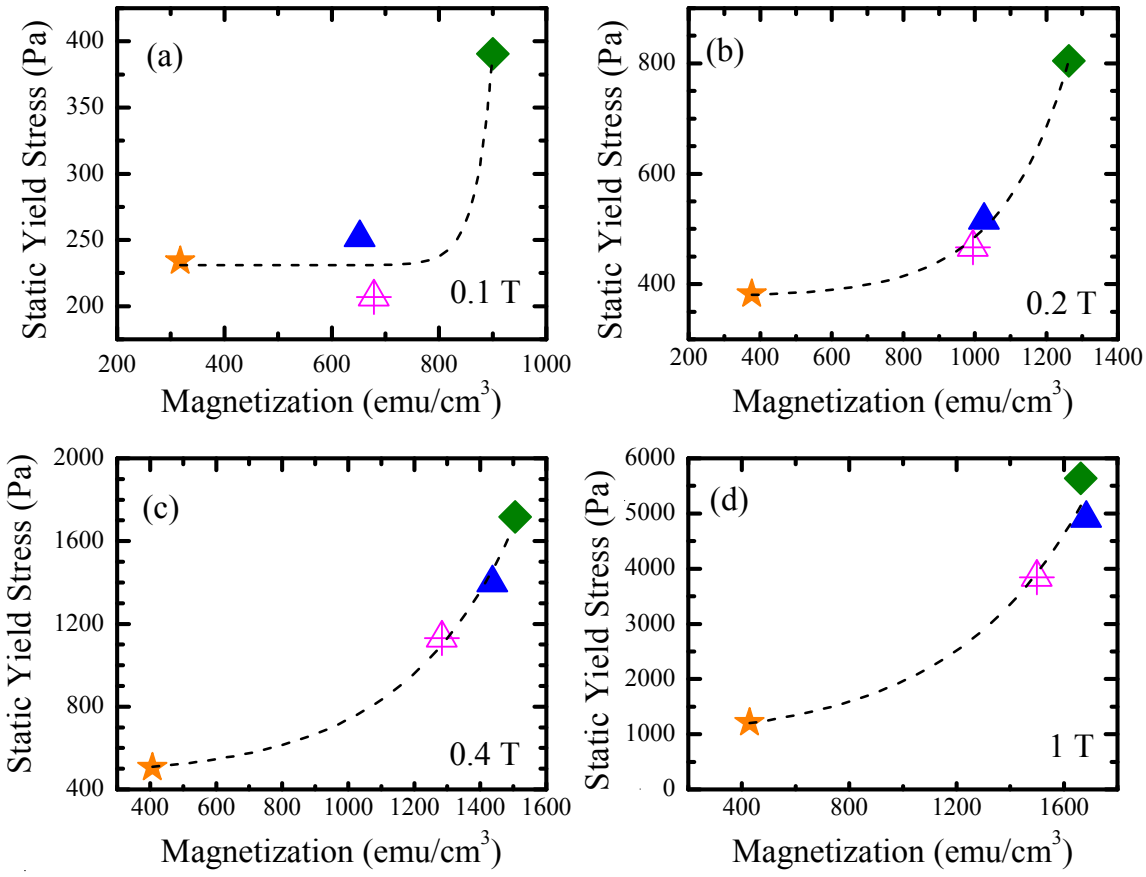

Figure 6.7 Plot showing the relationship between static yield stress (measured using stress growth curves) of the MR paste and magnetization of the magnetic particles at the specified magnetic field strengths. Star in orange represents yield stress of *$4Fe_3O_4$* vs. magnetization of *Fe_3O_4;* open triangle with cross hairs *(4Fe(H)* vs. *Fe(H));* solid triangle in blue (*4CIP* vs. *CIP)*; solid diamond in green *(4Fe(E)* vs. *Fe(E))*. The dashed black line is an exponential fit.

the yield stres of a field induced MR paste is mainly dependent on the magnetization values of the magnetic particles.

6.3 SUMMARY

It was found that magnetization values of the magnetic particles have a strong influence on the viscoelastic response of a cement-based MR fluid. By comparing the response of *4Fe(E)* with that of *4CIP,* it was concluded that larger magnetization values of *Fe(E)* particles lead to a better viscoelastic response compared to that of *4CIP* at lower magnetic field strengths (up to 0.4 T) for the first 60 minutes. At higher levels and at later stages, both the samples behave similarly. Similar correlation between magnetization and values of *G'* were observed in the case of *4Fe(H)* when compared with the response of *4CIP*. Finally, for *4Fe_3O_4,* even though the magnetization values of *Fe_3O_4* are significantly smaller than those of *CIP,* it was found that the viscoelastic response of the sample was better than that of *4CIP* at low levels of applied magnetic field (up to 0.4 T). At higher levels they had a similar response. Thus at low magnetic fields, there seems to be an influence of the flocculation behavior of the *4Fe_3O_4* on the viscoelastic response of the cement-based MR fluid. It was also found that magnetization values of the magnetic particles also had a direct correlation with the trends observed in the static yield stress measurements

CHAPTER 7: PRACTICAL APPLICATIONS OF CEMENT-BASED MR FLUID

In the previous chapters a cement-based MR fluid was developed whose fresh state rheological properties could be altered in real time. It was also shown that by varying the applied magnetic field strength, a significant change could be achieved in the magnitude of both the viscoelastic shear modulus and the yield strength of the cement paste. But the question to ask is what do these rheological changes mean practically? Section 7.1 gives information regarding permanent magnets used to conduct the experiments in this chapter. Sections 7.2 and 7.3 answer the above posed question through simple experiments and relate the results to actual applications on field

7.1 PERMANENT MAGNETS

For the rheological measurements conducted in the previous chapters, a current was passed through a coil and a uniform magnetic field was generated (see Figure 7.1 (a)). At high levels of applied current, the electric coils have to be continuously cooled to avoid the coils from heating which could potentially increase the sample temperature. Another way to generate a magnetic field is by using permanent magnets (see Figure 7.1 (b)). Permanent magnets are made up of hard magnetic materials that have a high coercivity. Permanent magnets are a fast and easy way to apply a magnetic field without the need for electricity or water for cooling the coils. They can also be manufactured in any shape

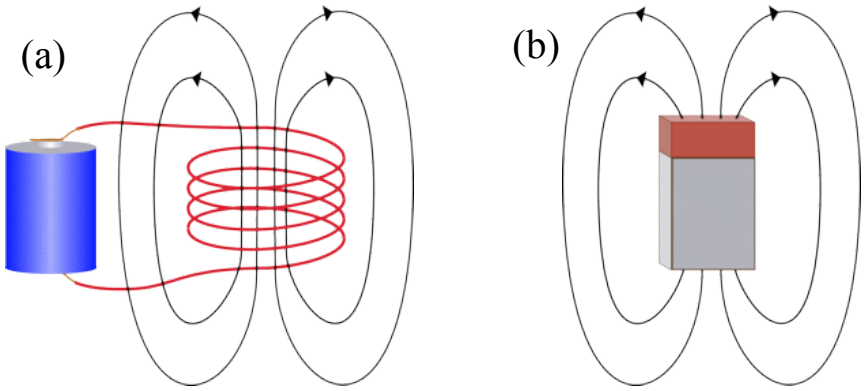

Figure 7.1 (a) Magnetic field being generated perpendicular to the direction of current. Source: www.thenakedscientists.com

desired. In a disc shaped permanent magnet (similar to the magnets shown in Figure 7.2) the highest magnetic field strength occurs on the surface of the magnet (at the center). Table 7.1 gives a list of neodymium magnets (Magnets A-D) that were obtained from K & J Magnetics, Inc. Magnet E was available in the lab and its composition is unknown, but Magnet E had higher field strength values.

Table 7.1 Dimensions of the permanent magnets used in this study

Magnet #	*Diameter (in.)*	*Height (in.)*
Magnet A	0.5	0.25
Magnet B	0.5	0.5
Magnet C	1	0.25
Magnet D	1	0.5
Magnet E	1.5	-

Figure 7.2 Disc shaped permanent magnets. Source: www.cmmagnets.com

Figure 7.3 shows the changes in the magnetic field strength of the magnets as you move away from the surface of the magnet. From the figure it can be seen that as you go further away from the surface of the magnet, the magnetic field strength decreases in value. Because of which if a sample has a thickness then it will not be subjected to a uniform

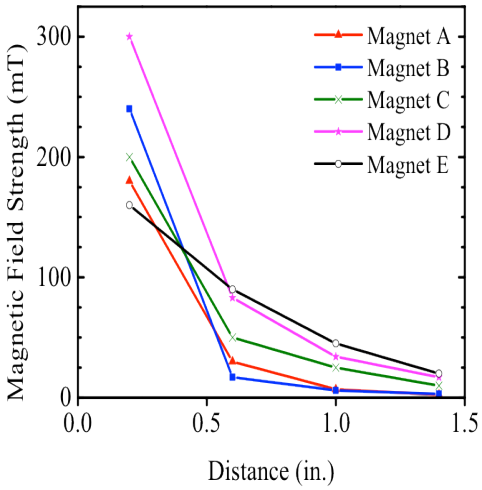

Figure 7.3 Strength of permanent magnets with increasing distance from the magnet

field. For example, if the thickness of the cement paste whose rheological properties are to be modified is 0.5 in. thick, and if Magnet A is used, then the sample will be subjected to varying fields from 180 mT to 30 mT; there will be a gradient with the highest field occurring closest to the magnet. The magnetic field strengths were measured using a Lakeshore 450 Gaussmeter and an MFT-3E03-VG flex-probe. It can be seen that for samples A-D. (i.e. all the neodymium magnets) the drop in field strength is faster than in Magnet E.

7.2 ABILITY TO WITHSTAND PRESSURE

The ability for cement to withstand pressure is a feature that is in particularly important for self-consolidating concrete. According to ACI 237R, *Self-consolidating concrete* (SCC) is defined as a "highly flowable, nonsegregating concrete that can spread into place, fill the formwork, and encapsulate the reinforcement without any mechanical consolidation" (ACI-237 2007). With respect to SCC, formwork pressure development is a concern, and currently the formwork is designed to withstand the full hydrostatic head of fresh SCC (which leads to increase in construction costs to build strong formwork or limits heights of the vertical elements that can be cast). This problem can be solved to an extent by using the cement-based MR fluid. In field-induced pastes, a structure is formed due to alignment of the magnetic particles along the direction of applied field. It has been shown in Chapter 4, that the applied field changes the viscoplastic nature of cement pate to that of a viscoelastic solid. Thus a field-induced cement-based fluid will be able to hold additional pressures, which can potentially increase construction heights and reduce

formwork thicknesses. An extension to the test presented here would be to build a long column and to apply additional pressure on the top on the fluid. This would give an indication about the pressures that the field-induced portion of the fluid would be able to hold.

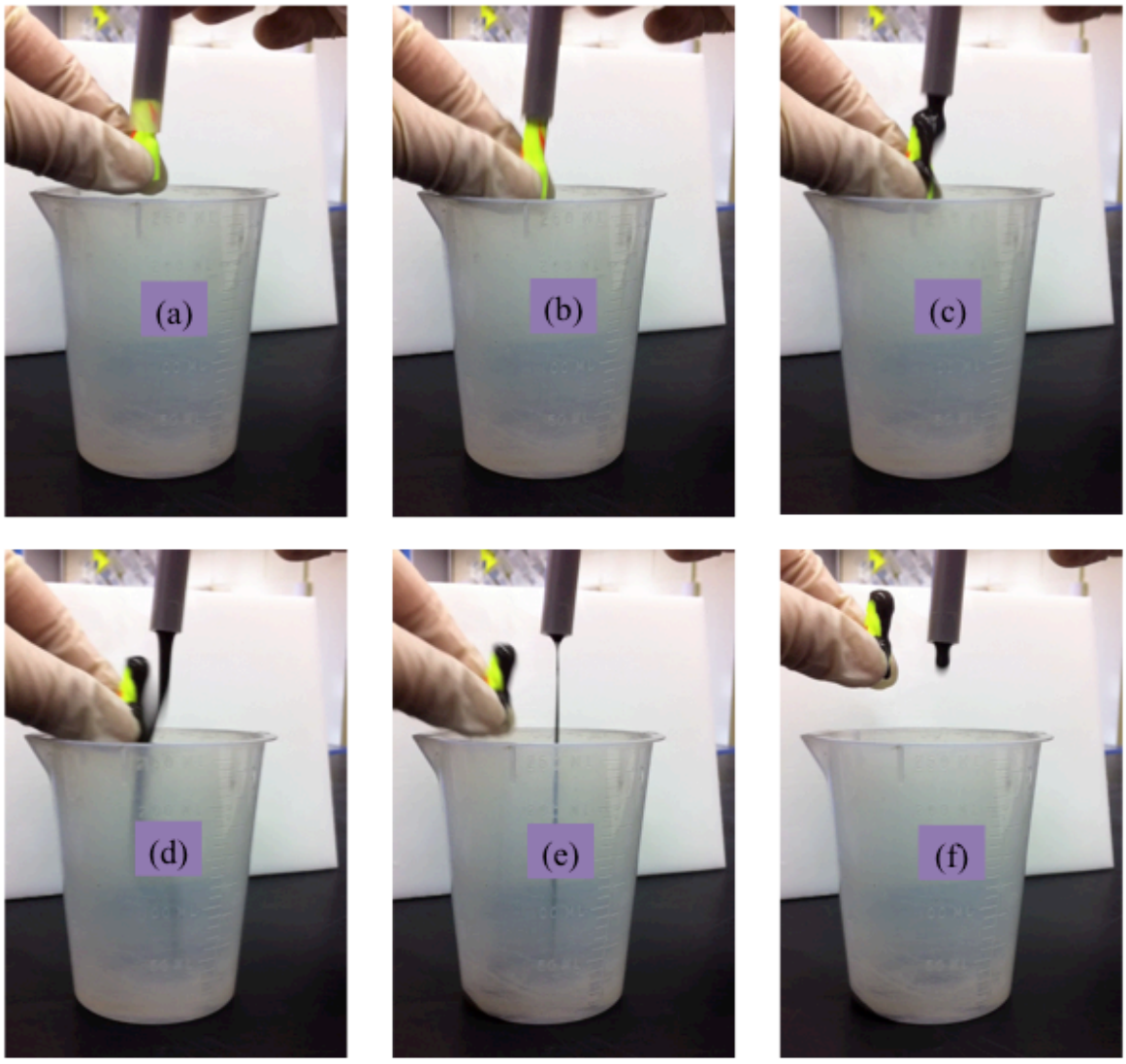

Figure 7.4 Still images from a video showing flow behavior of a magnetorheological cement paste (*4CIP)* when no external magnetic field is applied.

In Figure 7.4 a tube (inner diameter = 10mm, outer diameter = 13mm, length = 70 mm) was filled with *4CIP* right after mixing the sample in the high shear mixer (consult chapter 3 for more details on sample preparation). As shown in Figure 7.4, when the stopper holding the fluid is removed (c.f. Figure 7.4 (c)), the fluid immediately starts

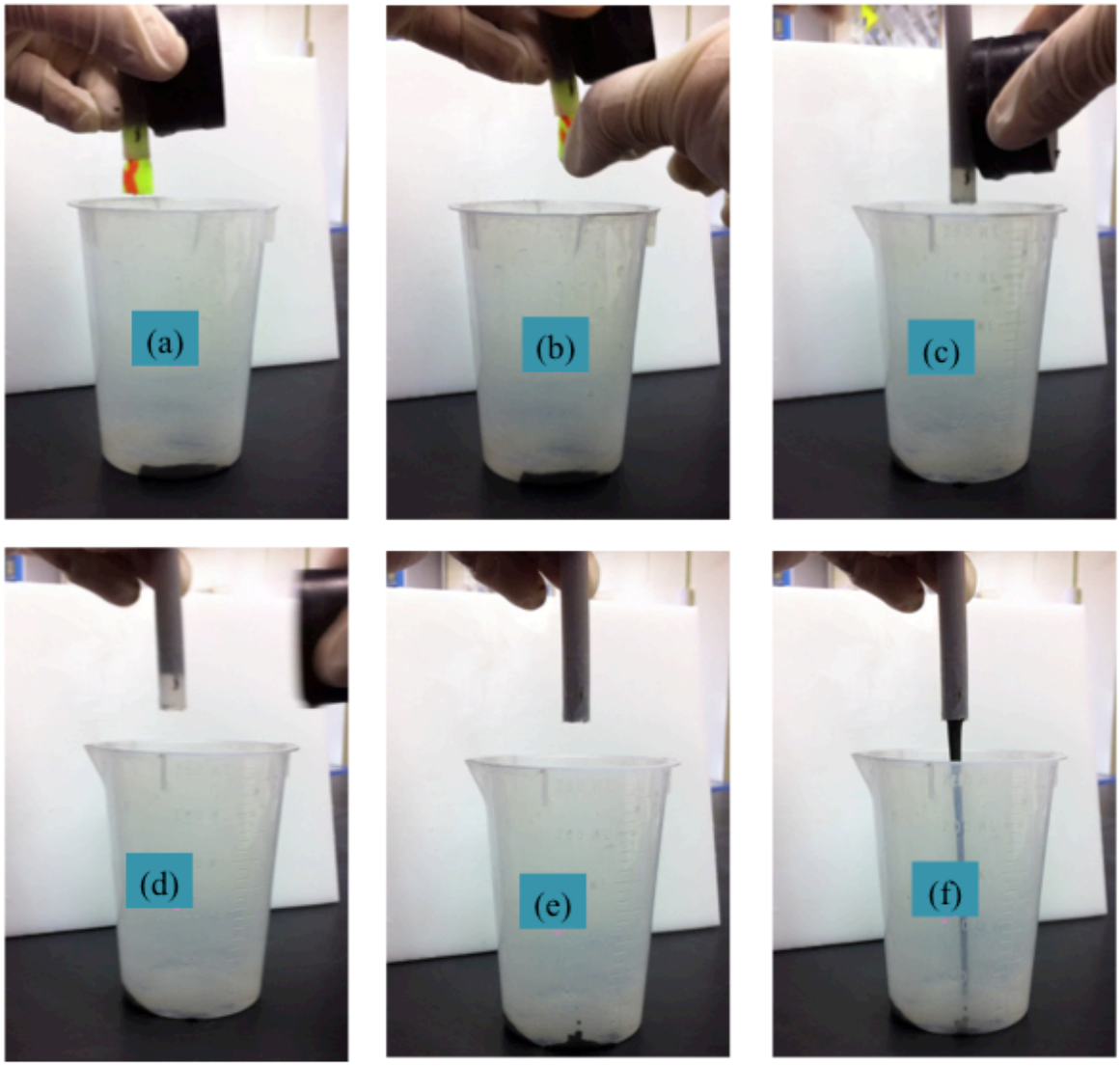

Figure 7.5 Snapshots from a video showing the ability of cement paste *(4CIP)* to withstand hydrostatic pressure in the presence of a magnetic field.

flowing out of the tube (c.f. Figure 7.4 (d) through Figure 7.4 (f)). All the figures shown are a sequence of snapshots from a very short video (≈ 10 seconds).

The tube was again filled with *4CIP* and this time Magnet E was held next to the bottom of the tube (see Figure 7.5 (a)). Initially a plug is placed in the tube to prevent fluid flow (see Figure 7.3a). Even if the plug is removed, if the sample is in the presence of a magnetic field, the fluid does not flow (see Figure 7.3d). Magnetic particles form chains in the regions in close proximity to the magnet. The magnetic particle chains that have formed have the capability to withstand the hydrostatic pressure generated from the rest of the fluid (Figure 7.5 (c)) and are able to stop the fluid flow. When the magnet is removed, the paste starts flowing freely (Figure 7.5 (f)). A similar response was observed with the use of Magnets A-D.

These "plug-flow" experiments were repeated with *4Fe(E), 4Fe(H)* and $4Fe_3O_4$. Of all the three samples, $4Fe_3O_4$ exhibited the most resemblance to the behavior of *4CIP*, which can be attributed to their relatively smaller particle sizes and almost spherical surfaces. On the other hand, *4Fe(E)* and *4Fe(H)* exhibited a plug effect wherein, even when the magnet was removed, the fluid flow was restricted. This plug effect in the cement-based MR fluid when the magnet is removed might be because the not all the stiffness induced in the sample is lost (see section 4.7 for more details regarding the influence of removing a magnetic field). This behavior was not observed here in the case of *4CIP,* probably because of their spherical shape *CIP* particles are able to avoid severe interlocking (*Fe(E)*

and *Fe(H)* are made up of irregularly shaped particles). But as shown in Section 4.7, when a magnetic field is applied for 30 minutes, even *4CIP* would show a plug effect.

All the particles used thus far have particles that are smaller than 100 μm. Thus to investigate the effect of using much larger magnetic particle sizes, cement paste containing 4% iron filings (based on volume of cement) was prepared. The shape and particle size distribution of the iron particles are shown in Figure 7.6. d_{50} of iron filings is 200 μm (considerably higher than all the other magnetic particles) and in addition the particles are irregularly shaped. When the "plug flow" experiment was repeated with cement paste containing iron filings, all the iron filings in the vicinity of the applied field migrated towards the magnet (region with highest field) and the rest of the fluid could freely flow down the tube. Thus in the presence of magnetic fields, cement paste

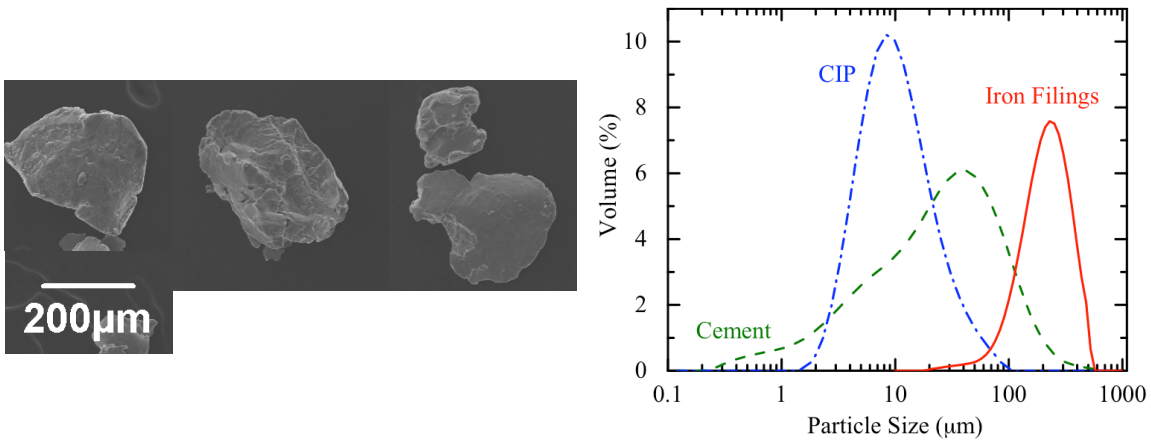

Figure 7.6 (a) Shape of iron filings (b) particle size distribution on iron filings in comparison to CIP and cement psd

containing large particles would probably lead to segregation which promotes the idea that there exists a critical magnetic particle size below which the magnetic particles would be better dispersed within an MR paste.

7.3 DISPLACEMENT OF CEMENT PASTE

As shown in Figure 7.7, 3 ml volume of cement paste (*4CIP)* was placed on top of a plastic sheet. By using a magnet at the bottom of the sheet the cement paste was displaced horizontally (note, the magnet was not in contact with the cement paste). In the displacement experiment it was found that the magnet size had an influence on the

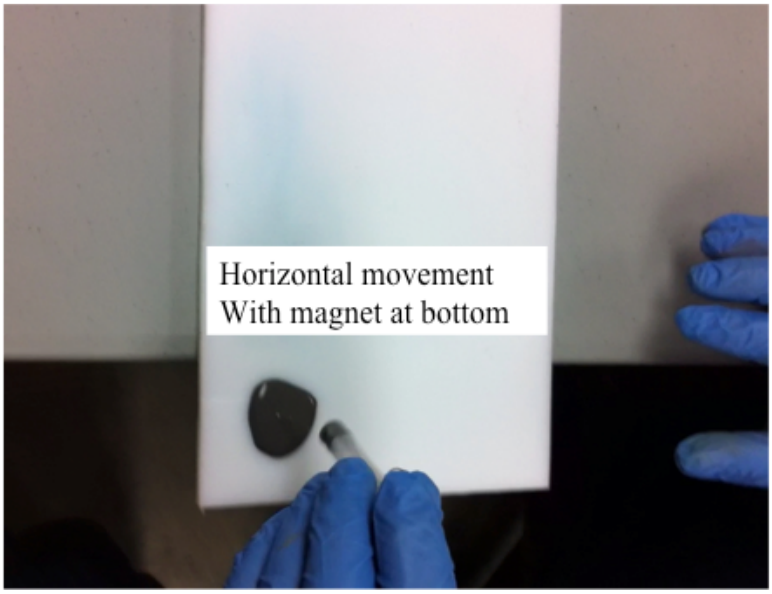

Figure 7.7 Investigation of cement displacement. Magnetorheological cement paste was placed on top of a plastic sheet and a permanent magnet was placed at the bottom of the plastic sheet to investigate if cement paste can be displaced horizontally.

distance by which cement paste could me moved. Specifically, as shown in Figure 7.8 (b), by using Magnet A (0.5" dia), the paste could only be displaced by a short distance. By using Magnet B (0.5" dia, higher magnetic field strength), the paste could be displaced further (see Figure 7.8 (c)). But by using Magnet C (1" dia) the cement paste could be displaced horizontally by a significant distance (see Figure 7.9 (e)). Thus the size and the magnetic field strength of the permanent magnet have an influence on the quantity of paste that can be displaced as well as the distance to which it can be displaced.

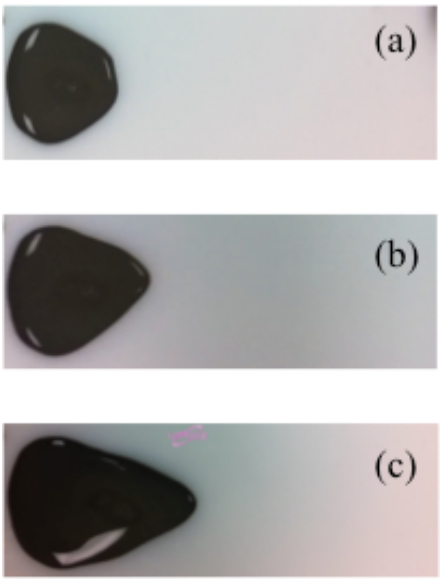

Figure 7.8 (a) Magnetorheological paste before application of magnet (b) Displacement with Magnet A (c) Displacement with Magnet B. The images shown are snapshots from a video.

Figure 7.10 shows the ability of displacing the cement paste vertically by using Magnet E. Cement paste is placed inside a glass beaker and the Magnet E is held outside the beaker. As seen from Figure 7.10, when the Magnet E is placed next to the paste, the influence of the magnet is visible almost to the center of the beaker. Beyond a certain distance as the magnetic field dies down; thus, the paste that can be displaced is the quantity of paste that is under the influence of the magnetic field.

Before an oil/gas well is cemented, the borehole is filled with drilling fluid (or mud). A

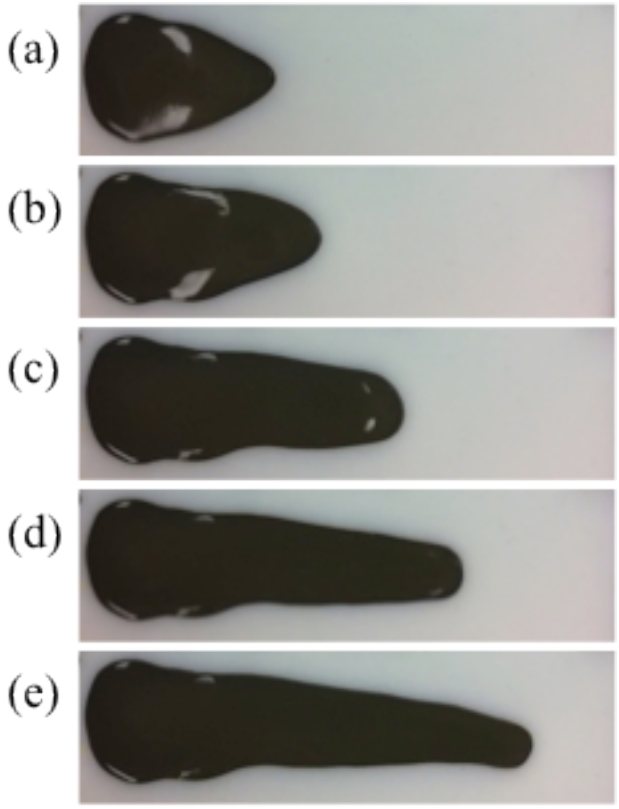

Figure 7.9 Displacement of cement paste (*4CIP)* using Magnet C. The images shown are snapshots from a video.

casing is placed in the borehole and the drilling fluid in the annulus between the casing and borehole is displaced by cement slurry. In certain situations, the cement slurry takes a least resistive path and does not displace the drilling fluid. As discussed in Chapter 1, zonal isolation is very important and has serious consequences if the cement sheath in the annulus is not continuous. To understand the ability of MR cement paste to displace drilling fluids, a polymer based fluid (simulating a drilling fluid) was placed in a beaker on top of freshly mixed cement paste. From Figure 7.11 it can be seen that in the presence of magnetic field, cement paste can indeed displace drilling fluids. Thus by using an MR approach, cement paste can be displaced in regions where it would not otherwise go when pumped conventionally.

Therefore by a combination of results from the horizontal displacement and vertical displacement it can be concluded that cement paste can be displaced along any desired

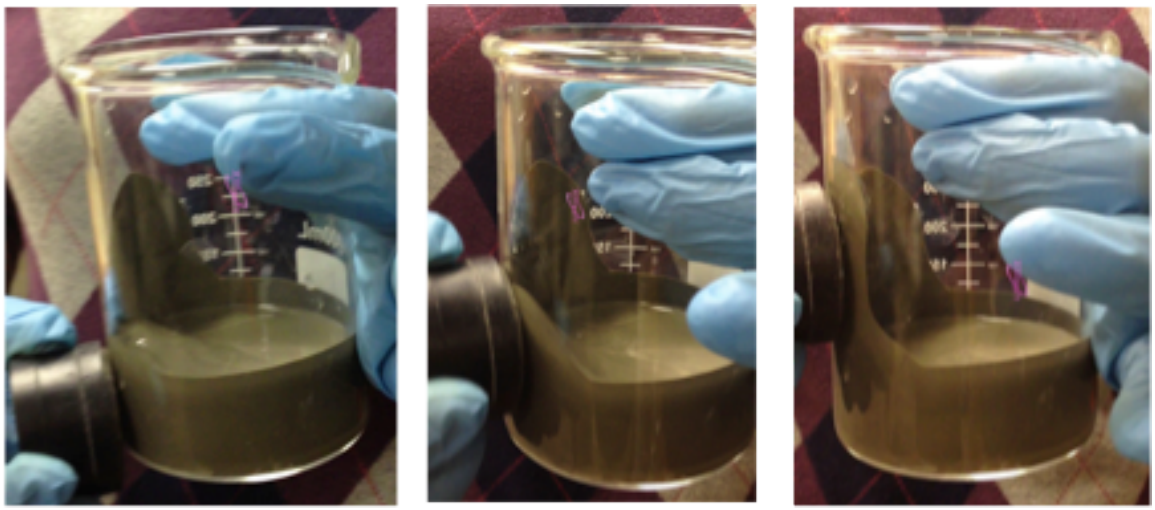

Figure 7.10 Vertical displacement of *4CIP* using Magnet E. The images shown are snapshots from a video.

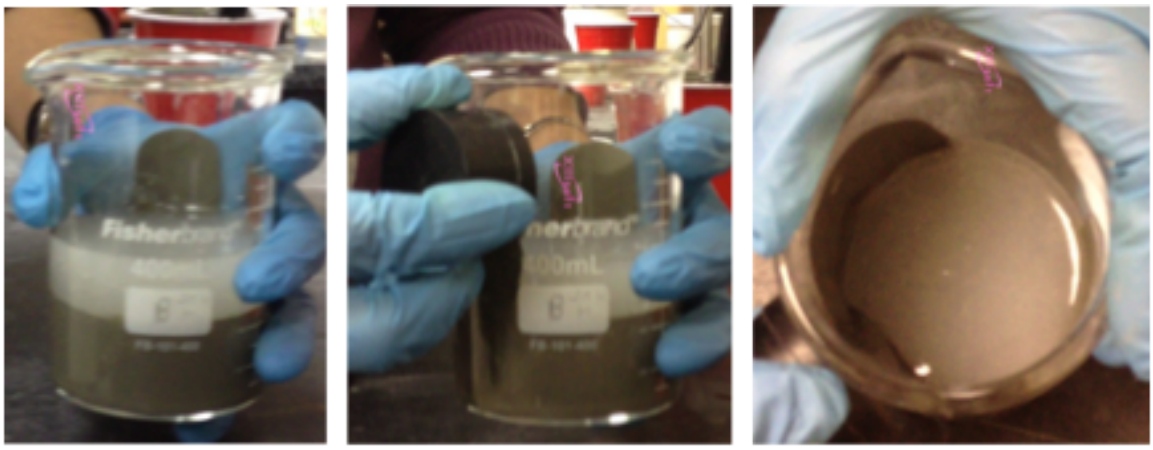

Figure 7.11 Cement paste (*4CIP*) displacing a polymer based mud.

path as long as the magnetic field lines are present in the entire sample that has to be displaced.

7.4 SUMMARY

Through preliminary testing with permanent magnets it has been shown that the behavior of fresh cement paste can be manipulated in real-time. It has been shown that field induced MR cement paste can withstand hydrostatic pressures and can potentially decrease the pressures experienced by formwork. It was also shown that cement-based MR fluids could be displaced in regions where the paste would not flow using conventional approaches. Apart from the magnetic field strength having an influence on the ability to manipulate the cement paste, the size of the magnet (and thus the region in which magnetic field lines are present) also has an impact on the maneuverability of

cement-based MR fluids. The results prove that a cement-based MR fluid can be used to manipulate flow behavior in real time.

CHAPTER 8: CONCLUSIONS AND FUTURE WORK

The main goal of this research was to develop a smart concrete whose fresh-state rheological properties can be controlled in real-time. In this dissertation such a material was indeed developed based on the principles of magnetorheology wherein micron sized magnetic particles were added to cement pastes and by applying a magnetic field, the rheological behavior of cement paste was altered in real-time. By extension, similar behavior can potentially be obtained from mortar/concrete. Background information about rheology, magnetorheology and magnetism was provided in Chapter 2. Chapter 3 dealt with information regarding the materials used in this research and the sample preparation procedure. Chapter 4 described the rheological tests used to characterize the samples and the rheological properties of cement paste containing carbonyl iron powder (*CIP)*. Chapter 5 investigated the influence of the magnetic particles and magnetic field on the hydration kinetics of cement paste. Chapter 6 investigated the influence of magnetic particle type, particle size, shape (hollow or solid) and surface chemistry on the response of a cement-based MR fluid. Chapter 7 focused on practical applications and investigated whether the changes in the rheological properties would actually translate into changes in the fresh state performance. Finally this chapter provides the key findings of this study along with ideas for future work.

8.1 CONCLUSIONS

It has been shown that although unhydrated cement is a weak ferromagnetic material the rheological response of cement paste is not affected by the applied magnetic field. But, by incorporating magnetic particles and by applying a magnetic field, the fresh state properties of cement paste were altered remarkably. By varying the level of applied magnetic field, the response of the paste can be custom tailored to the required behavior. The key findings and conclusions of this research study are stated below.

- The response of the smart fluid can be tweaked by varying the ***dosage of the magnetic particles***. Within the first 30 minutes, by doubling the quantity of *CIP* particles, the shear moduli values also doubled in value. At 90 minutes, they reach similar values suggesting that *CIP* magnetic particle concentration plays a minor role on the magnitude of the later age (> 90 min) rheological response, and leads to the possibility of optimizing the magnetic particle dosage for a certain response requirement, especially at earlier ages. At later ages, the similarities in the viscoelastic properties are attributed to the effects of hydration.

- The ***suspending medium rheological properties*** had an impact on the field induced properties only at low magnetic fields (up to ~ 0.4 T). At larger magnetic field strengths, the rheological response was dominated by the magnetic dipole-dipole interactions.

- By varying the ***particle size distribution*** of *CIP* from a d_{50} of 8.7 μm to d_{50} of 3.3 μm, neither the shear moduli nor the yield stress values of the cement paste were significantly affected.
- Through ***cyclic variation of applied magnetic field***, it was found that the structural rigidity of the sample depend on the, initial level of applied field, the level to which it is changed and the age of the sample. The points worth noting from that experiment are:

    1. At 30 minutes when the magnetic field is increased to a larger value, the value of *G'* is dependent on the elastic properties induced due to formation of chains from the alignment of magnetic particles and most probably many of the flocs are broken down.
    2. At 30 minutes when the magnetic is decreased to a smaller value, the storage modulus has a contribution from both the magnetic particle chains as well as the flocculated structure. So, the intensity of breakdown of flocs must depend on the level of applied magnetic field.
    3. At 60 minutes, the bond strength between the flocs appears to be stronger compared to those at 30 minutes, because when the magnetic field is either increased or decreased, there appears to be a relatively higher contribution from the structural rigidity of the cement paste.
    4. By removing the magnetic field (at any age), the elastic properties of cement paste are not completely lost and that there is some residual structural integrity left in

the sample. This is could be beneficial wherein the magnetic field can be applied for a certain period of time and then removed to change the viscoelastic properties of the cement paste.

- By comparing the responses of *4CIP, 4Fe(E)* and *4Fe(H*) it was found that the viscoelastic behavior of field induced samples are dependent on the magnetization values of the corresponding magnetic particles. In addition, by comparing the viscoelastic response of the *4CIP* sample with that of $4Fe_3O_4$ it was found that along with the magnetization values of the magnetic particles, there is an influence of the flocculation behavior of Fe_3O_4 on the viscoelastic properties at low field strengths (up to 0.4 T)
- By comparing the responses of *4CIP, 4Fe(E), 4Fe(H*) and $4Fe_3O_4$ it was also found that ***magnetization values have a direct (exponential) correlation with the trends observed in the static yield stress measurements***. MR fluid made with magnetic particles with higher magnetization values had comparatively higher yield stresses.
- From ***heat of hydration curves*** it was found that *CIP* magnetic particles did not have cementitious properties and that they do not affect early age hydration of cement paste (measured up to 72 hours).
- Through crystalline phases detected using ***X-ray diffraction*** it was found that *CIP* particles do have an effect on the groeth of hydration products up to 90 days (the maximum observed duration in this study). There was also no significant change in

early age hydration products when different levels of magnetic fields were applied to the cement-based MR fluid for 4 hours.

- Even though *CIP* particles did not have any cementitious properties, they did not adversely affect the increase in ***compressive strength*** up to 90 days (the maximum observed duration in this study).
- With the use of permanent magnets and video still images it was shown that the cement-based MR paste could be transported horizontally or vertically against gravity. It was also shown that the cement paste with magnetic field can withstand hydrostatic pressures.

In conclusion, a cement-based magnetorheological fluid has been developed whose properties depend upon the type, dosage and size of magnetic particles, the age of the cement sample as well as the level of applied magnetic field. Therefore, the cement paste can be custom tailored to the desired properties for an application. This cement-based MR fluid would allow for better control over stiffening/setting behavior of concrete and can be useful in applications in which controlling the fresh-state behavior of concrete is critical. Having better control improves the quality and durability of the cementing operation. This improvement in durability can extend the service life and the improvement in quality control reduces the need for costly repairs and reduces the need to have to use more materials to conduct the repairs.

8.2 FUTURE WORK

8.2.1 Low Cost Alternatives for Magnetic Particles

The minimum cost of the magnetic particles used in this study is approximately $10 per pound. If producing 1 yd^3 of normal concrete costs about $50, then MR based concrete (with addition of 4% of magnetic particles based on volume of cement) would increase the cost by $450. In order to reduce the cost of a cement-based MR composite, future research should be focused on incorporating low-cost alternative materials and/or waste materials containing ferromagnetic fractions. These waste materials would not only help to reduce the cost of the cement-based MR fluid, but would also increase the "greenness" of this smart fluid since the waste materials can now be recycled into the cement-based MR fluid instead of being disposed of, especially since these waste materials often have significant consequences to the environment (Dewan 2009; Huang et al. 2012). A few probable cheap magnetic materials include:

- Ball-milled iron filings
- Magnetic iron separated from fly ash (Russeil and Zawacizki 1963; Norton, Markuszewskl, and Shanks 1986; Shoumkova 2011)
- Iron tailings (Redman 2009; Li et al. 2010; Bao-kuan et al. 2011)
- Waste/spent magnetic ink toner (Yildirim, Hazlett, and Davio 2004)

8.2.2 Use of Hard Magnetic Particles

All the magnetic particles used in the current study are made up of soft magnetic particles. As mentioned in Section 2.4.5, upon removal of magnetic field, all the domains of soft magnetic particles become randomly oriented and are thus completely demagnetized. When a magnetic field is applied to the cement-based MR fluid containing these soft magnetic particles, the elastic component of the shear modulus increases because of the magnetic dipole interactions. When the magnetic field is removed, it was found that the elastic properties of cement paste were not completely lost (because the magnetic particles cannot completely disperse as they are suspended in a concentrated suspension of cement particles).

In the case of hard magnetic materials, when the magnetic field is removed there is a residual magnetization left in the sample. Which means that when the cement-based MR fluid containing hard magnetic particles is first magnetized, there would be an increase in the elastic component of shear modulus and when the magnetic field is removed, the elastic properties of the sample might be higher than those experienced by the cement-based MR fluid containing soft magnetic particles. This would mean that the magnetic field does not have to be applied continuously to achieve higher viscoelastic properties. At the end of "actual" setting of cement paste through hydration a magnetic field (also known as coercivity) can be applied in the opposite direction to demagnetize the material.

8.2.3 Visualzation of magnetic particle chains

Many authors have presented techniques to visualize the magnetic particle chains that are formed due to the magnetic dipole interactions. As the response time of MR fluids is very fast, conventional CCD cameras cannot be used to capture the formation of magnetic chains. To get around this problem Deshmukh (2007) suspended small dosages of magnetic particles in silicone oil based fluid and visualized the chains using high-speed video microscopy. It would be interesting to visualize the chains formed in a cement-based MR fluid. Cement paste being a concentrated suspension of particles would pose additional difficulty in visualizing the aggregation and breakage of magnetic chains. This can be circumvent by using a small dosage of cement to understand the interaction between the cement particles and the magnetic chains.

8.2.4 Compressive Rheology

In all the rheological tests performed in this study the magnetic field was applied in the perpendicular direction of shear flow. It would be interesting to see the changes in the rheological response of the sample when the magnetic field is applied in the same direction as applied field. This is also known as compressive rheology (or bi-axial squeeze flow), wherein the upper plate is lowered to reduce gap between the plates at a certain rate and the changes in the normal forces (or tensile stresses) are monitored. The current literature is split between the use of smooth lubricated surfaces (perfect slip condition) or serrated/rough surfaces (no slip condition). But according to literature, achieving a perfect slip or no-slip condition is hard and partial slip occurs in most cases

(De Vicente et al. 2011). The appropriate testing conditions and the relevant equations have to be figured out before this rheology technique can be used.

8.2.5 Measuring mortar/concrete MR properties

The current study was focused on understanding the changes in the rheological behavior of MR based cement paste. A uniform magnetic field (using an electromagnet) was generated in parallel plate geometry and a sensitive rotational rheometer was used to measure the rheological properties. By building an appropriate electromagnet, the same rheometer can be used to measure properties of mortar (cement paste + sand) in a cup and vane geometry. Several rheometers have been developed in the past for measuring the rheological properties of concrete. They include the Tattersall two point device, IBB rheometer, BML viscometer, Bertta apparatus, BTRHEOM, CEMAGREF-IMG, ICAR rheometer etc (Tattersall and Banfill 1983; Ferraris and Brower 2001; Koehler and Fowler 2004). One of these rheometers can potentially be outfitted with a magnetic source to measure the rheological properties of MR based concrete.

8.2.6 Small scale setup for simulating placing/pumping operations

In Chapter 7 it was shown that using magnetic fields cement-based MR fluids can be directed to flow in any desired direction and this would be helpful in transporting the fluids to regions where it would not want to flow on it's own (for example constricted regions). It would be beneficial to build a small scale set up (maybe 1 foot in dimension) to gain a better understanding of potential problems that might arise in field.

8.2.7 Use of magnetic particles for structural health monitoring

There are several non-destructive techniques that are used to detect cracks and monitor crack growths in ferromagnetic metals. Some of these methods include magnetic flux leakage, eddy current inspection, magneto acoustic emission magneto optic emission (Jiles 1988; Jiles 1990). The magnetic particles are embedded throughout the matrix of the cement-based material and as the material as a whole exhibits ferromagnetic behavior. Therefore it would be interesting to know one or more of the techniques mentioned above would work for a distributed network of magnetic particles. Such monitoring could be critical to assess the performance of important structures (Brownjohn 2007), to reduce the risk of failures, to maintain the structures and to prolong their useful life.

Bibliography

ACI-237. 2007. *Self Consolidating Concrete*. Farmington Hills, MI.

Amziane, S., and C. F. Ferraris. 2007. "Cementitious Paste Setting Using Rheological and Pressure Measurements." *ACI Materials Journal* 104 (2): 137–145.

API-10A. 2011. *Specification for Cements and Materials for Well Cementing*. Washington, DC.

ASTM-C150. 2012. *Standard Specification for Portland Cement*. West Conshohocken, PA.

ASTM-C1738. 2011. *Standard Practice for Standard Practice High-shear Mixing of Hydraulic Cement Pastes*. West Conshohocken, PA.

Banfill, P. F. G. 2003. "The Rheology of Fresh Cement and Concrete - A Review." In *11th International Congress on the Chemistry of Cement*, edited by G. Grieve and G. Owens, 1:50–62. Durban, South Africa.

Banfill, P. F. G., and M. Frias. 2007. "Rheology and Conduction Calorimetry of Cement Modified with Calcined Paper Sludge." *Cement and Concrete Research* 37: 184 – 190. doi:10.1016/j.cemconres.2006.11.013.

Bao-kuan, N., M. Jin, R. Yi-nan, J. Tong, and C. Xiao-lei. 2011. "Preliminary Approach to Mechanical Characteristics of Cement Mixed Superfine Iron Tailings." *Advanced Materials Research* 299-300. Materials and Manufacturing: 718–721. doi:10.4028/www.scientific.net/AMR.299-300.718.

Barker, A. P. 1990. "Conduction Calorimetric Studies of Cements Containing 5% Additions." *Cement and Concrete Research* 20 (2): 219 – 226. doi:10.1016/0008-8846(90)90074-8.

Barnes, H. A., and D. Bell. 2003. "Controlled-stress Rotational Rheometry : An Historical Review." *Korea-Australia Rheology Journal* 15 (4): 187–196.

Barnes, H. A., J. F. Hutton, and K. Walters. 1989. *An Introduction to Rheology*. Amsterdam: Elsevier.

Barnes, H. A., H. Schimanski, and D. Bell. 1999. "30 Years of Progress in Viscometers and Rheometers." *Applied Rheology* 9 (2): 69–76.

Barnes, H. A., and K. Walters. 1985. "The Yield Stress Myth?" *Rheologica Acta* 24: 323–326.

BASF. 2012. "Carbonyl Iron Powder; General Brochure." http://www.monomers.basf.com/.

Bentz, D. P., and C. F. Ferraris. 2010. “Rheology and Setting of High Volume Fly Ash Mixtures.” *Cement and Concrete Composites* 32 (4): 265–270. doi:10.1016/j.cemconcomp.2010.01.008.

Bentz, D. P., C. F. Ferraris, M. A. Galler, A. S. Hansen, and J. M. Guynn. 2012. “Influence of Particle Size Distributions on Yield Stress and Viscosity of Cement and Fly Ash Pastes.” *Cement and Concrete Research* 42 (2): 404–409. doi:10.1016/j.cemconres.2011.11.006.

Bica, I. 2006. “Advances in Magnetorheological Suspension: Production and Properties.” *Journal of Industrial and Engnering Chemistry* 12 (4): 501–515.

Brian, R. M., R. S. Cohen, and O. Knudsen. 2007. *Hans Christian Ørsted and the Romantic Legacy in Science*. Vol. 241. Boston Studies in the Philosophy of Science. Springer.

Brownjohn, J. M. W. 2007. “Structural Health Monitoring of Civil Infrastructure.” *Philosophical Transactions of the Royal Society A: Mathematical, Physical and Engineering Sciences* 365 (1851): 589–622. doi:10.1098/rsta.2006.1925.

Camp, J. M., and C. B. Francis. 1920. *The Making, Shaping and Treating of Steel*. Second. Pittsburgh, PA: The Carnegie Steel Company.

Carlson, J. D., D. M. Catanzarite, and K. A. St. Clair. 1995. “Commertial Magnetorheological Fluid Devices.” In *5th International Conference on Electro-Rheological, Magneto-Rheological Suspensions and Associated Technology*. Sheffield.

Carlson, J. D., W. Matthis, and J. R. Toscano. 2001. “Smart Prosthetics Based on Magnetorheological Fluids.” In *Smart Structures and Materials 2001: Industrial and Commercial Applications of Smart Structures Technologies*, 4332:308–316. Bellingham: SPIE.

Chen, Q., and Z. J. Zhang. 1998. “Size-dependent Superparamagnetic Properties of MgFeO Spinel Ferrite Nanocrystallites.” *Applied Physics Letters* 73 (21): 3156. doi:10.1063/1.122704.

Cheng, D. C-H. 1986. “Yield Stress: A Time-dependent Property and How to Measure It.” *Rheologica Acta* 25: 542–554.

Chong, J. S., E. B. Christiansen, and A. D. Baer. 1971. “Rheology of Concentrated Suspensions.” *Journal of Applied Polymer Science* 15 (8): 2007–2021. doi:10.1002/app.1971.070150818.

Chung, D. D. L. 2010. *Functional Materials: Electrical, Dielectric, Electromagnetic, Optical and Magnetic Applications*. Vol. 2. Engineering Materials for Technological Needs. World Scientific.

Claracq, J., J. Sarrazin, and J. P. Montfort. 2004. “Viscoelastic Properties of Magnetorheological fluids.” *Rheologica Acta* 43 (1): 38–49. doi:10.1007/s00397-003-0318-7.

Cullity, B. D., and C. D. Graham. 2009. *Introduction to Magnetic Materials*. 2nd ed. Wiley.

Deshmukh, S. 2007. “Development, Characterization and Applications of Magnetorheological Fluid Based `smart’ Materials on the Macro-to-micro Scale”. PhD Dissertation, Massachusetts, USA: Massachusetts Institute of Technology.

Dewan, S. 2009. “Metal Levels Found High in Tributary After Spill.” January 1. http://www.nytimes.com/.

Domone, P. L. 2003. “Fresh Concrete.” In *Advanced Concrete Technology: Concrete Properties*, edited by J. Newman and B. S. Choo, First. Burlington, MA: Elsevier.

Dyke, S. J., B. F. Spencer, M. K. Sain, and J. D. Carlson. 1996. “Modeling and Control of Magnetorheological Dampers for Seismic Response Reduction.” *Smart Materials and Structures* 5 (5): 565–575.

EPMA. 2013. “Powder Manufacture.” *European Powder Metallugy Association*. http://www.epma.com/powder-manufacture.

EPRI. 2000. “Metal Powder Production”. SIC 33991. Industry Segment Profile. EPRI Center for Materials Production.

Feng, Y. B., T. Qiu, C. Y. Shen, and X. Y. Li. 2006. “Electromagnetic and Absorption Properties of Carbonyl Iron/rubber Radar Absorbing Materials.” *IEEE Transactions on Magnetics* 42 (3): 363–368.

Ferraris, C. F., and L. E. Brower. 2001. “Comparison of Concrete Rheometers: International Tests at LCPC (Nantes, France) in October 2000”. NISTIR 6819. Gaithersburg, MD: National Institute of Standards and Technology.

Ferraris, C. F., and J. M. Gaidis. 1992. “Connection Between the Rheology of Concrete and Rheology of Cement Paste.” *ACI Materials Journal* 88 (4): 388–393.

Ferraris, C. F., K. H. Obla, and R. Hill. 2001. “The Influence of Mineral Admixtures on the Rheology of Cement Paste and Concrete.” *Cement and Concrete Research* 31 (2): 245–255.

Ferraris, Chiara F., W. Guthrie, A. I. Avilés, M. Peltz, R. Haupt, and B. S. MacDonald. 2006. *Certification of SRM 114q: Part II (Particle Size Distribution). NIST Special Publication 260-166*. Technology Administration, U.S. Department of Commerce.

Ferron, R. D., Z. Gregori, Z. Sun, and S. P. Shah. 2007. “Rheological Method to Evaluate Structural Buildup in Self-consolidating Concrete Cement Pastes.” *ACI Materials Journal* 104 (3): 242–250.

Ferron, R. D., S. P. Shah, E. Fuente, and C. Negro. 2013. “Aggregation and Breakage Kinetics of Fresh Cement Paste.” *Cement and Concrete Research* 50: 1–10. doi:10.1016/j.cemconres.2013.03.002.

Foner, S. 1959. “Versatile and Sensitive Vibrating‐sample Magnetometer.” *Review of Scientific Instruments* 30 (7): 548–557. doi:10.1063/1.1716679.

Gartner, E. M., J. F. Young, D. A. Damidot, and I. Jawed. 2002. “Hydration of Portland Cement.” In *Structure and Performance of Cements*, edited by J. Bensted and P. Barnes, 57–113. New York: Spon Press.

Genc, S., and P. P. Phule. 2002. “Rheological Properties of Magnetorheological Fluids.” *Smart Materials and Structures* 11: 140–146.

Gorodkin, S. R., R. O. James, and W. I. Kordonski. 2009. “Magnetic Properties of Carbonyl Iron Particles in Magnetorheological Fluids.” In *Journal of Physics: Conference Series*. Vol. 149. Dresden, Germany: IOP Publishing. doi:10.1088/1742-6596/149/1/012051.

Grant, K. J., G. L. Paul, and J. A. O’Neill. 1991. “Quantitative Elemental Analysis of Iron Ore by Laser-induced Breakdown Spectroscopy.” *Applied Spectroscopy* 45 (4): 701–705. doi:10.1366/0003702914336949.

Helmuth, R., L. M. Hills, D. A. Whiting, and S. Bhattacharja. 1995. “Abnormal Concrete Performance in the Presence of Admixtures”. RP333. Skokie, Illinois, USA: Portland Cement Association.

Hsieh, Y. Z., and S. T. Lin. 2001. “Diamond Tool Bits with Iron Alloys as the Binding Matrices.” *Materials Chemistry and Physics* 7 (2): 121–125.

Huang, X. X., H. B. Ji, C. Li, F. Qin, Q. Li, and Y. L. Liang. 2012. “A Comparative Study on the Pollution and Speciation Characteristics of Heavy Metals Between the Gold and Iron Mine Tailings of the Upstream Area of Miyun Reservoir, Beijing.” *Advanced Materials Research* 518-523. Advances in Environmental Science and Engineering: 1412–1416.

Izon, D., E. Danenberger, and M. Mayes. 2004. “Absence of Fatalities in Blowouts Encouraging in MMS Study of OCS Incidents 1992-2006.” *Drilling Contractor*, August.

Jarl, J. 2012. “Cement Mill Sheet”. Texas Lehigh Cement Company.

JCPDS. 1989. *Powder Diffraction File Search Manual (Hanawalt Method): Inorganic*.

Jiang, S. P., J. C. Mutin, and A. Nonat. 1995. “Studies on Mechanism and Physico-chemical Parameters at the Origin of the Cement Setting. I. The Fundamental Processes Involved During the Cement Setting.” *Cement and Concrete Research* 25 (4): 779–789. doi:10.1016/0008-8846(95)00068-N.

Jiles, D. C. 1988. “Review of Magnetic Methods for Nondestructive Evaluation.” *NDT International* 21 (5): 311–319.

———. 1990. “Review of Magnetic Methods for Nondestructive Evaluation (Part 2).” *NDT International* 23 (2): 83–92.

Jolly, M. R., J. W. Bender, and J. D. Carlson. 1999. “Properties and Applications of Commercial Magnetorheological Fluids.” *Journal of Intelligent Material Systems and Structures* 10 (1): 5–13.

Jozwiak, W. K., E. Kaczmarek, T. P. Maniecki, W. Ignaczak, and W. Maniukiewicz. 2007. “Reduction Behavior of Iron Oxides in Hydrogen and Carbon Monoxide Atmospheres.” *Applied Catalysis A: General* 326 (1): 17–27. doi:10.1016/j.apcata.2007.03.021.

Kciuk, M., and R. Turczyn. 2006. “Properties and Application of Magnetorheological Fluids.” *Journal of Achievements in Materials and Manufacturing Engineering* 18 (1-2): 127–130.

Kern, E. F. 1908. “Electrolytic Refining of Iron.” In *Transactions of the American Electrochemical Society*, 13:103–119. Albany, NY: The American Electrochemical Society.

Khayat, K. H., and A. F. Omran. 2009. “Evaluation of SCC Formwork Pressure.” In *Second International Symposium on Design, Performance and Use of Self-Consolidating Concrete*, 43–55. Beijing, China.

Kim, J. H., R. P. Ferron, and S. P. Shah. 2012. “Fresh Concrete and Its Significance for Sustainability.” *Journal of Sustainable Cement-Based Materials* 1 (1-2): 16–23. doi:10.1080/21650373.2012.726821.

Klar, E., and P. K. Samal. “Process for Electrolytic Iron Powder.”

Klingenberg, D. J. 2001. “Magnetorheology: Applications and Challenges.” *American Institute of Chemical Engineers Journal* 47 (2): 246–249.

Klingenberg, D. J., C. H. Olk, M. A. Golden, and J. C. Ulicny. 2010. “Effects of Nonmagnetic Interparticle Forces on Magnetorheological Fluids.” *Journal of Physics: Condensed Matter* 22: 324101.

Koehler, E. P., and D. W. Fowler. 2004. “Development of a Portable Rheometer for Fresh Portland Cement Concrete”. ICAR 105-3F. Austin, TX: International Center for Aggregates Research.

Kordonski, W. I., and S. D. Jacobs. 1996. “Magnetorheological Finishing.” *International Journal of Modern Physics B* 10 (23-24): 2837–2848.

L’Hermite, R. 1949. “Vibration and the Rheology of Freshly Mixed Concrete.” *Revue Des Materiaux De Construction* 1 (405): 179–187.

Larson, R. G. 1998. *Structure and Rheology of Complex fluids*. USA: Oxford University Press.

Lee, J. K., T. Sefzik, Y. H. Son, T. X. Phuoc, Y. Soong, and M. K. Chyu. 2009. “Use of Magnetic Nanoparticles for Smart Drilling Fluids.” In *American Association of Drilling Engineers: National Technical Conference and Exhibition*. New Orleans.

Lemaire, E., A. Meunier, G. Bossis, J. Liu, D. Felt, V. Bashtovoi, and N. Matoussevitch. 1995. “Influence of the Particle Size on the Rheology of Magnetorheological Fluids.” *Journal of Rheology* 39 (5): 1011–1020.

Lepinski, J. A., J. C. Myers, and G. H. Geiger. 2005. “Iron.” In *Kirk-Othmer Encyclopedia of Chemical Technology*. John Wiley and Sons.

Li, C., H. Sun, J. Bai, and L. Li. 2010. “Innovative Methodology for Comprehensive Utilization of Iron Ore Tailings: Part 1. The Recovery of Iron from Iron Ore Tailings Using Magnetic Separation After Magnetizing Roasting.” *Journal of Hazardous Materials* 174 (1–3): 71–77. doi:http://dx.doi.org/10.1016/j.jhazmat.2009.09.018.

Li, W. H., G. Chen, and S. H. Yeo. 1999. “Viscoelastic Properties of MR fluids.” *Smart Materials and Structures* 8 (4): 460–468. doi:1088/0964-1726/8/4/303.

Li, Z. C., and J. Wang. 2012. “A Gun Recoil System Employing a Magnetorheological Fluid Damper.” *Smart Materials and Structures* 21: 105003. doi:10.1088/0964-1726/21/10/105003.

Lim, S. T., M. S. Cho, I. B. Jang, and H. J. Choi. 2004. “Magnetorheological Characterization of Carbonyl Iron Based Suspension Stabilized by Fumed Silica.” *Journal of Magnetism and Magnetic Materials* 282: 170–173.

Luidold, S., and H. Antrekowitsch. 2007. “Hydrogen as a reducing agent: State-of-the-art science and technology.” *JOM* 59 (6): 20–26. doi:10.1007/s11837-007-0072-x.

Lynch, S. R. 2005. “The Impact of Iron Fortification on Nutritional Anaemia.” *Best Practice & Research Clinical Haematology* 18 (2): 333–346. doi:10.1016/j.beha.2004.09.003.

Macosko, C. W. 1994. *Rheology Principles, Measurements and Applications*. Wiley-VCH.

McCurrie, R. A. 1994. *Ferromagnetic Materials, Structure and Proeprties*. Academic Press.

Mehta, P. K., and P. J. M. Monteiro. 2006. *Concrete: Microstructure, Properties and Materials*. Edited by L. S. Hager. Third. USA: McGraw Hill.

Mewis, J., and N. J. Wagner. 2012. *Colloidal Suspension Rheology*. First. Cambridge Series in Chemical Engineering. Cambridge University Press.

Mindess, S., J. F. Young, and D. Darwin. 2003. *Concrete*. Second. USA: Prentice Hall.

Nelson, E. B., and D. Guillot. 2006. *Well Cementing*. Second. Texas, USA: Schlumberger.

Nguyen, Q. D., and D. V. Boger. 1992. “Measuring the Flow Properties of Yield Stress Fluids.” *Annual Review of Fluid Mechanics* 24 (1): 47–88. doi:10.1146/annurev.fl.24.010192.000403.

Norton, G. A., R. Markuszewskl, and H. R. Shanks. 1986. “Morphological and Chemical Characterization of Iron-rich Fly Ash Fractions.” *Environmental Science & Technology* 20 (4): 409–413.

Van Oss, H. G. 2013. “Cement Statistics and Information.” *Minerals Information*. http://minerals.usgs.gov/minerals/pubs/commodity/cement/.

Papo, A., and L. Piani. 2004. “Effect of Various Superplasticizers on the Rheological Properties of Portland Cement Pastes.” *Cement and Concrete Research* 34 (11): 2097–2101. doi:10.1016/j.cemconres.2004.03.017.

Park, B. J., F. F. Fang, and H. J. Choi. 2010. “Magnetorheology: Materials and Application.” *Soft Matter* 6 (21): 5246–5253.

Piotter, V., W. Bauer, T. Benzler, and A. Emde. 2001. “Injection Molding of Componenets for Microsystems.” *Microsystem Technologies* 7 (3): 99–102.

Rabinow, J. 1948. “The Magnetic Fluid Clutch.” *AIEE Transactions* 67: 1308–1313.

Rahhal, V., V. Bonavetti, L. Trusilewicz, C. Pedrajas, and R. Talero. 2012. “Role of the Filler on Portland Cement Hydration at Early Ages.” *Construction and Building Materials* 27 (1): 82 – 90. doi:10.1016/j.conbuildmat.2011.07.021.

Rankin, P. J., A. T. Horvath, and D. J. Klingenberg. 1999. “Magnetorheology in Viscoplastic Media.” *Rheologica Acta* 38 (5): 471–477.

Red, R. 2009. “Refraction of Light.” http://interactagram.com/physics/optics/refraction/.

Redman, C. 2009. “The Next Iron Rush.” *CNN Money*. http://money.cnn.com/2009/05/19/magazines/fortune/redman_iron.fortune/index.htm.

Rich, J. P., P. S. Doyle, and G. H. McKinley. 2012. “Magnetorheology in an Aging, Yield Stress Matrix Fluid.” *Rheologica Acta* 51: 579–593.

Roberts, L. R., and P. C. Taylor. 2007. “Understanding cement-SCM-admixture Interaction Issues: Staying Out of the Sensitive Zone.” *Concrete International*, January.

Roussel, N., G. Ovarlez, S. Garrault, and C. Brumaud. 2012. “The Origins of Thixotropy of Fresh Cement Pastes.” *Cement and Concrete Research* 42 (1): 148–157. doi:10.1016/j.cemconres.2011.09.004.

Russeil, H. H., and E. A. Zawacizki. 1963. “Factors Affecting the Upgrading of Iron Oxide Derived from Fly Ash.” In *Symposium on Non_fuel Uses of Coals*, 7:47–54. 1. Cincinnati, Oh: ACS.

Sabins, F. 2002. “Ultra-lightweight Cement Slurries Improve Cement Performance.” *GasTIPS*. http://www.netl.doe.gov/technologies/oil-gas/publications/GasTIPS/GasTIPS_Fall%2002.pdf.

Schultz, Mark A., and Leslie J. Struble. 1993. “Use of Oscillatory Shear to Study Flow Behavior of Fresh Cement Paste.” *Cement and Concrete Research* 23 (2): 273 – 282. doi:10.1016/0008-8846(93)90092-N. http://www.sciencedirect.com/science/article/pii/000888469390092N.

Shackelford, J. F. 1996. *Introduction to Materials Science for Engineers*. Fourth. NJ, USA: Prentice Hall.

Sheng, R., G. A. Flores, and J. Liu. 1999. “In Vitro Investigation of a Novel Cancer Therapeutic Method Using Embolizing Properties of Magnetorheological Fluids.” *Journal of Magnetism and Magnetic Materials* 194 (1–3): 167–175.

Shoumkova, A. S. 2011. “Magnetic Separation of Coal Fly Ash from Bulgarian Power Plants.” *Waste Management & Research* 29 (10): 1078–1089. doi:10.1177/0734242X10379494.

Son, K. J., and E. P. Fahrenthold. 2012. “Evaluation of Magnetorheological fluid Augmented Fabric as a Fragment Barrier Material.” *Smart Materials and Structures* 21: 075012. doi:10.1088/0964-1726/21/7/075012.

Stöhr, J., and H. C. Siegmann. 2006. *Magnetism: From Fundamentals to Nanoscale Dynamics*. Springer.

Takata, S., K. Hosoo, Y. Inoue, R. Hanaoka, T. Fukami, and K. Shima. 2007. “Properties of Clutch Using Thixotropic MR Fluid with Surfactants.” In *International Conference on Smart Materials and Nanotechnology in Engineering*. Vol. 6423. Harbin, China.

Tattersall, G. H., and P. F. G. Banfill. 1983. *The Rheology of Fresh Concrete*. London: Pitman.

Taylor, H. F. W. 1997. *Cement Chemistry*. Second. London: Thomas Telford.

Taylor, P. C., V. Johansen, L. Graf, R. Kozikowski, J. Zemajtis, and Chiara F. Ferraris. 2006. “Identifying Incompatible Combinations of Concrete Materials: Volume I - Final Report”. FHWA-HRT-06-079. Virginia, USA: Federal Highway Administration.

Taylor, P. C., S. H. Kosmatka, G. F. Voigt, and et al. 2006. “Integrated Materials and Construction Practices for Concrete Pavement”. A State-of-the-Practice Manual HIF-07-004. Washington, DC: Federal Highway Administration.

Tregger, N. A. 2010. “Tailoring the Fresh State Properties of Concrete”. PhD Dissertation, Illinois, USA: Department of Civil and Environmental Engineering, Northwestern University.

ULCOS. 2013. “Alkaline Electrolysis.” http://www.ulcos.org/en/research/electrolysis.php.

De Vicente, J., D. J. Klingenberg, and R. Hidalgo-Alvarez. 2011. “Magnetorheological Fluids: a Review.” *Soft Matter* 7: 3701–3710. doi:10.1039/c0sm01221a.

De Vicente, J., J. A. Ruiz-López, E. Andablo-Reyes, J. P. Segovia-Gutiérrez, and R. Hidalgo-Alvarez. 2011. "Squeeze Flow Magnetorheology." *Journal of Rheology* 554: 753–779. doi:10.1122/1.3574932.

Wallevik, J. E. 2009. "Rheological Properties of Cement Paste: Thixotropic Behavior and Structural Breakdown." *Cement and Concrete Research* 39 (1): 14–29.

WBCSD. 2012. "The Cement Sustainability Initiative - 10 Years of Progress and Moving on into the Next Decade". World Business Council for Sustainable Development. http://www.csiprogress2012.org/CSI_ProgressReport_Summary.pdf.

Wereley, N. M., A. Chaudhuri, J. H. Yoo, S. John, S. Kotha, A. Suggs, R. Radhakrishnan, B. J. Love, and T. S. Sudarshan. 2006. "Bidisperse Magnetorheological Fluids Using Fe Particles at Nanometer and Micron Scale." *Journal Of Intelligent Material Systems And Structures* 17: 393–401.

West, L. 2011. "How Do Oil Spills Damage the Environment?" http://environment.about.com.

Williams, D. A., A. W. Saak, and H. M. Jennings. 1999. "The Influence of Mixing on the Rheology of Fresh Cement Paste." *Cement and Concrete Research* 29 (9): 1491–1496.

Yang, M., and H. M. Jennings. 1995. "Influences of Mixing Methods on the Microstructure and Rheological Behavior of Cement Paste." *Advanced Cement Based Materials* 2 (2): 70–78. doi:10.1016/1065-7355(95)90027-6.

Yellishetty, M., P. G. Ranjith, and A. Tharumarajah. 2010. "Iron Ore and Steel Production Trends and Material Flows in the World: Is This Really Sustainable?" *Resources, Conservation and Recycling* 54 (12): 1084–1094. doi:http://dx.doi.org/10.1016/j.resconrec.2010.03.003.

Yildirim, Y., D. Hazlett, and R. Davio. 2004. "Toner-modified Asphalt Demonstration Projects." *Resources, Conservation and Recycling* 42 (3): 295–308. doi:10.1016/j.resconrec.2004.04.008.

Zhang, B., Y. Feng, J. Xiong, Y. Yang, and H. Lu. 2006. "Microwave-absorbing Properties of De-aggregated Flake-shaped Carbonyl-iron Particle Composites at 2-18 GHz." *IEEE Transactions on Magnetics* 42 (7): 1778–1781. doi:10.1109/TMAG.2006.874188.

Zhang, H., L. R. Moore, M. Zborowski, P. S. Williams, S. Margel, and J. J. Chalmers. 2005. "Establishment and Implications of a Characterization Method for Magnetic Nanoparticle Using Cell Tracking Velocimetry and Magnetic Susceptibility Modified Solutions." *Analyst* 130 (4): 514–527. doi:10.1039/B412723D.

Zhang, J., and G. W. Scherer. 2011. "Comparison of Methods for Arresting Hydration of Cement." *Cement and Concrete Research* 41: 1024–1036.